Aalto University
School of Engineering

Farhang Shamaei

Analysis of methods for the prediction of ice loading on a ship's hull

Thesis submitted in partial fulfilment of the requirements for the degree of Master of Science in Technology

Espoo 26.11.2018
Supervisor: Prof. Pentti Kujala
Advisor: Prof. Pentti Kujala
Dr. Martin Bergström

Aalto University
School of Engineering

Aalto University, P.O. BOX 11000, 00076 AALTO
www.aalto.fi
Abstract of the master's thesis

Author Farhang Shamaei

Title of thesis Analysis of methods for the prediction of ice loading on a ship's hull

Degree programme Mechanical Engineering

Major/minor Marine Engineering

Thesis supervisor Prof. Pentti Kujala

Thesis advisor(s) Prof. Pentti Kujala, Dr. Martin Bergström

Date 26.11.2018 **Number of pages** 41+51 **Language** English

Abstract

The hull of a ship operating in ice might be exposed to significant ice loading, originating from a complex and stochastic interaction between the hull and the ice. In order to analyze such ice loading, taking into account the stochastic nature of the hull-ice interaction, statistical methods might be used. In this context, the estimation of the local ice pressures on various locations of a ship's hull is required. This thesis aims to analyze a semi-empirical method known as the event-maximum method, which estimates the maximum local pressures as the function of the contact area and the ice condition. To this end, this study uses the full-scale ice load measurements to determine a new set of curves, which describe the relationship between the contact area and the local pressures. The obtained curves are subsequently compared with the previous studies corresponding curves, which had been obtained from different sets of full-scale ice pressure measurements. In addition, the maximum local pressures obtained from this study are compared with the maximum local pressures obtained using the design curve proposed in previous studies. Furthermore, for studying the effect of the variation of the load height on maximum local pressures, a sensitivity analysis is performed for the bow. The results show that the curves obtained in this study are close to the curves obtained in previous study. Furthermore, the sensitivity analysis shows that the variation of the load height causes small changes in maximum local pressures at the bow. The study shows that the event-maximum method is well-suited for the estimation of the maximum local pressures at all the locations of the hull. This research may help naval architects to design safe and efficient hull structures for Arctic ships.

Keywords Ship-ice interaction, probabilistic methods, ice-induced loading, local ice pressures, event-maximum method.

Acknowledgement

I would like to express my great appreciation to everyone who has assisted me during this thesis work. First, I want to express my sincere gratitude to my supervisor, Prof. Pentti Kujala, for providing me with this research opportunity. I would like to thank him for his invaluable guidance, supports and encouragements throughout the whole process. Then I am grateful to my thesis advisor, Dr. Martin Bergström, for all of his helpful discussions, comments and advice which assisted me to learn about the academic writing process and criteria and have a better understanding about the topic. I would also like to thank my colleagues, Fang Li, Mikko Kotilainen, and Sunil Basnet, Ghalib Humayun Taimuri for their tremendous technical guidance and supports, which assisted me throughout the entire process. Furthermore, I really appreciate the SEDNA project for providing financial support to the current study. The project has received funding from the European Research Council (ERC) under the European Union's Horizon 2020 research and innovation programme (grant agreement n° 723526). Finally yet importantly, I am deeply grateful to my parents and wife, Afsoon, for their constant supports and encouragements, which assisted me in managing all the challenges throughout my life and studies.

Farhang Shamaei

26 November 2018
Espoo, Finland

Table of contents

List of figures

List of tables

List of abbreviations

Abbreviation	Description
#	Frame number
CDF	Cumulative Density Function
FEA	Finite Element Analysis
FYI	First-Year Ice
HPZs	High Pressure Zones
IB	Icebreaker
MYI	Multi-Year Ice
NM	Nautical Mile
PDF	Probability Density Function

List of variables

Variable	[Unit]	Description
A	$[m^2]$	Nominal contact area
a	$[m^2]$	Actual contact area
C	[-]	Constant coefficient
D	[-]	Constant coefficient
D_t	[NM]	Total distance operating in ice
F	[kN]	Maximum global force
f	[-]	Frequency of ice impacts
F (x)	[-]	Cumulative density function
f (x)	[-]	Probability density function
F_{max}	[kN]	Maximum total force
H	$[m]$	Load height
L	$[m]$	Load length
n	[-]	Number of impacts
P	[MPa]	Global pressure
P_e	[-]	Probability of exceedance
P_l	[MPa]	Local ice pressure
r	[-]	Number of direct hits
t	[Sec]	Average duration of ice interaction referring to expected ice condition
t_k	[Sec]	Average duration of ice interaction referring to ISO 2010 design curve
v	[-]	Expected number of ice impacts
X_i	[-]	Random quantity of the ice load
x_0	[MPa]	Best fitting line x-intercept
z_e	[MPa]	Design pressure
$\hat{z}_l$	[MPa]	Most probable extreme value
z_n	[MPa]	Characteristic largest value
α	[MPa]	Inverse slope of the best fitting line
μ	[-]	Ice exposure

1 Introduction

1.1 Background

In recent years, the existence of potential natural resources of hydrocarbons and minerals in the Arctic and the possibility of a shorter shipping route through the Arctic seas has stimulated the demand for ice class ships. In order to design safe and efficient ice going ship for protecting the human life and the environment, a vast knowledge of ice loading on the hull of ships is required. The Arctic area in this thesis refers to the seas, which are covered by seasonal ice, and has a cold weather. Figure 1 shows the Arctic area.

Figure 1. The Arctic area (Ehlers, et al., 2015).

Ice loads on the hull of an ice-going ship arise from interaction between ice features and ship hull. It exerts significantly high pressures on the hull of a ship and consequently causes elastic and plastic deformation on structural elements (Suominen, 2018). Hence, it is important to evaluate possible structural failure that could occur once a single load exceeds the critical value of the system's structural strength. For that purpose, the determination of the ice load extreme value, which a ship will experience throughout the lifetime, is crucial. Generally, the extreme value is defined as the largest value expected to occur in a certain number of interactions or in a certain period (Ochi, 1981). Thus, its magnitude and frequency of occurrence must be estimated as design requirements.

The ice loads on the structures of a ship have a stochastic nature which is influenced by different variables such as the ice conditions, ice mechanical properties, the speed of ship, the speed of ice, and the ice fracture mechanisms (Suyuthi, et al., 2012b). There are different approaches for the evaluation of the ice loads and pressures on hull of a ship such as numerical studies, discrete element and finite element simulations, and full-scale measurements (Suominen, 2018). Ice loading can be assessed using data from full-scale ice load measurements. Furthermore, the statistical analysis can also be employed for the approximation of the ice loads on the hull of a ship (Kujala & Vuorio, 1985). Hence, different statistical methods are proposed for estimating the most likely maximum ice loads from the short-term and long-term full-scale ice load measurements (Kujala & Vuorio, 1985).

Due to the existence of high magnitude local ice pressure zones within the global contact area, localized damage can happen. Hence, the maximum local ice pressure corresponding to the specific probability of exceedance, i.e., 10^{-2} is an important criterion for structural design. In this respect, Jordaan et al. (1993) developed the event-maximum method for the evaluation of the maximum local pressure on particular area of hull of a ship, i.e., a plate between the frames. However, few studies have been done for the evaluation of the proposed method. The availability of full-scale measurements data from Aghulas II enables further examine the method.

1.2 Research objectives

For the evaluation of the maximum local pressures on different areas of ship's hull, this thesis aims to analyze a semi-empirical method known as the event-maximum method, using the ice loads from full-scale measurements. Furthermore, the results of this study will be compared with the results of a previous study by Taylor et al. (2010). In addition, the obtained maximum local pressures will be compared with the maximum local pressures defined based on the curve proposed by Jordaan et al. (1993). As the contact area plays the main role for approximating the ice pressures from the measured ice loads, the study also examines the effect of variation of load height on maximum local pressures by conducting sensitivity analysis.

1.3 Structure of the thesis

Chapter 2 presents the state of art, which focuses on previous studies related to the ice loads and pressures on hull of ships. Then, Chapter 3 comprises the research background and theories for the approximation of the local ice pressures. It discusses about the application of the extreme statistics for estimating the design ice loads and ice pressures from the full-scale measurements. Furthermore, it describes the event-maximum method, which is used in this study for the estimation of the maximum local pressure from the measured ice loads. Next, chapter 4 provides a description and analysis of full-scale measurement on board of S.A Agulhas II. Then, Chapter 5 describes the methods, which are used in this study. In addition, the study results are presented in this chapter. Moreover, the results from using the event-maximum method are compared with the results presented by Jordaan et al. (1993) and Taylor et al. (2010). Furthermore, the outcomes of the sensitivity analysis are also presented. Next, the results from previous chapter are discussed in Chapter 6. Finally, the conclusion and future possibilities are provided in Chapter 7 and Chapter 8 respectively.

2 State of the art

The prediction of the extreme ice load acting on a ship's hull requires extensive knowledge of ice conditions, ice mechanical properties and integration of those with ship speed and ice load. To this end, different methods are being used for measuring the ice loads on ship hull structures for better understanding about the ice-loading phenomenon. Full-scale measurement is a common methods for studying ice loading on the hull of a ship (Kujala & Vuorio, 1985). Full-scale measurements have the advantages that all the complexities like the variety of different ice regimes and mechanical processes through the ship voyage are embedded in the measurements (Suominen, 2018). Kheisin and Popov (1973) have started full-scale measurements from 1960's, and later Vuorio et al. (1978) has measured ice loads on board icebreaker (IB) Sisu in the winter 1979 in Bothnian Bay. Furthermore, Kujala and Vuorio (1985) have conducted extensive full-scale measurements on board IB SISU during the winters 1979-1985 in the Baltic Sea and by Kujala (1994) in Antarctic Sea. Similarly, Leira et al (2009) conducted full-scale measurements on board KV Svalbard during the winters 2007-2008.

Even though the ice interaction (ice breaking) process is random, in principle the probability theory can be used to predict design ice loads statistically (Ochi, 1981) (Kujala & Vuorio, 1985). The main purpose of the statistical analysis is firstly to generate a statistical model using the full-scale data to study the phenomena associated with the ice-breaking processes (ice interactions) and secondly to generate a basis for extremal analysis (Kujala & Vuorio, 1985).

In principle, the approximation of maximum ice loads is based on extreme value theory (Kujala & Vuorio, 1985). In the case of known initial ice load distribution, the extreme value distribution can be defined if the initial distribution raised to the power of expected ice interactions (Ochi, 1981). Practically, in most cases, the initial distribution is not known, so extreme ice loads should be approximated (Ochi, 1981). To this end, some known probability distributions (i.e. exponential distribution) can be fitted into the load amplitude time history and the extreme value in a desired period can be estimated based on approximated probability distribution (Ochi, 1981). The previous studies of short-term measured ice loads have reported different probability distributions as the best fit into the full-scale measurements in the Baltic Sea, i.e., weibull distribution with the shape parameter of 0.75 by Suominen and Kujala (2010), lognormal distribution by Kujala and Vuorio (1985). Furthermore, Kujala and Vuorio (1986) have analyzed both, short-term and long-term measurements, on board IB Sisu between the years 1979-1985 by using the Exponential and gumbel I asymptotic distribution respectively. They reported that the maximum ice load, which resulted from the modeling of the measured daily maxima with gumbel I distribution, is fairly close to the extrapolation of the maximum ice load resulted from fitting the Exponential distribution into the measured peak amplitudes. Similarly, Vuorio et al. (1979) studied the measured daily maximum ice loads and pressures from the full-scale measurement on board IB Sisu in winter 1978. They have concluded that the gumbel distribution followed quite closely the measured daily maxima of the ice pressures and the ice loads. Moreover, Jordaan et al. (1993) suggested that the best fitting line into the tail of the ice loads follows the exponential distribution. Furthermore, Suyuthi et al. (2012b) has conducted a broad study of fitting different probability distributions to the full-scale measured ice loads. The study reported that, for the most of the cases, weibull and exponential distribution provide better fits to the measured ice forces than by gumbel and lognormal distributions for modeling the ice loads. On the other hand, another approach called time-window was used by Lensu (2002) for the evaluation of short-term ice loads.

Analysis of the ice pressures data from various full-scale measurements by (Sanderson, 1988) (Frederking, et al., 1990) (Daley, et al., 1990) showed that the ice pressure is not uniformly distributed on the area of ice interaction with the hull of a ship. As a result, the pressure-area curve became a common approach for the representation of ice pressure as a function of the area (Daley, 2007). Furthermore, Sanderson (1988) concluded from many tests that the relationship between the ice pressure and the contact area can be modeled in the form of $P = CA^D$. Moreover, Frederking (1999) proposed two different concepts of process and spatial pressure-area relationship. The process pressure-area relationship represents how the average ice pressure is related to the nominal area of contact (Frederking, 1999) (Daley, 2004). In contrast, the spatial describes the relationship between the local maximum pressures with the local contact area (Frederking, 1999) (Daley, 2004). The result of the study by Frederking (1999) showed a decreasing trend in both process and spatial pressure-area curves as the contact area increases. Daley (2007) has conducted further study for the investigation of the relationship between the process, and the spatial pressure-area model. The results of this study revealed the fact that in the process model, for some of the cases, pressure increases as the nominal contact area grows. On the other hand, in the spatial model, for all of the cases, the pressure decreases as the actual area of the interaction increases. Today, the spatial and the process pressure-area models are being used for the evaluation of the global and local maximum pressures respectively (Daley, 2004).

Consideration of the pressure-area relationship, and the global and local pressure have resulted in development of different methods for the prediction of the global and local maximum ice pressure. Jordaan et al. (1993) has developed the event-maximum method for the approximation of the maximum local ice pressures on a ship's hull. The method uses parameters of α and x_0, which are obtained from the best fitting lines to the peak pressures. Parameter α as a function of contact area is represented by the α-area curve. Furthermore, Taylor et al. (2010) has compared the α–area curves obtained from several full-scale ice pressures data with the design curve proposed by Jordaan et al. (1993). The study shows that the constant coefficients of the curves are varied and dependent on the ice type and the ice condition.

3 Research background

3.1 Ice-breaking process and peak load events definition

Ice load is a force on the hull of a ship raised from the interaction between the ship hull and ice floes (Kotilainen, et al., 2017). As ship moves forward in ice it causes ice to break, immerse or slide against the hull (Kotilainen, et al., 2017). The continuous ice-breaking process can be categorized into three phases: *approaching*, *crushing*, and *disengaging* stage (Kotilainen, et al., 2017). Figure 2 represents a typical ice-breaking process. The approaching phase starts as the ice load starts to grow (Kotilainen, et al., 2017). At this time, the ice is still not touched the frame of interest but the load is reflected from the neighboring frames (Kotilainen, et al., 2017). Next, in the crushing phase starts when the ice feature interacts the hull of the ship and the ship starts penetrating into the ice sheet until the maximum penetration is achieved (Kotilainen, et al., 2017). Furthermore, the load is assumed to increase due to the crushing of ice at the location of the interaction until the ice edge breaks (Kotilainen, et al., 2017). Breaking of the ice can occur either due to microscopic shearing or due to bending failure (Kujala, 1994). The criteria for bending and shear failure determine the level of the peak load event (Kujala, 1994). At the time of the failure, the load reaches its maximum amplitude, which is called the peak value of the measured loads (Kotilainen, et al., 2017).

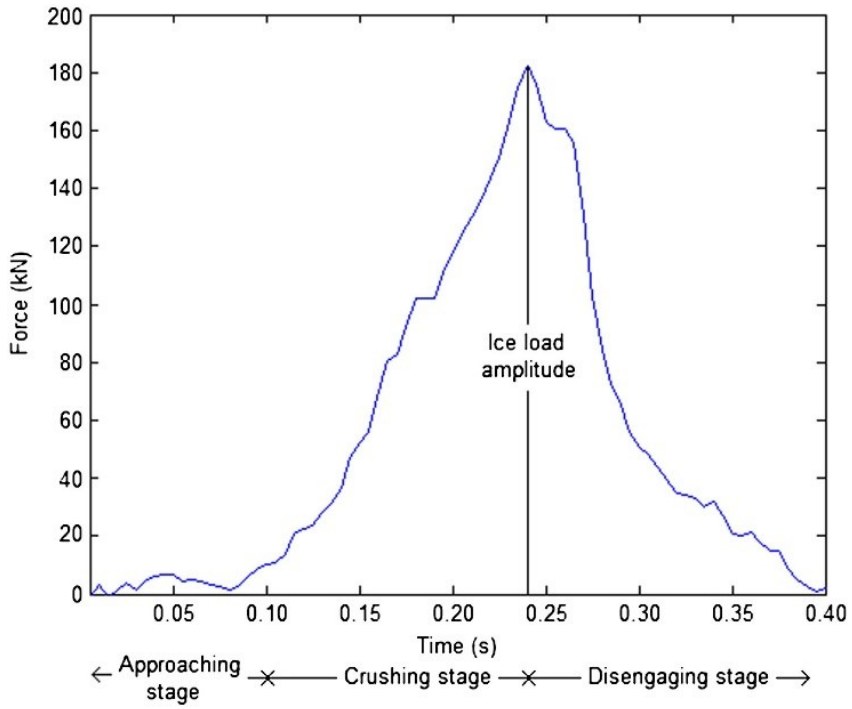

Figure 2. Different stages of a continues ice-breaking process (Kotilainen, et al., 2017).

The ice-breaking process and the ice loads are affected by mechanical properties, and ship hull shape (Kujala, 1994). The normal frame angle, β_n, as shown in Figure 3 is an important parameter that affects the ice failure process (Kujala, 1994). Ice breaks due to bending as ship moves into the ice and the normal frame angle increases and contact height, h, decreases (Kujala, 1994). At smaller normal frame angle, i.e., the side of the ship, ice breaks mainly by crushing (Kujala, 1994). Figure 3 represents an idealization of the failure process of the ice edge.

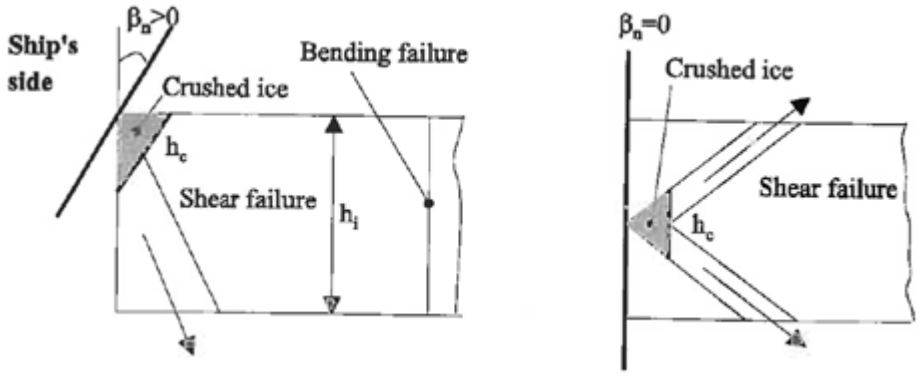

Figure 3. Idealization of the ice edge failure process (Kujala, 1994).

3.2 Stochastic nature of ice loads

The ice-breaking phenomena is complex process, which its complexity is originated from variety of parameters such as the mechanical properties of ice, the speed of ice, the ice fracture mechanisms, and the speed of ship (Kujala & Vuorio, 1985). Furthermore, the ice loading has a stochastic nature. Thus, as shown in Figure 4, the ice loads can considerably fluctuate even in a short time interval.

Although it has been assumed that in a constant ice conditions, the speed has a linear effect on ice loads, some extensive studies have shown that there is a weak correlation between the speed of the ship and the magnitude of the ice load (Hanninen, et al., 2001) (Suominen, et al., 2015). Furthermore, some studies also investigated the effect of the ice thickness on the ice load. The results have indicated that the ice thickness has a significant effect on the magnitude of the ice loads (Hanninen, et al., 2001) (Suominen, et al., 2015) (Kotilainen, et al., 2017). Moreover, Suominen et al. (2015) reported a correlation between the ice concentration and the magnitude of the ice load. This correlation may be the result of the increased number of impacts at the higher ice concentrations.

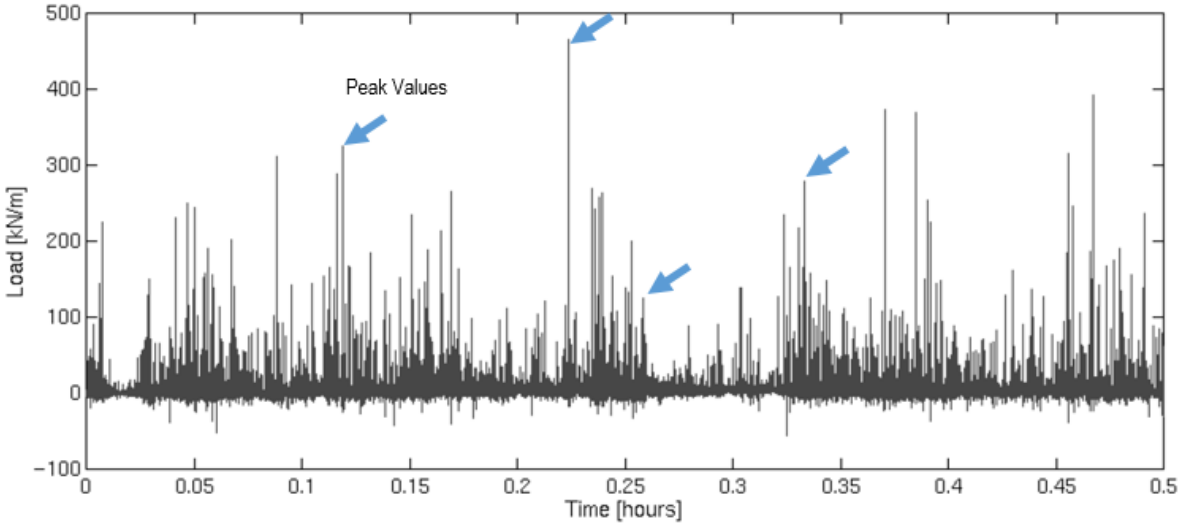

Figure 4. Representation of a random ice load measured on a ship frame (Lensu, 2002).

3.3 Full-scale ice load measurement and processing the data

Full-scale ice load measurement is being used for generating a random and stochastic time series of ice loads. The peak amplitude probability distribution can be defined from the measured ice loads, which then can be employed for the prediction of the probability of the extreme loads for a specific period.

In this method, during the time of the operation of a ship in ice, the ice loads are typically measured with the strain gauges installed in particular frames along the ship hull, i.e., bow, bow shoulder, and the stern shoulder (Kujala, et al., 2014). Then, the measured shear strains are converted into ice loads using Equation (1) (Kujala, et al., 2014).

$$\{F\} = [a] \cdot \{\Delta\gamma\} \tag{1}$$

where a is the stiffness matrix and $\Delta\gamma$ is the measured shear strain change between the two sensors on one frame (Kujala, et al., 2014). The stiffness matrix is a $n * n$ matrix where n corresponds to the number of instrumented frames and can be determined either by the Finite Element Analysis (FEA) or analytical solutions (Kujala, et al., 2014).

3.4 Methods for determining the ice load events

The time history of the ice load comprises a lot of information about the ice loading associated phenomena. Once the measured shear strains are converted into the loads, the ice load events can be specified from the time history if the associated noises, i.e., open water wave loads are excluded from the data. Generally, two different methods could be used for the defining the ice load time histories: the peak amplitude and the time window. These are presented in the following.

3.4.1 Peak amplitude method

The measured loads through the full-scale ice measurements are connected with some noises such as open water wave loads and measurement errors. In order to have a reliable time history of the ice loads, the associated uncertainties must be ignored. To this end, we can easily assume that each individual load peak starts when the force exceeds a specific threshold and ends when it again goes below the threshold (Kotilainen, et al., 2017). This method does not consider a new ice-breaking process when the previous one is still in its disengaging stage (Kotilainen, et al., 2017). To avoid the dependency on the threshold, Rayleigh separator can be used as an additional criterion (Kujala, et al., 2014). As shown in Figure 5, it distinguishes two local maxima, as two separate load peaks if the minimum value of the force in the time series between those two local maxima is less than $100 * r$ percent of the lower maxima, where r is the separator value (Lensu, 2002). The separator value can be determined based on the load peaks, which typically is 0.5 (Lensu, 2002). Once Rayleigh criterion is used, first Rayleigh separated maxima are defined; then the values that exceed the threshold are selected and indexed by their corresponding time instants, which form the peak amplitude time history (Lensu, 2002). The selected indexed maxima constitute the peak amplitude time series (Lensu, 2002). Figure 5 provides an example of using Rayleigh separator for identifying the ice load event

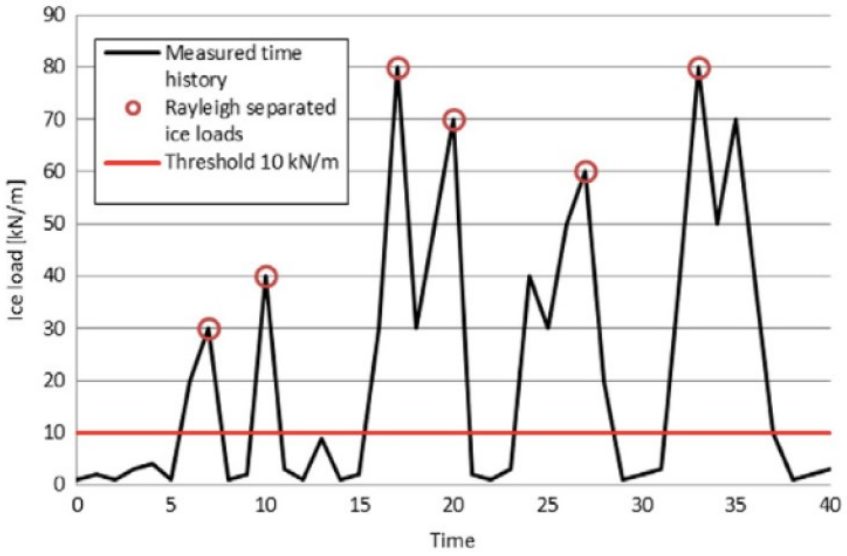

Figure 5. The load peaks separated by the Rayleigh method with the parameter value of 0.5 and the threshold value of 10 kN / m (Kujala, et al., 2014).

3.4.2 Time window method

In the time window method, the time series are divided into the time windows of the same duration, i.e., 10 minutes, 1 hour, or 1 day. Therefore, in each time window the maximum ice load can be identified easily (Suyuthi, et al., 2010). The method is straightforward to implement and has the following benefits (Leira, et al., 2009):

- There is no need for using the threshold value
- It can derive reliable statistical models from the shorter time series

Figure 6 provides an example for determining the ice load measured maxima by using the time window method.

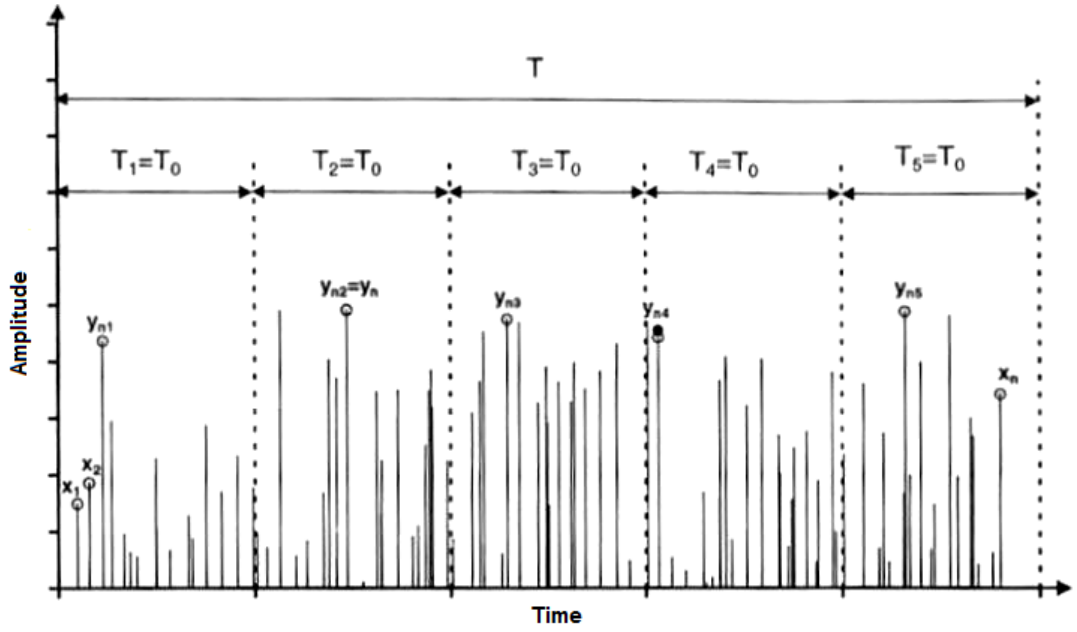

Figure 6. The time window method for determining the ice load measured maxima (Hanninen, et al., 2001).

3.5 Design requirements

Designing a safe ship to protect human life and environment requires knowledge of load carrying capacity of ship structures and extreme forces. Once the resistance of the structure and distribution of the extreme loads are defined, the probability of failure and safety targets (i.e. the probability of exceedance of 10^{-4}) can be specified (Ralph, 2016). The possible failure, as shown in Figure 7, can happen if a single load exceeds the structure capacity (Ralph, 2016). As a result, for the prediction of the extreme loads, the magnitude and the frequency of occurrence of the maximum forces must be taken into account. A well-defined extreme load distribution could benefit the designers as they can avoid an unreliable or overly conservative design as shown in Figure 7.

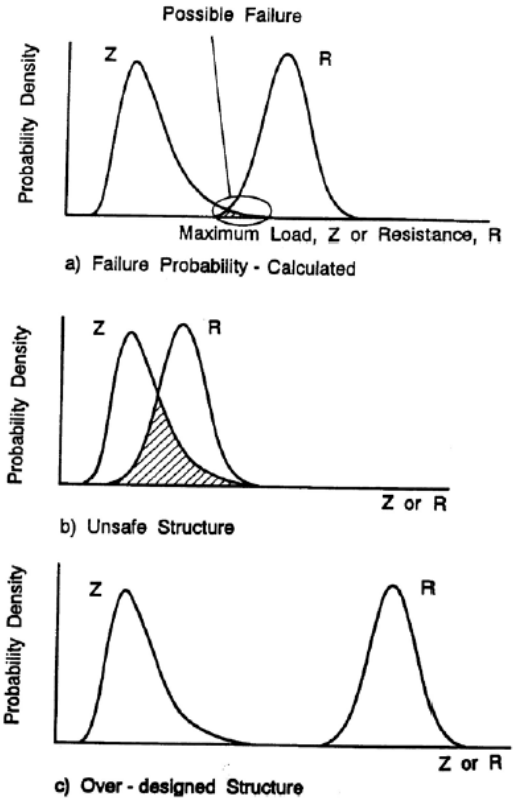

Figure 7. Definition of safe, unreliable, and overly conservative design (Ralph, 2016).

3.6 Statistical approaches for the prediction of the ice loading on hull of a ship

Generally based on the extreme statistics, three different statistical approaches of the exact-method, the approximate method, and the asymptotic formulation are being used for the prediction of the extreme values (Ochi, 1981). The selection of the method for the estimation of extreme values depends on the level of knowledge concerning the initial or parent distribution (Kujala & Vuorio, 1985). The Exact method is the classic application of the extremal analysis for prediction of the extreme loads when the initial distribution of ice loads is known. On the other hand, when the initial distribution in not known, the semi-empirical methods, either the approximate or the Asymptotic formulation, can be used for estimating the ice loads within a specific period. The details for the implementation of these methods are discussed in the following.

3.6.1 Exact-method for the estimations of the extreme values

To define the maximum ice load out of n expected ice impacts in a specific period, the distribution of the extreme loads must be identified from the measured ice loads (Kujala & Vuorio, 1985). A typical measured load distribution is shown in Figure 8. As presented in the figure, the most probable events are concentrated around the peak of the distribution while less likely ones are scattered at the tail (Ralph & Jordaan, 2013). This distribution is the parent distribution of the loads, which can't be utilized directly for defining the design load (Ralph & Jordaan, 2013). As a result, the exposure of ship to the ice crushing failure must be taken into account (Ralph & Jordaan, 2013). Exposure is defined as the expected number of impacts during a given period (or encounter frequency) that typically is being considered one year in design processes (Ralph & Jordaan, 2013).

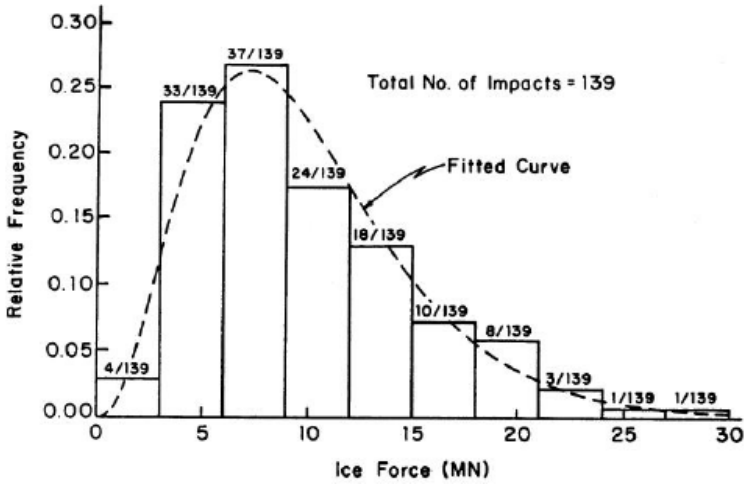

Figure 8. Typical histogram of measured ice loads at the bow frame of a ship encountering the sea ice during a specific period (Ralph & Jordaan, 2013).

The distribution of the extreme value can be defined as Equation (2)

$$Z = \max(X_1, X_2, \dots, X_n) \tag{2}$$

where X_i is the random quantity of the ice load, and n is the number of impacts within a specific duration of time, i.e., one year (Ralph & Jordaan, 2013).

The distribution of extreme values follows its own probability law; and is mathematically related to the initial distribution and frequency of occurrence (Ochi, 1981). The impact of the exposure on the extreme value design distribution is shown in Figure 9 (Jordaan, 2005a). As the number of impacts rises, the design distribution shifts to the right of the initial distribution (Jordaan, 2005a). On the other hand, in the case of rare events, the initial distribution moves to the left of the initial distribution (Jordaan, 2005a). In other words, when the initial distribution is known, the extreme values can be simply estimated by analytical formulation through application of order statistics to the initial probability distribution (Ochi, 1981). In this case, the Probability density Function (PDF), and the Cumulative Distribution Function (CDF) of the extreme value distribution can be defined by Equation (3) and Equation (4) respectively (Jordaan, 2005a).

$$f_Z(z) = n\, F_X^{n-1}(z) f_X(z) \tag{3}$$

$$F_Z(z) = F_X^n(z) \tag{4}$$

where f_X is the PDF, and F_X is the CDF of the ice load, and z is the extreme value of , n , the expected number of impacts (Jordaan, 2005a).

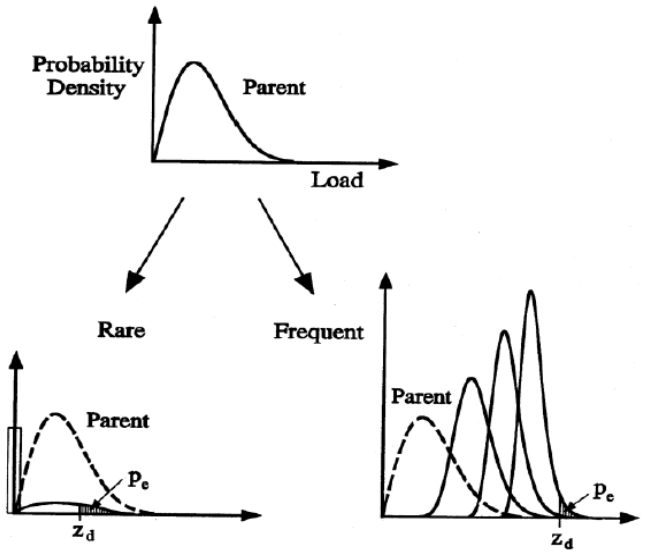

Figure 9. Effect of number of ice interaction on parent distribution of ice loads (Ralph & Jordaan, 2013).

Various statistical properties of extreme values can be obtained from Equation (3) and Equation (4) (Ochi, 1981). For instance, the most probable maximum value to occur in n observation ($\hat{z}_l$) can be defined as the modal value of the probability density function $f_Z(z)$ as shown in Figure 10 (Ochi, 1981).

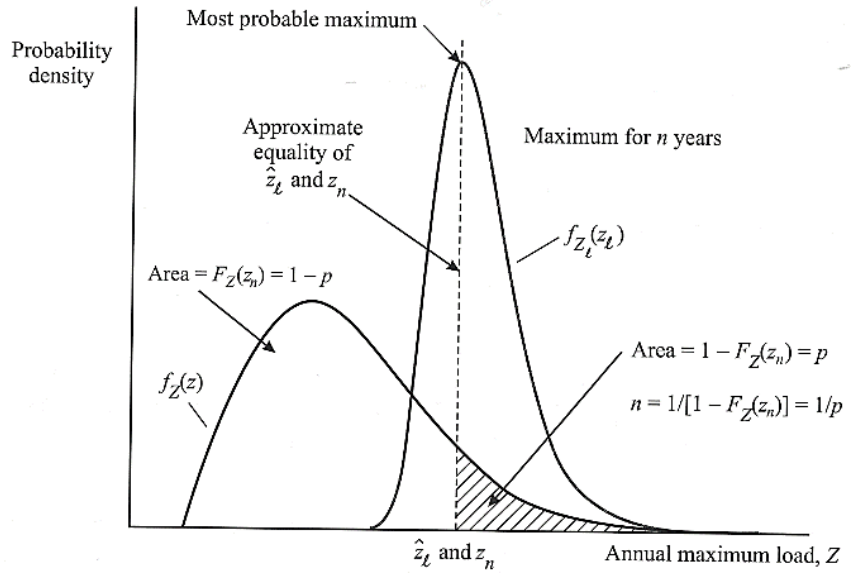

Figure 10. Representation of the most probable maximum (Jordaan, 2005a).

3.6.2 Approximate method for the estimation of the extreme values

Practically, the information for the parent distribution is often not accurately known (Ochi, 1981). However, the function can be constructed from the accumulation of the measured data over an adequate long period without accurate information of the parent distribution (Ochi,

1981). In such cases, the extreme ice load values can be estimated by an approximate method that is applicable to any probability distribution if specific conditions are satisfied (Ochi, 1981). In this respect, the approximated cumulative distribution can be defined by fitting some known probability distribution, i.e., exponential, weibull, and lognormal to the peak amplitude time history (Suyuthi, et al., 2012a). Table 1 lists some of the most commonly used probability distributions for the prediction of ice loads from the full-scale measurements, which are used in this thesis as well.

Table 1. Formula of the PDF and CDF of common probability distributions for modeling the ice loads *(Suyuthi, et al., 2012a).*

Distribution	Cumulative density function, $F\ (x)$	Probability density function, $f\ (x)$
Weibull	$F\ (\mathrm{x}) = 1 - \exp\left\{\left(\frac{x}{\theta}\right)^k\right\}$	$f\ (x) = \frac{k}{\theta}\ (\frac{x}{\theta})^{k-1}\exp\left\{(\frac{x}{\theta})^k\right\}$
Exponential	$F\ (x) = 1 - \exp(-\lambda x)$	$f\ (x) = \lambda \exp(-\lambda x)$
Lognormal	$F(x) = \frac{1}{2} + \frac{1}{2}\mathrm{erf}\left[\frac{lnx - \mu}{\sqrt{2\sigma^2}}\right]$	$f\ (\mathrm{x}) = \frac{1}{x\sqrt{(2\pi\sigma^2)}}\exp\left\{-\frac{(lnx - \mu^2)}{2\sigma^2}\right\}$

3.6.3 Asymptotic Formulation for the estimation of the extreme values

The most likely maximum ice load that a ship will encounter in her lifetime can also be estimated from the full-scale measured maxima when the initial probability distribution is unknown (Ochi, 1981). The measured maxima can be defined as the largest observed ice load during a certain period such as 5 minutes, 30 minutes or even some days. Hence, the time window approach is being used for the determination of the measured maxima for the specific period (Leira, et al., 2009).

The cumulative distribution function of the measured maxima can be determined by using gumbel *I* asymptotic distribution (Kujala, 1994). The significant feature of the asymptotic distribution is that the parent distribution tends asymptotically to an extreme distribution of the same type as number of impacts (n) increases (Ochi, 1981). Figure 11 represents a typical extrapolation of the full-scale measured maximum ice by means of the PDF of the gumbel *I* probability distribution (Riska & Kämäräinen, 2012).

The mean, $E[z]$, and variance, $Var[z]$, can be computed form the data, thus the cumulative distribution function of the extreme value could be expressed as

$$F_Z(z) = e^{-e^{-\alpha(z-u)}} \tag{5}$$

$$\alpha = \frac{\pi/\sqrt{6}}{\sqrt{Var[z]}} \tag{6}$$

$$u = E[z] - \frac{\gamma}{\alpha} \tag{7}$$

Where α and u are gumbel distribution parameters, and γ is the Euler-Mascheroni constant; equals to 0.5772 (Ochi, 1981) (Kujala, 1994).

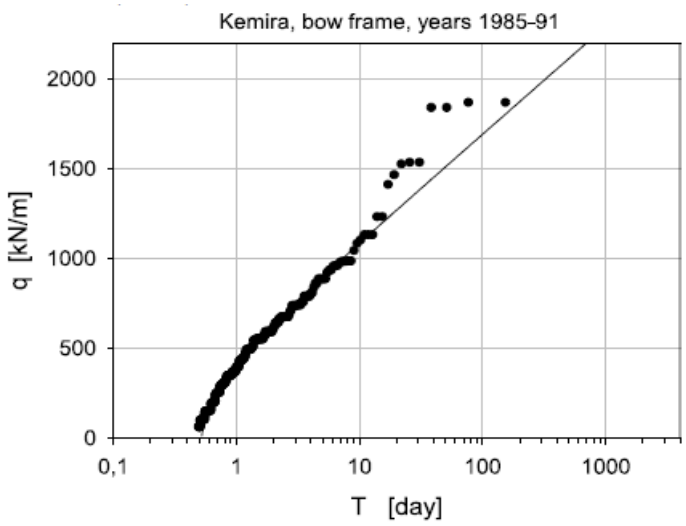

Figure 11. Extrapolation of the full-scale measured maximum ice load at the bow frame, using gumbel I PDF (Riska & Kämäräinen, 2012).

3.7 Design strategy and return period

The determination of appropriate design loads having low probability of occurrence is one of the key criteria for engineers, to design safe structures (Ralph, 2016). The design strategy (limit state) refers to a specific level of the ice load acting on structures, which is based on PDF of the annual maxima that corresponds to the target probability of exceedance, P_e (Ralph, 2016). One strategy may reflect design for the annual probability of the exceedance of 10^{-2} which accounts for one extreme level ice event (ELIE) in one hundred years (Ralph & Jordaan, 2013) (ISO, 2010). The consequence of exceedance of this load level may be some minor localized failure on the structure, i.e., dents but no major safety issues (Ralph & Jordaan, 2013). The other strategy may follow the design for the annual probability of the exceedance of 10^{-4} which considers one abnormal level ice event (ALIE) in ten thousand years (Ralph & Jordaan, 2013) (ISO, 2010). Exceedance of a load level of this kind can end up with the loss of human life or severe environmental footprints, i.e., oil spills due to collision of ships (Ralph & Jordaan, 2013). Figure 12 represents the relationship between the PDF and the CDF of the measured annual maxima, and the probability of exccedance of the specific load level (P_e).

$f_Z(z) = \text{PDF}$

$F_Z(z) = \Pr(Z \leq z) = \text{CDF}$

$P_e = 1 - F_Z(z)$

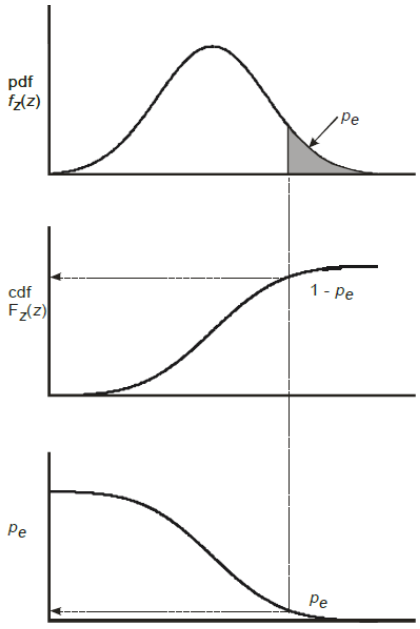

Figure 12. Definition of the probability of exceedance (P_e), (Ralph & Jordaan, 2013).

The return period is another important parameter for the determination of the design loads. It is the number of realizations that are needed to obtain the characteristic largest value, z_n (Vuorio, et al., 1978). The Equation (8) represents the relationship between the expected number of peak amplitudes and the initial cumulative distributions, which is valid for all exponential distribution types for large number of observation, n (Kujala & Vuorio, 1985). In other words, $1 - F_Z(z_n)$ is the probability of exceedance of the characteristic largest value, and n is the return period in terms of number of events per specific period, i.e., one year (Castillo, 1988).

$$n = \frac{1}{1 - F_Z(z_n)} \tag{8}$$

3.8 Global and local design

Analysis of ice pressures data of various full-scale measurements by (Sanderson, 1988), (Frederking, et al., 1990), and (Daley, et al., 1990) revealed the fact that the distribution of the ice pressure in the area of ship-ice interaction is nonlinear. This may occur due to the flaking process, which reduces the nominal contact area and consequently leave a line-like feature in the area of interaction, where a high ice pressure is acting (Riska, 2010). The total force is transmitted into the hull of the ship through the High Pressure Zones (HPZs) existing in the local contact area (Ralph, 2016). Accordingly, for approximating the global and local design pressures, the variation of the ice pressure on the nominal and local contact area must be accounted (Ralph, 2016). Hence, details are discussed in the following.

3.8.1 Global and local design areas

For the global design, we are interested in approximating the maximum global pressure on a ship's hull during a collision or ramming event. Thus, the global force and the global contact area are the only required input data of global design (Ralph, 2016). As the ship reaches the ice floe, it starts to penetrate into the ice and leaves the imprint of the bow at the ice feature (Ralph, 2016). Figure 13 shows the contact area during a ramming process. The global contact area, also termed nominal contact area, as shown in Figure 14, is simply the area of the imprint of

the bow into the ice feature without any reduction due to the spalls (fractured ice) (Ralph, 2016). The global load starts to grow as the penetration process is initiated; and meet the peak as the ship reaches the maximum penetration (Ralph, 2016).

On the other hand, for the local design, we are concerned about the maximum ice pressure on a particular area of the structure, i.e., a plate between the frames (Ralph, 2016). Furthermore, in contrast to the global forces, HPZs can occur any time during the interaction and vary spatially across the global contact area as shown in Figure 14 (Ralph, 2016).

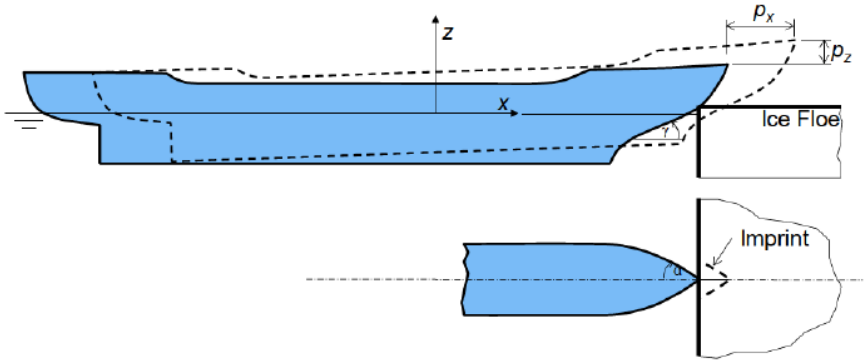

Figure 13. The contact area during a ramming process (Ralph, 2016).

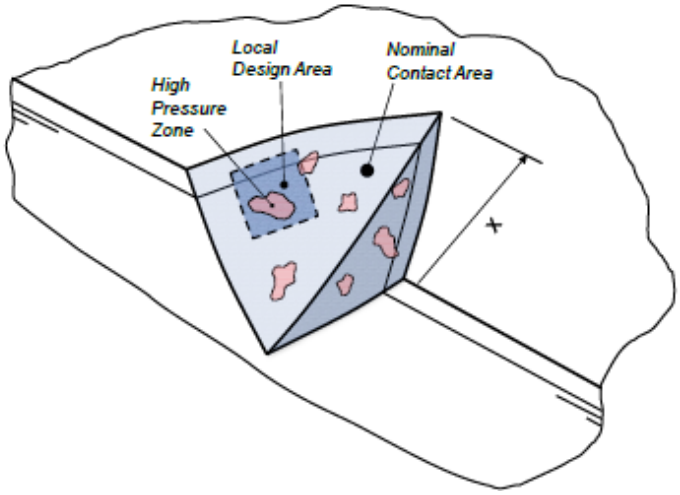

Figure 14. The global and local design area (Ralph & Jordaan, 2013).

3.8.2 Ice pressure data

There are two different methods for measuring the ice pressure on the hull of a ship termed as the exterior measurement and interior measurement (Daley, 2007). The exterior measurement determines the average ice pressure by dividing the total ice force into the nominal contact area (Daley, 2007). On the other hand, for analyzing the actual ice pressure and the actual contact area, the ice pressure has to be measured directly on the surface of the structure; this called the interior measurement (Daley, 2007).

Generally, there are three different approaches for defining the actual pressure and the actual contact area (Daley, 2004). First, the nominal pressure can be obtained if the measured total force is divided by the nominal area as shown in Figure 15 (a) (Daley, 2004). This does not provide us with any information about local pressures (Daley, 2004). Second, as shown in Figure 15 (b), the true pressure distribution can be determined by performing a continuous

measurement of the pressure over the whole surface which is not practical in reality (Daley, 2004). Third, the actual pressure can be determined well if the pressure is being measured on the local panels though there are some uncertainties such as the effect of the pressures on the neighboring panels are associated with the measured data (Daley, 2004). The third approach as represented in Figure 15 (c), is the common method for the evaluation of the local pressures (Daley, 2004).

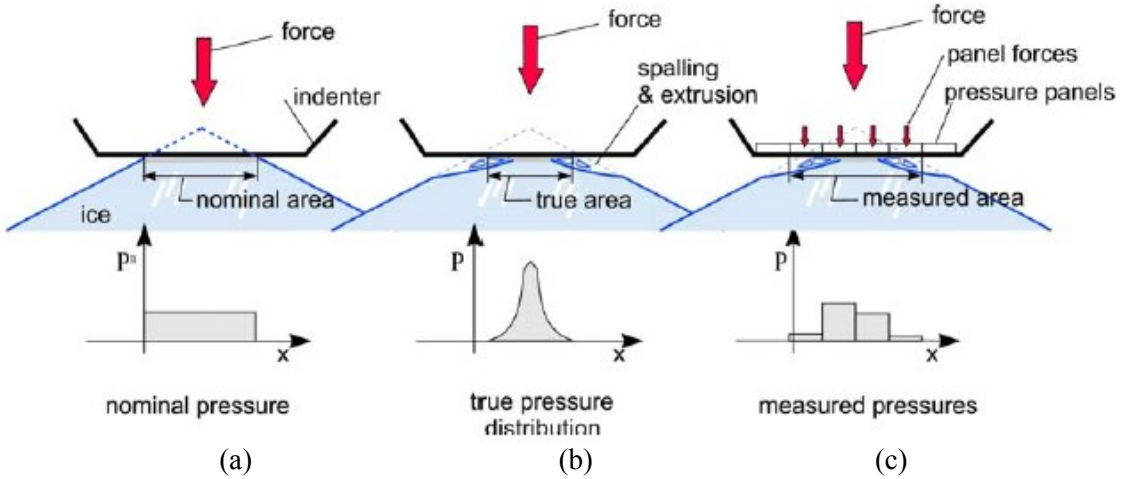

Figure 15. Representation of different approaches for measuring the pressure and the actual area (Daley, 2004).

3.8.3 Pressure-area relationship

In order to study the distribution of the ice pressure in a particular contact area, many full-scale and laboratory measurements have been conducted by (Sanderson, 1988), (Frederking, et al., 1990), (Daley, et al., 1990), and (Riska, 2010). These studies have shown the variation of the ice pressure within the contact area to be non-uniform, varying considerably from panel to panel (Daley, 2007). As a result, the concept of the pressure-area relationship has been developed to describe the variation of ice pressure versus the area (Daley, 2007).

Pressure-area models are being used to define both global and local ice pressure on the hull of the ships and fixed structures (Daley, 2007). There are two different pressure-area relationships. The *process* pressure-area model defines how the mean pressure changes as a function of the global contact area during an impact; such as a ship ramming into a massive ice feature (Daley, 2007). This model might be used for the calculation of the global pressure (Daley, 2007). On the other hand, the *spatial* pressure-area model defines that how the local peak pressures during an impact relate to the area of the sub-panels of different sizes inside the entire contact area. The *spatial* pressure-area model is commonly used to define the design pressure on local structures, such as plate between the frames. (Frederking, 1999) (Daley, 2004)

3.8.4 Estimation of the global pressure

According to the result of the study of the full-scale measured ice pressures, Frederking (1999) reported a decreasing trend in both models of the process and spatial pressure-area. It means that the ice pressure decreases as the as the contact area increases. As a result, the global pressure-area relationship can be modeled using the Equation (9) (Jordaan, et al., 1993) (Jordaan, et al., 2005b)

$$P = CA^D \tag{9}$$

The global force can also be defined based on the nominal pressure and nominal contact area as given in the Equation (10) (Jordaan, et al., 2005b).

$$F = CA^{D+1} \tag{10}$$

where A is the nominal contact area, and the parameters of C_p and D_p are constant coefficients. These constant coefficients could be varied for different ice condition scenarios (Ralph, 2016).

3.8.5 Estimation of the local pressure with the event-maximum method

The local pressure can arise either from the collision with large ice features in the bow area or other ice interactions at the shoulder of a ship (Ralph, 2016). The local pressure can cause significant localized damages on the area of interaction, which may occur due to the existence of HPZs within the nominal contact area (Kendrick & Daley, 2011). Hence, the local design for the specific areas of the structure, i.e., plate between the frames must be based on the maximum local pressure during a specific time interval or event (Taylor, et al., 2010). The maximum local pressures, corresponding to a specific probability of exceedance, i.e., 10^{-2}, can be defined with the event maximum method, which is developed based on the extreme statistics by Jordaan et al (1993).

The event maximum method implies that the peak pressures on a specific contact area can be represented by fitting a linear line into the tail of the sorted pressures, which are plotted versus the natural logarithm of the probability of exceedance (P_e) (Jordaan, et al., 2005b). The fitted line is assumed to agree with an exponential distribution as given in the Equation (11) (Jordaan, et al., 2005b).

$$F_X(x) = 1 - \exp\left(-\frac{x - x_0}{\alpha}\right) \tag{11}$$

where parameters of x_0 and α are constant values for the specific area. The parameter x is a random event that defines the local pressure (Jordaan, et al., 2005b). As shown in Figure 16, parameter α is the inverse slope of the best fitting line and parameter x_0 is the intercept of the line with the abscissa (x axis) (Jordaan, et al., 2005b).

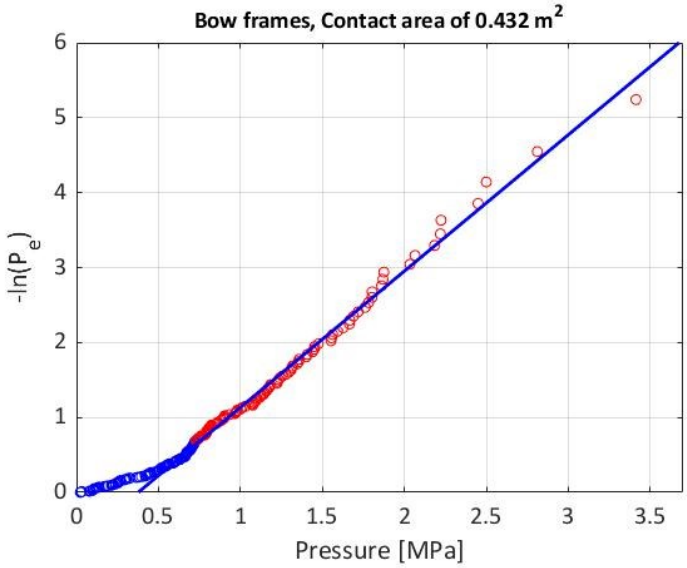

Figure 16. Representation of best fitting line (blue line) into ten-minute maximum ice pressures at the tail (red dots), the contact area of 0.432 m^2 of two frames at the bow of S.A. Agulhas II, Antarctica 2031-2014. Blue dots are ten-minute maximum ice pressures smaller than the median.

The maximum pressure, Z, that encountering to a specific panel during a specific period is defined as

$$Z = \max(X_1, X_2, \dots, X_N) \tag{12}$$

where X_i is the random quantity represents pressure and N is the total number of impacts (Jordaan, et al., 1993). Applying the extreme statistics to the Equation (11), defines the cumulative distribution function of the maximum local ice pressure for a particular area as

$$F_Z(z) = \exp\left\{-\exp\left(-\frac{(z - x_0 - x_1)}{\alpha}\right)\right\} \tag{13}$$

where, $x_1 = \alpha(ln\mu)$. The parameter μ denotes the exposure, which will be explained in Section 3.8.6, and the parameter α represents the pressure decrease with the area (Jordaan, et al., 2005b). In addition, the relationship between α and area can be defined as given in the Equation (14) (Jordaan, et al., 1993).

$$\alpha = Ca^D \tag{14}$$

The parameter a is the local contact area and parameters C and D are constant coefficients, which are connected with the ice type and ice condition (Jordaan, et al., 1993).

The parameter of x_0 given in Equation (13), is also a function of the area corresponding to the ice condition scenario (Taylor, et al., 2010). Considering the α, x_0, and the exposure (μ), the maximum local pressure, z_e, corresponding to a specific probability of exceedance, i.e., 10^{-2} can be determined as given in the Equation (15) (Taylor, et al., 2010).

$$z_e = x_0 + \alpha\{-\ln[-\ln F_Z(z_e)] + \ln\mu\} \tag{15}$$

3.8.6 Exposure

The exposure can be expressed as the proportion of total number of interactions, presenting the direct panel hits per specific period. The exposure can be defined from Equation (16).

$$\mu = r.v.\frac{t}{t_k} \tag{16}$$

where the parameter v denotes the expected number of ice interactions in a specific period, and the parameter r represents the proportion of interaction events obtained from direct hits on a specific panel. The direct hit is an ice interaction on a particular panel with the pressure amplitude greater than zero. Parameter t denotes the average duration of the ice interactions for a specific ice condition scenario, and t_k is the average duration of the ice interactions associated with α-area curve presented by Jordaan et al. (1993). (Taylor, et al., 2010).

Another important aspect of the exposure is the location of the panels on the hull of the ship. For instance, panels that are located at the bow, are more prone to experience the ice pressure than other panels to the side or stern. For designing an ice class ship, typically the above-mentioned issue is taken into account, applying the hull area factors (Taylor, et al., 2010) (IACS, 2016).

3.8.7 Estimation of the expected number of impacts

The expected number of ice interactions per specific period, i.e., 1 year can be defined using Equation (17).

$$v = f * D_t \tag{17}$$

where, f is the impact frequency, i.e., per nautical mile (NM), and D_t is the total distance that ship operates in ice. The frequency of the impacts can be defined based on full-scale measurements and the total distance can be either defined from ship ice trial data or simulation (Bergström, et al., 2016).

4 Measurements and data processing

4.1 Full-scale ice load measurements

To obtain additional full-scale ice load measurements, a full-scale ice experiment was conducted on board of S.A Agulhas II in the Antarctica. The voyage was started on 28th of the November 2013 and finished on 12th of the February 2014. During the ice trial, extensive measurements were carried out for different ice conditions. The measurements comprise the measurement of the ice loads on different areas of the hull of the ship, the visual observation of the ice condition, and the measurement of the ice thickness. The ice thickness data used for this study are recorded based on visual observations. The details of this full-scale measurements are reported by Kujala et al. (2014). Figure 17 represents the route that ship was operating in Antarctica. Figure 18 presents the ship speed during the whole voyage.

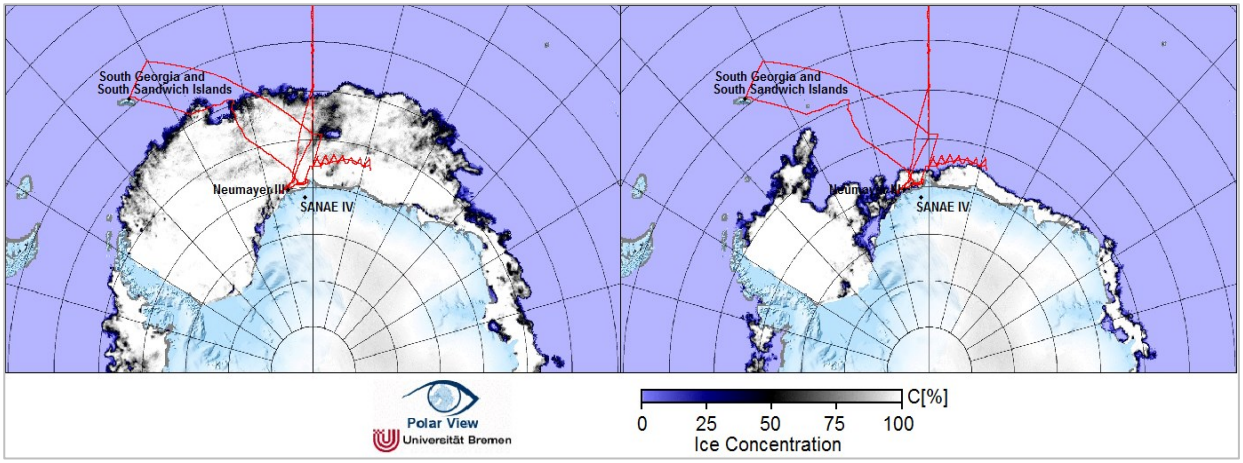

Figure 17. The voyage route and the sea-ice extent in Antarctica on (a) December 6,2013, and (b) February 2, 2014 (Kotilainen, et al., 2018).

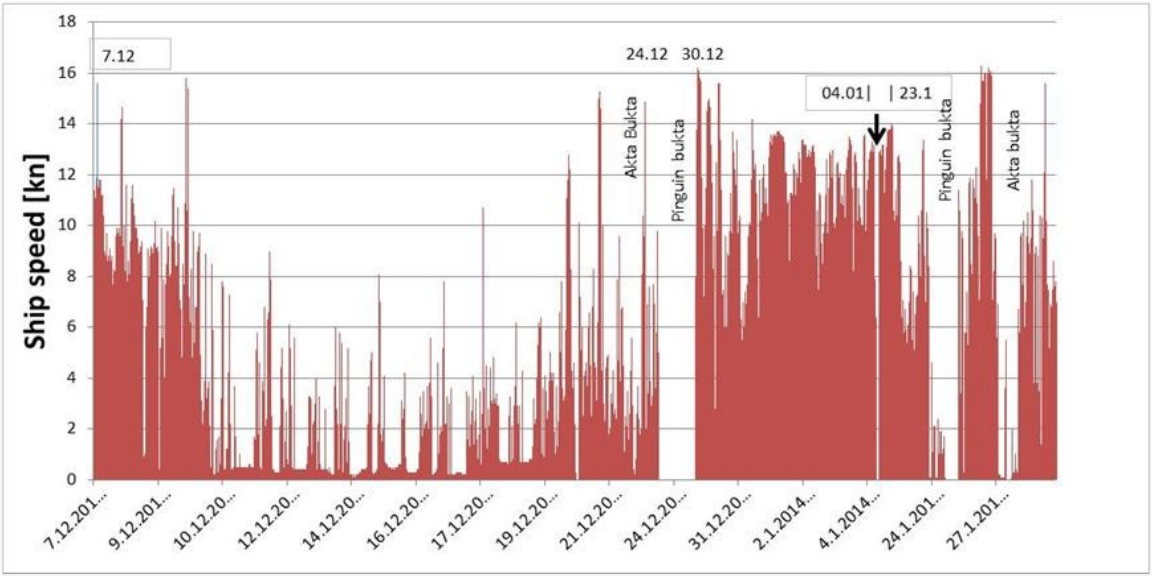

Figure 18. 10-minutes average speed in knots. Time is in UTC+0h (Kujala, et al., 2014).

4.2 Ship main dimensions and instrumentation set up

S.A. Agulhas II was built by STX Finland in the Rauma shipyard in April 2012. The ship has Polar ice class PC 5. The strength of the hull of ship is in accordance with DNV ICE-10. The main dimensions and parameters of the ship are listed in Table 2. The ship is operating with the propulsion power of 9 MW. (Kujala, et al., 2014)

Table 2. The main dimensions and parameters of the S.A. Agulhas II

Length, overall [m]	135.0
Length, between perpendiculars [m]	121.8
Breadth [m]	21.7
Draught, design [m]	7.65
Deadweight at design draught [t]	5,000
Service speed [kn]	14.0

The hull of the ship is instrumented with the strain gauges at two frames at the bow (#134+400, and #134), three frames at the bow shoulder (#113, #112+400, and #112), and four frames at the stern shoulder (#41, #40+400, #40, and #39+400) for measuring the ice loads. Furthermore, ten strain gauges were installed on the hull plating for strain measurements – two gauges at the bow, two at the bow shoulder, and six at the stern shoulder. Figure 19 represents setup of the strain gauges on the hull of S.A. Agulhas II.

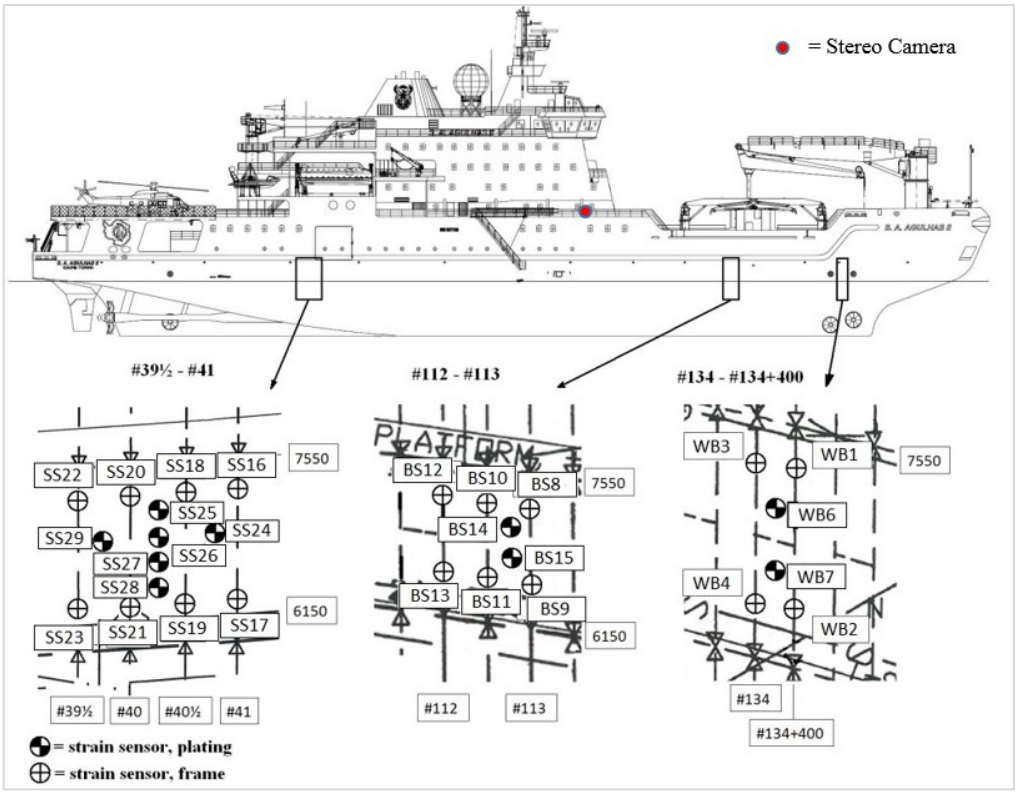

Figure 19. Representation of the setup of the strain gauges on the hull of the S.A. Agulhas II.

4.3 Determination of the ice load time history

In order to define the ice loads acting on ship frames and hull plating, the differences of shear strain between the upper and lower strain gauges mounted on the frames were measured with the frequency of 200 Hz during the whole voyage. In addition, the shear strains occurring in the hull plating have been measured with one directional strain gauges. Thereafter, the measured shear strains on each frame have been converted into ice loads time history by means of the stiffness matrix; using Equation (1). The stiffness matrix for the bow (a_b), was obtained from the FEA. Furthermore, the stiffness matrices for the bow shoulder (a_{bs}) and the stern shoulder (a_{ss}) were defined from the calibration pull. The stiffness matrices for the bow, bow shoulder and the stern shoulder are provided in Appendix A.

5 Results and analysis

5.1 Determination of frames of interest

For studying the maximum local pressures on different locations of the hull, the time history of the ice loads on nine different frames and their combinations are defined. For that purpose, frames #134+400, #134, and their combinations are studied at the bow. In addition, frames # 113, #112 ½ , #112 and their combinations are analyzed at the bow shoulder. Moreover, frames # 41, #40 ½ , #40, #39 ½ and their combinations are studied at the stern shoulder. Figure 20 shows the graphical representation for combinations of the different frames.

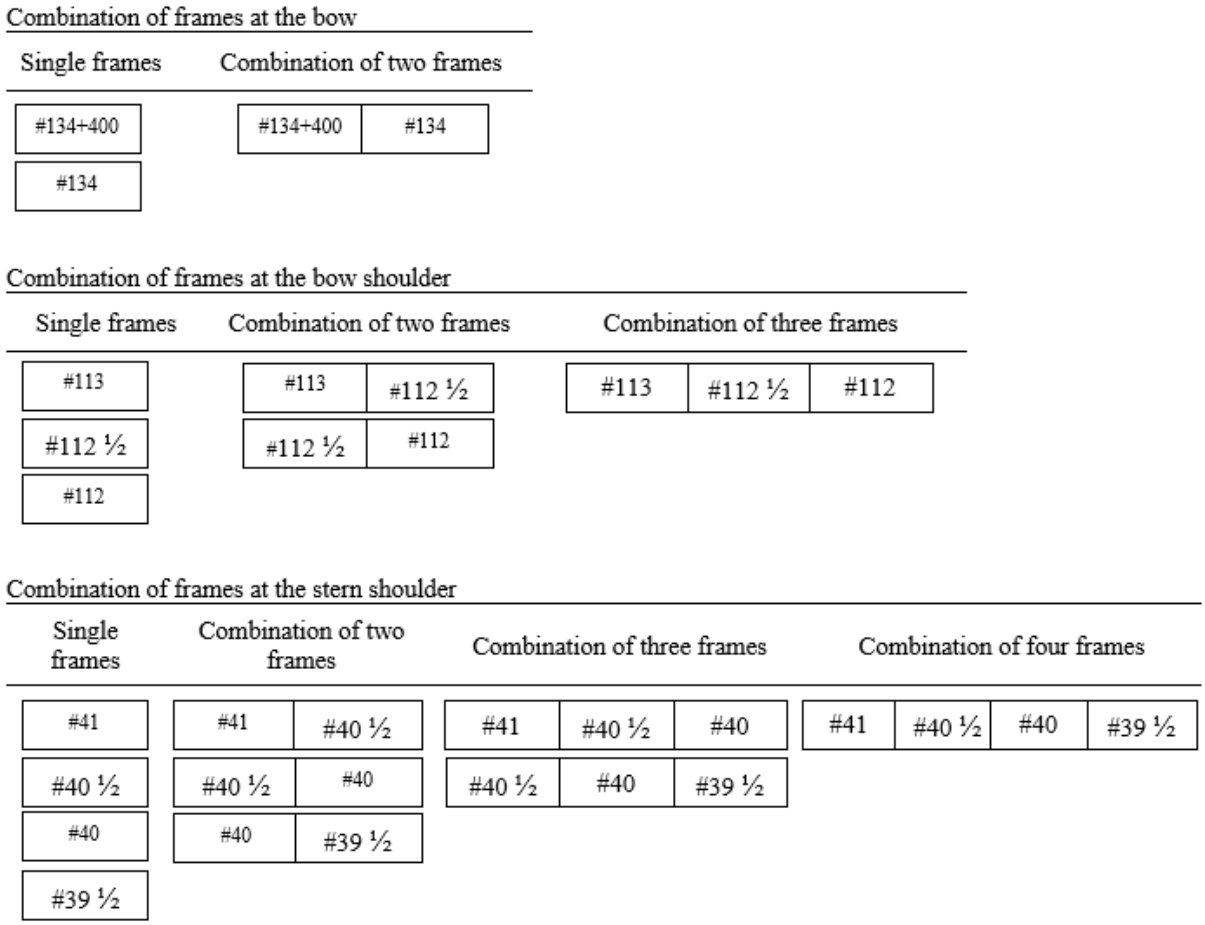

Figure 20. Combination of frames at different locations of hull

5.2 Determination of the ice load events

In order to define the ice loads on combined frames, the loads transferring between the frames needs to be taken into consideration. For that purpose, the ice loads on adjacent frames at each time stamp (instant) are added. Then, for filtering the potential noises and effect of open water, the threshold of 10 kN is applied to the data. Finally, ten-minute maximum ice loads for individual frames and their combinations are defined. Figure 21 provides an example that shows how a particular load event typically transfers from one frame to the neighboring ones.

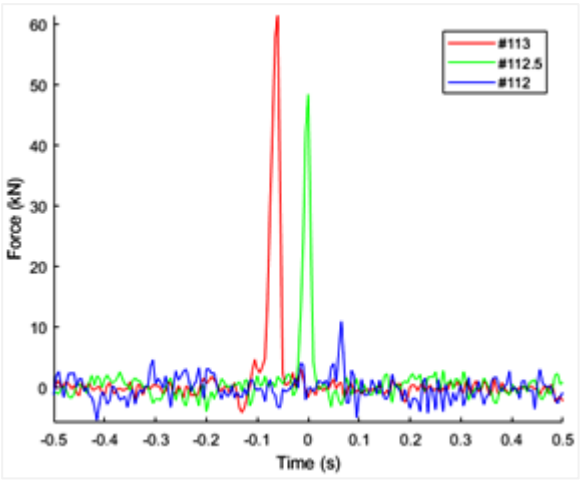

Figure 21.The process of single load event traveling to the adjacent frames at the bow shoulder of Agulhas II.

Figure 22 represents an example of ten-minute maximum ice loads histogram on two frames at the bow. The ten-minute maximum ice loads histograms for other frames combinations are presented in Appendix B.

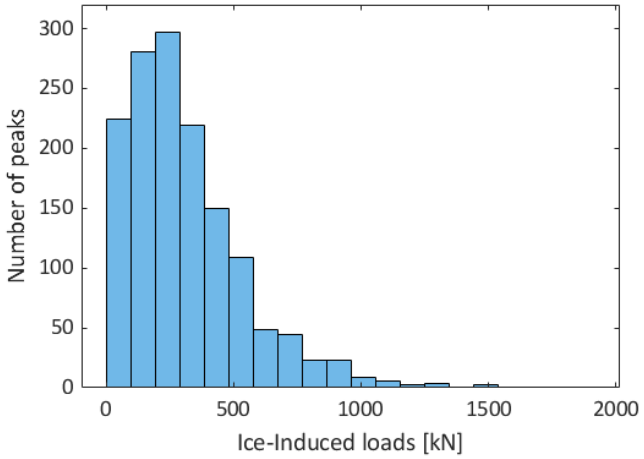

Figure 22. Ten-minute maximum ice loads on two frames at the bow (#134, and #134+400). , Threshold 10 kN is applied. Mean value is 312.61 kN and standard deviation is 240.85 kN.

5.3 Ice condition classification and frequency of ice impacts

As the local ice pressure measurements were not available, the study aims to define the ice pressures from the measured ice loads. For that purpose, the maximum ice load for a specific period is assumed to be connected with the maximum ice thickness. Hence, the maximum ice thickness and corresponding ten-minute maximum ice load at different area of hull are determined based on ten-minute intervals visual observations. Furthermore, the ice thicknesses average of 2 meter and the standard deviation of 0.73 meter are obtained from the maximum ice thicknesses of ten-minute periods. Figure 23 represents the distribution of maximum ice thicknesses, which is obtained from the ten-minute period visual observations.

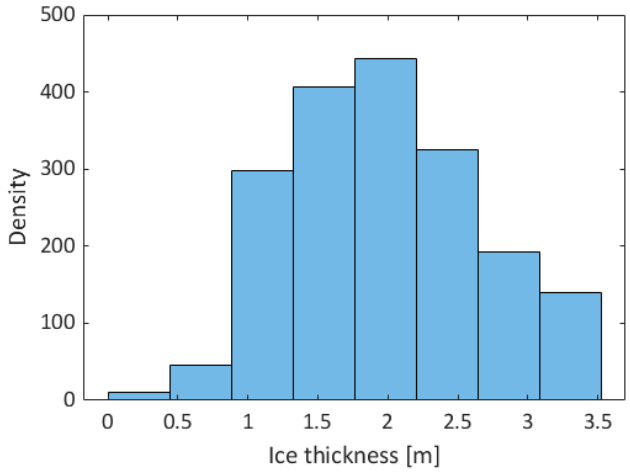

Figure 23. Histogram of maximum ice thicknesses of ten-minute periods, mean 2 meters and standard deviation 0.73 meter.

The frequency of the ice loads is the other required parameter for the approximation of the maximum local ice pressures. In order to define number of the ice load events per nautical miles (NM), the following steps are performed. First, the observed ice condition data are categorized into thick, medium, and thin First-Year Ice (FYI) in accordance with Table 3. Second, the total distance that ship was operating in each ice condition is determined based on the navigation data of ship through the whole voyage. Third, the total number of ten-minute maximum ice loads at the bow, bow shoulder, and the stern shoulder are defined from the full-scale measured ice loads during 500 hours (h) operating in ice. Finally, the average numbers of ten-minute maximum ice loads per nautical mile at different areas of the hull in each ice condition are defined as presented in Table 4.

Table 3. Ice condition classification based on the ice thickness (m) *(WMO, 2014)*

	Thin first- year ice	Medium first- year ice	Thick first- year ice
Ice thickness (t)	$t \leq 0.7$	$0.7 < t \leq 1.2$	$t > 1.2$

The frequency of the ice impacts at different areas of hull of ship are defined according to the information in Table 4 and using Equation (17). The frequency of the ten-minute maximum ice loads per nautical mile at the bow, bow shoulder, and the stern shoulder are equal to 0.97, 0.45, and 0.58 respectively.

Table 4. Analysis of the ship operation data in different ice conditions through the whole voyage

	Thin FYI	Medium FYI	Thick FYI	Voyage
Total distance [NM]	145	507	836	1488
Time of operation [h]	146	113	241	500
Number of ten-minute maximum at the bow	29	265	1154	1448
Number of ten-minute maximum at the bow shoulder	2	69	604	675
Number of ten-minute maximum at the stern shoulder	1	38	839	878

5.4 Calculation of the ice pressures from the full-scale ice loads

In order to convert the measured ice load into the local ice pressure, the actual contact area must be defined. Hence, in accordance with Finnish-Swedish Ice Class Rules (FSICR) for 1A super ice class, the load height (H) is assumed as 30% of the maximum ice thickness, corresponding to each ten-minute maximum ice load. Moreover, the load length (L) is considered as ship frame spacing at the location of interest (0.4 meter). Thus, the actual contact areas (A_l) and the local ice pressures(P_l) are being defined from Equation (18) and Equation (19) respectively.

$$A_l = L * H \tag{18}$$

$$P_l = \frac{F_{max}}{A_l} \tag{19}$$

where F_{max} is the maximum of the total force at the frame(s) of interest within specific period , i.e., ten-minute maximum ice loads on two bow frames. Figure 24 represents an example of ten-minute maximum ice pressures histogram on two frames at the bow. The ten-minute maximum ice pressures histograms for other frames combinations are presented in Appendix C.

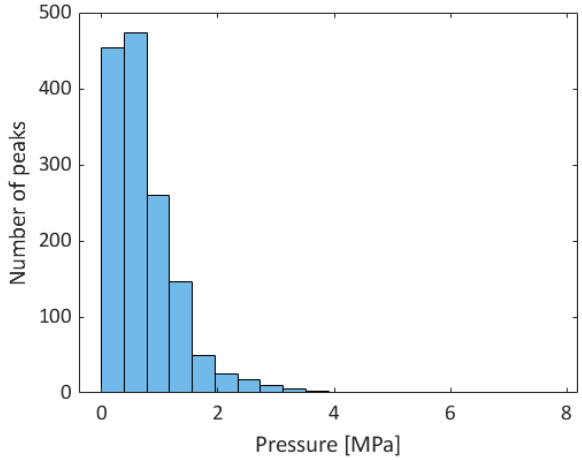

Figure 24. Distribution of ten-minute maxima local ice pressure at two bow frames. Mean value is 0.7352 MPa and standard deviation is 0.6190 MPa

5.5 Evaluation of the maximum local pressure using the event-maximum method

In the current study, the event maximum method is being used for estimating the maximum local ice pressures on the bow, bow shoulder, and the stern shoulder of S.A. Agulhas II.

5.5.1 Peak pressure versus contact area

For estimating the maximum local pressures, the ice pressures on a specific contact area is required. For that purpose, ten-minute maximum ice pressures are categorized according to the area of ship-ice interaction at the bow, bow shoulder, and the stern shoulder for different frames combinations. Figure 25 shows an example of ice pressures versus the contact area on two frames at the bow. The results for other frames combinations are presented in Appendix D.

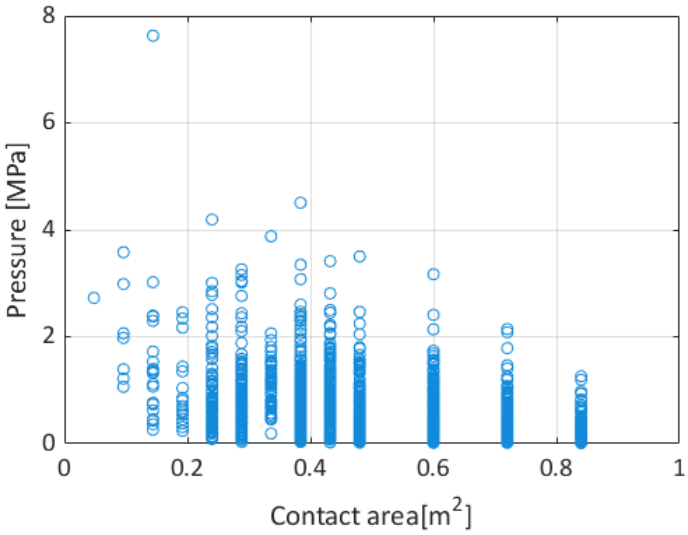

Figure 25. Ice pressures vs different contact areas at two frames at the bow (frames # 134+400 and #134)

5.5.2 Determination of the best fitting line into the pressures at the tail

The event-maximum method assumes that the local ice pressures can be obtained from the linear fits into the pressures at the tail, which follows the exponential distribution. Hence, ten-minute maximum ice pressures greater than the median are accounted as the pressures at the tail. Furthermore, a linear line, as given in Equation (20), is fitted into these pressures.

$$F_X(x) = ax + b \tag{20}$$

Where a and b are parameters of the best fitting line.

The lack of appropriate number of ice pressures in some contact areas resulted in unacceptable fits with high level of uncertainty. As a result, for minimizing the uncertainty, the contact areas with less than 40 data points at the bow were ignored. Similarly, at the bow shoulder and the stern shoulder the contact areas with less than 20 data points were excluded. As an example, Figure 26 presents the obtained best fitting lines for the combination of two frames at the bow. The red points indicate the pressures at the tail and the blue ones represent the pressures smaller than the median. As shown in Figure 26, in most cases the selection of the pressures greater than the median provides good fits. The obtained best fitting lines for other frames combinations are presented in Appendix D.

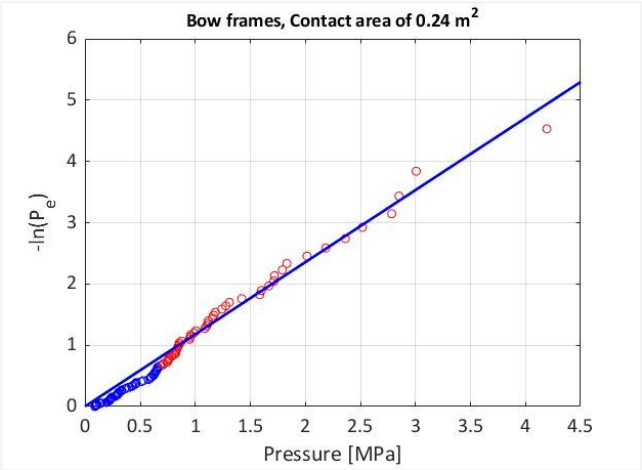
Bow frames, Contact area of 0.24 m2
-ln(Pe)
Pressure [MPa]

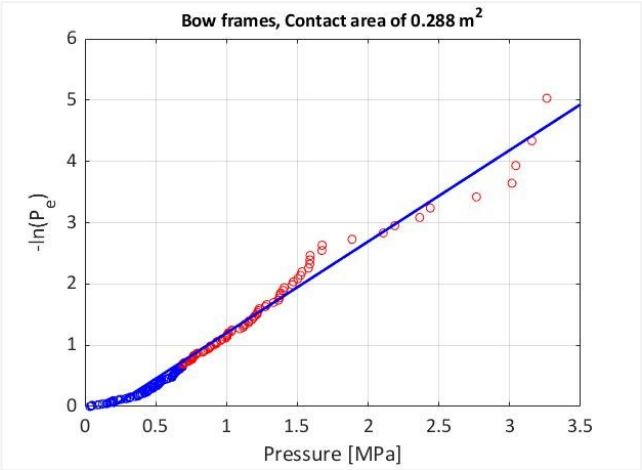
Bow frames, Contact area of 0.288 m2
-ln(Pe)
Pressure [MPa]

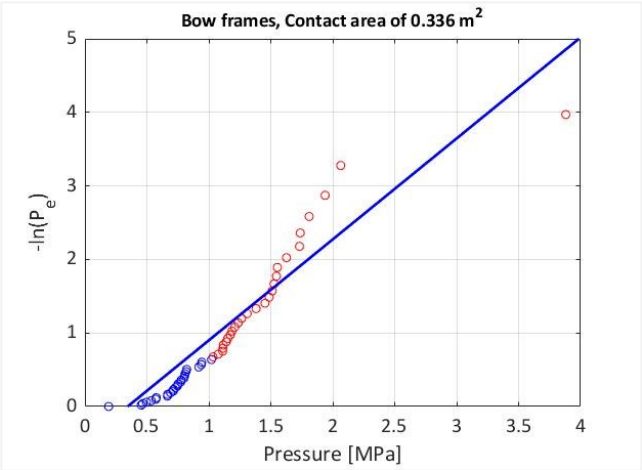
Bow frames, Contact area of 0.336 m2
-ln(Pe)
Pressure [MPa]

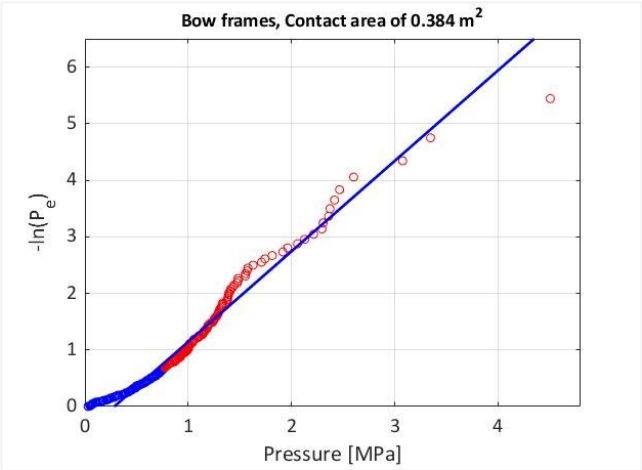
Bow frames, Contact area of 0.384 m2
-ln(Pe)
Pressure [MPa]

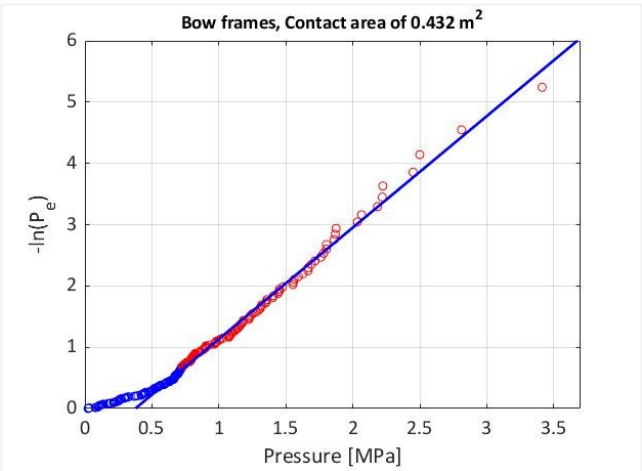
Bow frames, Contact area of 0.432 m2
-ln(Pe)
Pressure [MPa]

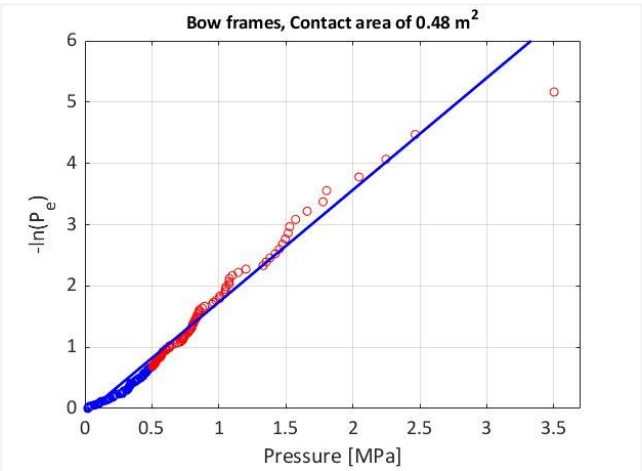
Bow frames, Contact area of 0.48 m2
-ln(Pe)
Pressure [MPa]

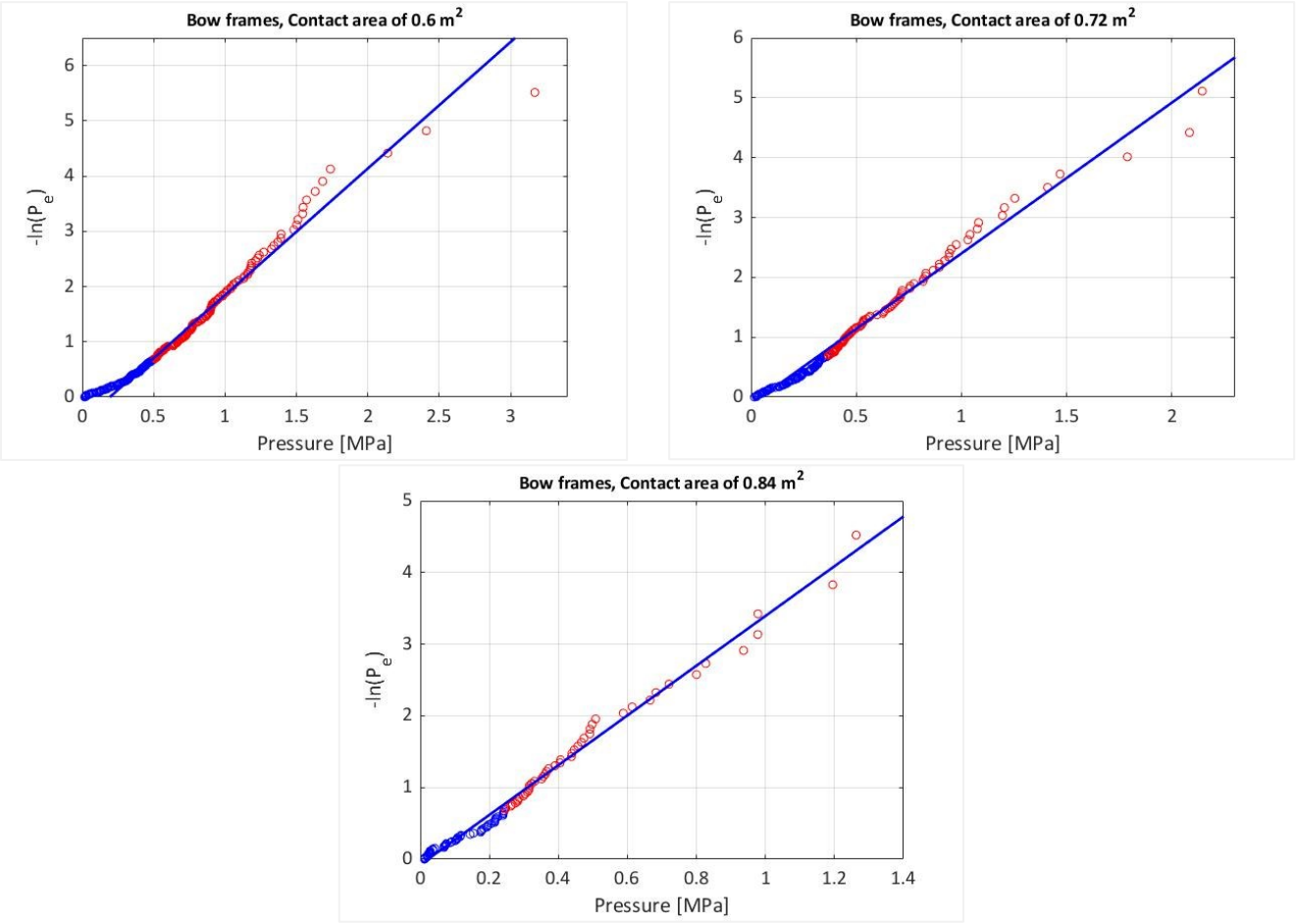

Figure 26. Best fitting line into the ten-minute maximum pressures at the tail on bow frames. Red points indicate the pressures at the tail and blue ones represent the pressures smaller than the median

5.5.3 Determination of α and x_0

For modeling the α-area relationship, the best fitting line of the measured ice peak pressures is assumed to follow the exponential distribution as given in Equation (11). Consequently, the parameters of α and x_0 are defined, using the Equation (21) and Equation (22).

$$\alpha = 1/a \tag{21}$$

$$x_0 = -\alpha * b \tag{22}$$

Where, parameter of α is the inverse slope of the best fitting line and a function of contact area, and x_0 is the x-intercept of that line. Furthermore, for modeling the α-area relationship at different locations of the hull, the curve given in Equation (14) is fitted to the α versus the area. As an example, Figure 27 presents the α-area curve for the combination of two frames at the bow. In addition, the parameters x_0 at different location of the hull are defined based on the parameters of the best fitting lines to the ten-minute maximum peak pressures. As an example, Figure 28 shows variation of x_0 versus different contact areas for the combination of two frames at the bow. The α-area curves, and the x_0 versus contact areas graphs for other frames combinations are presented in Appendix D.

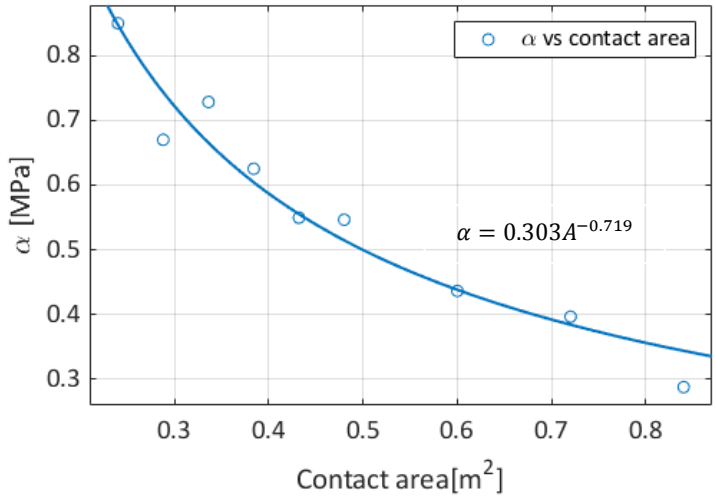

Figure 27. α-area curve for two frames at the bow. Curve equation, $\alpha = 0.303x^{-0.719}$. R-Square value 0.9421

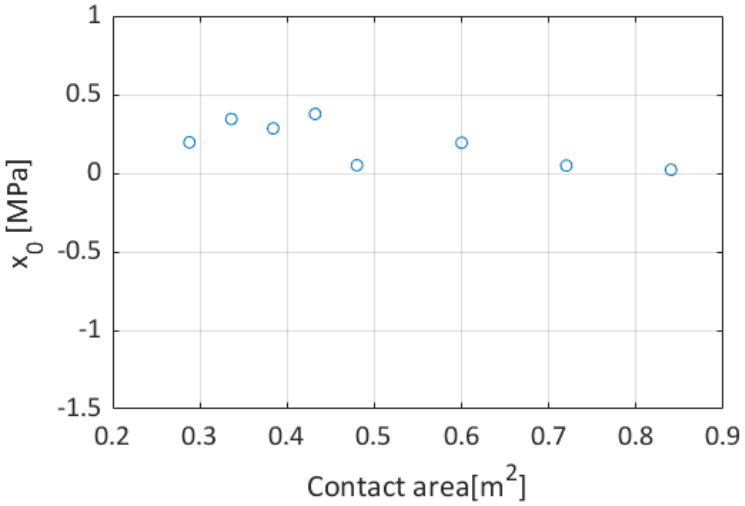

Figure 28. x_0 vs contact area for two frames at the bow

5.5.4 Determination of exposure

The exposure is the other required parameter for the estimation of the maximum local pressure using the event-maximum method. In this study, the ice exposure is calculated using Equation (16), where the parameters r, t_k, and t are assumed to be equal to one. Thus, the calculated total number of exposure (μ) at the bow, bow shoulder, and the stern shoulder are equal to 1448, 675, and 878 per year.

5.5.5 Determination of maximum local pressure

After determining parameters μ, x_0, and α (see Section 4.5.3 and 4.5.4), the maximum local pressures at different locations of hull are estimated using Equation (15). As an example, Table 5 presents parameters of α and x_0 for the contact area of 0.48 m^2. The obtained values at the bow are resulted from analyzing the combination of frames # 134+400 and #134, at the bow shoulder from the combination of frames #113 and #112 1/2 and at the stern shoulder from the combination of frames #41 and #40 ½. Table 6 shows the estimated maximum local pressure at the bow, bow shoulder, and the stern shoulder, based on the information in Table 5.

Table 5. Parameters of α and x_0 for the combination of two frames with contact area of 0.48 m^2

	$\alpha\ [MPa]$	$x_0[MPa]$
Bow	0.546	0.050
Bow shoulder	-0.179	0.228
Stern shoulder	-0.308	0.418

5.5.6 Comparison of the obtained α-area curves with the previous studies.

The obtained α-area curves at different locations of hull are compared with those presented by Taylor et al. (2010). As an example, Figure 29 shows the comparison between the obtained α-area curves for the combination of two frames at the bow with the curves presented by Taylor et al. (2010). The comparison results for other frames combinations are presented in Appendix E.

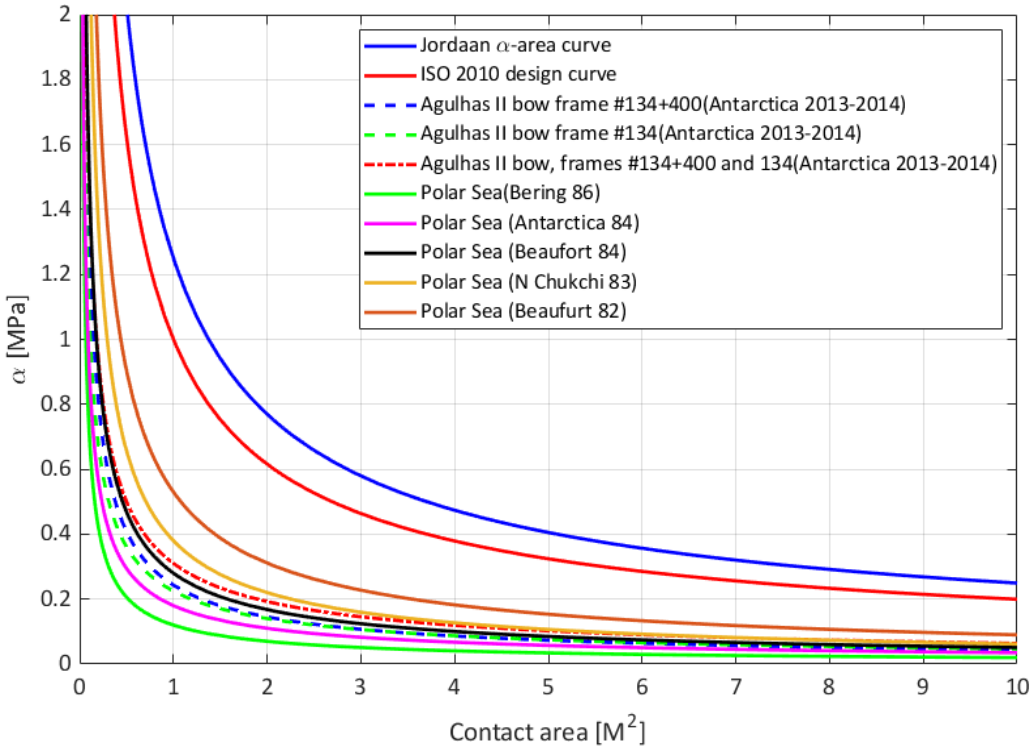

Figure 29. Comparison of α-area curves at different frames at the bow of S.A. Agulhas II with the curves presented by Taylor et al (2010).

5.5.7 Comparison of the obtained maximum local pressures with the previous studies.

The obtained maximum local pressures are compared with ones resulted from using the α-area curve presented by Jordaan et al. (1993) and the ice exposure according to Polar Class Rules (Appendix F). In accordance with the ice class PC5, the ice exposure is considered as one exposure to Multi-Year Ice (MYI) per year. Table 6 summarizes the estimated maximum local pressures at different locations of hull.

Table 6. Maximum local pressure at different locations of hull of the ship

	Max. local pressure ($P_e = 4 \times 10^{-2}$)	Max. local pressure ($P_e = 10^{-2}$)	Max. local pressure ($P_e = 10^{-4}$)
Bow	5.44	6.16	8.53
Bow shoulder	2.23	2.52	3.47
Stern shoulder	3.16	3.54	4.81
Bow, bow shoulder and stern shoulder[1]	6.68	9.61	19.24

5.6 Sensitivity Analysis

In current study, the load height was assumed to be 30 percent of the maximum ice thickness. Thus, for validating this assumption, a sensitivity analysis is performed, where the effect of the change in load height on local pressures is studied. As the bow of ship is more exposed to the ice floes, the sensitivity analysis is only performed for the combination of two frames at the bow with the contact area of 0.48 m^2. In this respect, the load height is varied from 20% to 50% of maximum ice thickness with the increment of 10 percent. The plots showing the effect of variation of the load height on α-area curves are presented in Figure 27 and Figure 30. The plots of x_0 and the ice pressures versus the contact areas are presented in Appendix G. Moreover, the obtained α-area curves of various load heights, as shown in Figure 31, are compared with the curves presented by Taylor et al. (2010). Furthermore, for assessing the sensitivity of the maximum local pressures to the load height, the coefficient of variations are defined, which corresponds to the ratio of the standard deviation to the mean. Table 7 shows the defined maximum local pressures corresponding to each load height and the coefficient of variations.

[1] The design curve proposed by Jordaan et al. (1993) with $t_k = 1$, $t = 1$, and $r = 1$

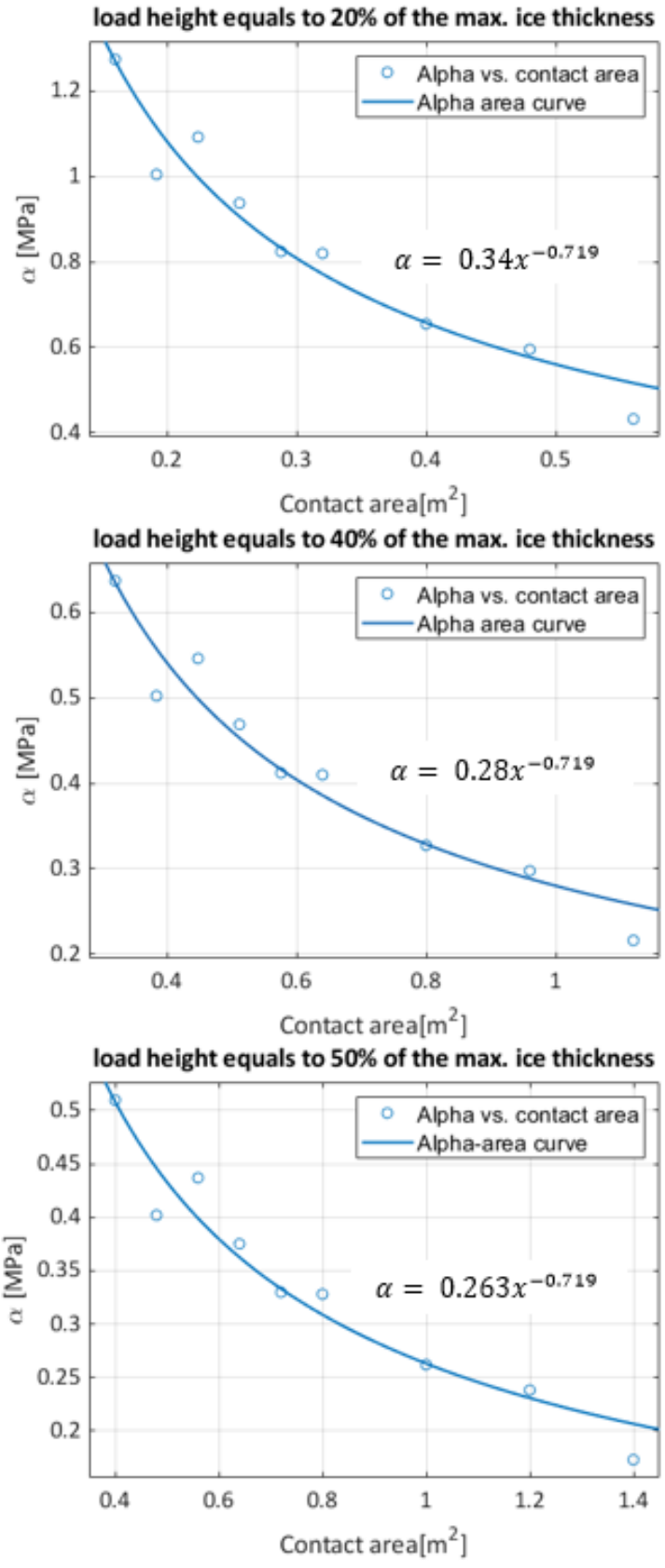

Figure 30. The effect of variation of load height on α-area curve for two frames at the bow.

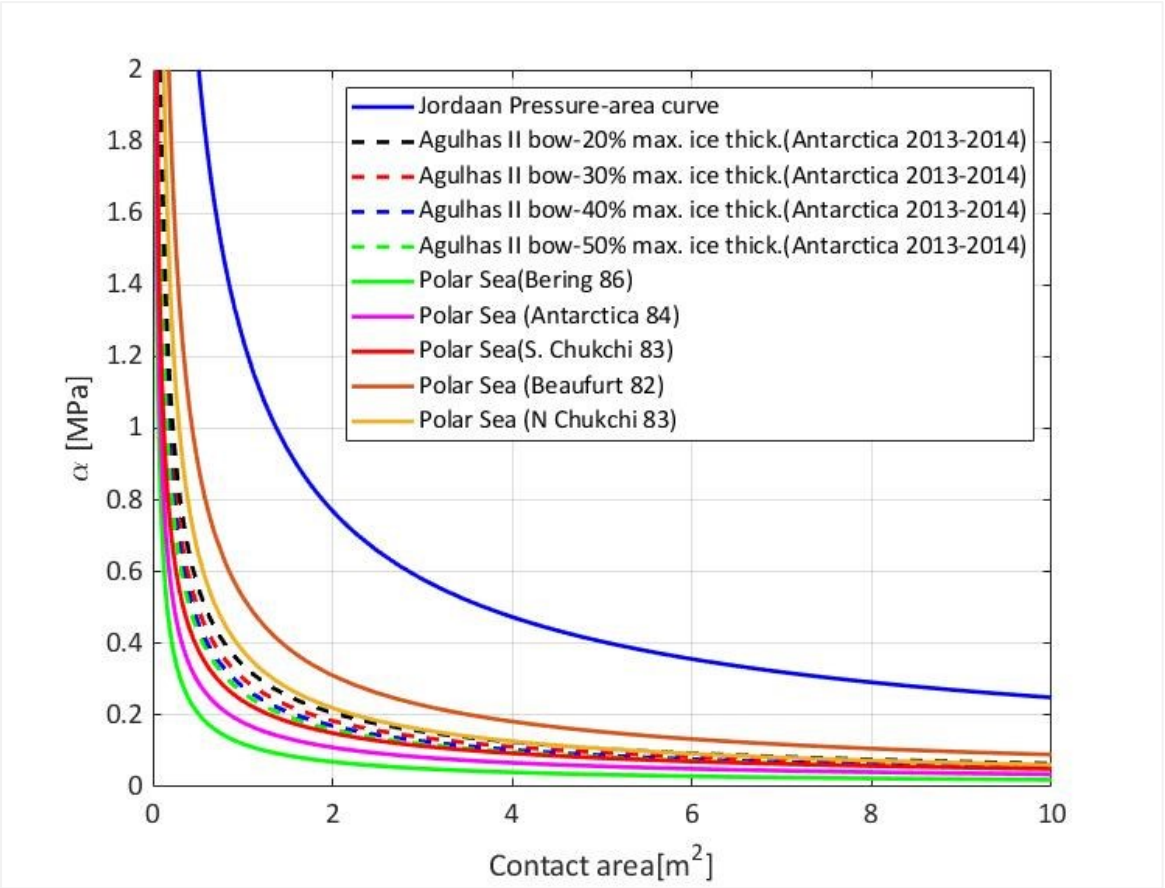

Figure 31. Comparison of the sensitivity analysis results with the α-area curves defined by Taylor et al (2010).

Table 7. Variation of the load height for defining the maximum local pressure on the contact area of 0.48 m^2at the bow

	Max. local pressure with probability of exceedance 10^{-2} [MPa]	Max. local pressure with probability of exceedance 10^{-4} [MPa]
Load height as 20 % of max. ice thick.	6.91	9.57
Load height as 30 % of max. ice thick.	6.16	8.53
Load height as 40 % of max. ice thick.	5.86	8.05
Load height as 50 % of max. ice thick.	5.41	7.46
Mean	6.08	8.40
Standard deviation	0.63	0.89
Coefficient of variation (%)	10.3	10.6

6 Discussion

The interaction between the ship's hull and ice features might arise significant ice loads on hull structures. For designing safe and efficient ice class ships knowledge of ice loading is required. The ice-breaking process has a complex and stochastic nature. Thus, statistical analysis can be used for analyzing the ice loads and ice pressures on ship's hull. This study used the event-maximum method for the evaluation of maximum local pressures on different locations of ship's hull. For this purpose, full-scale ice load measurements on board of S.A Agulhas II in the winter 2013-2014 are used to determine the ice pressures on different areas of hull.

The results shows that the largest number of ten-minute maximum ice loads was recorded at the bow when operating in thick ice condition. As presented in Table 4, the number of ten-minute maximum ice loads in thin ice condition are considerably low. It might have resulted due to applying the threshold of 10 kN for identifying the ice load events. As the thin ice condition contains large amount of open water and very thin ice, most of the measured ice loads are less than the set threshold. In addition, the expected number of impacts are connected with the location of ship-ice interaction. This looks reasonable because majority of the ice loads occur due to breaking of ice at the bow area. As Table 4 shows, the highest number of impacts was recorded at the bow when the ship operated in thick ice. This issue clarifies the necessity of defining the ice exposure from the ice condition similar to the one that is intended to be used for the design. For instance, for designing a ship to operate mostly in thin and medium ice in her lifetime, defining the expected number of interactions from a thick ice will result in overestimated maximum local pressures. Similarly, a conservative design can obtain if the number of interactions at bow is used for the evaluation of maximum local pressures at the bow shoulder and stern shoulder. Thus, to avoid a conservative design, the frequency of the ten-minute maximum ice loads are estimated for the bow, bow shoulder and the stern shoulder, which are 0.97, 0.45, and 0.58 per nautical mile respectively.

The results of the best fitting lines to peak pressures indicate that the selection of ten-minute maximum ice pressures greater than the median can result in acceptable fits for most cases. However, in some contact areas the exponential distribution cannot fit well into the peak pressures. The selection of the pressures at the tail affects the estimation of the maximum local pressures. Hence, the pressures at the tail must be defined carefully according to the data set.

The obtained α-area curves show that the parameter of α decreases as a function of contact area at all the locations of the ship's hull. The comparison between the obtained α-area curves and the design curves presented by Jordaan et al. (1993) and ISO (2010) show that all of the obtained curves are under the proposed design curves. Similarly, the obtained α-area curves are compared with those presented by Taylor et al. (2010), which resulted from full-scale measurements. The results of the comparison show that the obtained curves at the bow and bow shoulder are close to the curves presented in that study. Furthermore, the D value of these obtained curves are also in the range of observed D values presented by Taylor et al. (2010). On the other hand, for all of the frame combinations at the stern shoulder, the obtained D values do not fall in the range of D values presented by Taylor et al. (2010). The reported D values in that study were observed in full-scale measurements at the bow. Thus, the difference between the location of the measurement can be one possible reason for the difference between the obtained and observed D values. All the obtained α-area curves at the stern shoulder are also located below the ISO design curves and the curve proposed by Jordaan et al (1993). Moreover, the obtained x_0 values in all of locations are close to zero.

According to Table 6, the estimated maximum local pressures based on α-area curve proposed by Jordaan et al. (1993) are significantly higher than the approximated maximum local pressures based on the α-area curves of this study. This can be justified as the design curve proposed by Jordaan et al. (1993) is defined for the heavy ice conditions, i.e., MYI. While in this study the ship encountered easier ice conditions than those assumed by Jordaan et al (1993). Thus, the α-area equation for design should be defined from the ice condition similar to the one that the ship will encounter mostly in her lifetime.

The sensitivity analysis shows that the variation in the assumed load height has a small effect on the α-area curve. According to Table 7, the maximum local pressure with the probability of exceedance 10^{-2} and 10^{-4} decreases about 22% as the load height increases from 20% to 50% of maximum ice thickness. In addition, the variation of load height causes small changes in the coefficient of variation. Moreover, increasing the load height also affects the coefficient C while coefficient D remains constant.

7 Conclusion

The estimation of the maximum local pressures is required for designing safe and efficient ice class ships. This study analyzed the event-maximum method, which is a semi-empirical method for estimating the maximum local pressures on a ship's hull. As the measured local ice pressures were not available, the study used the full-scale ice load measurements for calculating the ice pressures. This study results are then compared with the previous studies.

The study outcomes indicate that the event-maximum method is suitable to estimate the maximum local pressures at ship's hull using the full-scale ice load measurements. Furthermore, the results of the best fitting lines to the peak ice pressures show that in the most contact areas, the best fitting lines follow the exponential distribution. However, in some cases the results show improper fits. Moreover, the results of this study indicate that the obtained α-area curves at all the locations of hull are close to the curves presented by Taylor et al. (2010), which were obtained from full-scale measurements. In addition, the coefficient D for all of the α-area curves at the bow and bow shoulder are in the range recommended by Taylor et al. (2010).

The study indicates that the use of design curve presented by Jordaan et al. (1993) results in conservative maximum local pressures estimation. This is most likely due to the fact that the design curve is defined for considerably heavier ice condition. Thus, using the appropriate design curve, which is derived from the ice condition similar to the one that is intended to be used for design, is recommended.

The results of sensitivity analysis indicate that the variation of the load height has small effect on α-area curves and estimated local pressures at the bow. In addition, variation of the load height only causes small changes in coefficient C while coefficient D remains constant. The result of sensitivity analysis and the similarity between the obtained α-area curves and the curves presented by Taylor et al. (2010) indicates that the assumption made in this study for defining the load height can be a valid approach. Furthermore, the results of the study indicate the expected number of ten-minute maximum ice loads is highly affected by prevailing ice condition and impact area. Hence, when designing a ship, it is recommended to define the ice exposure based on the ice condition, which the ship will encounter mostly in her lifetime.

8 Future Studies

The results of this study shows that the use of the exponential distribution in event-maximum method does not provide acceptable fits into the pressures at the tail in some bow contact areas. Thus, there is a need for assessing the application of other probability distributions in this method. As the weibull distribution is recommended for modeling the ice loads by Suyuthi et al. (2012b) and Suominen and Kujala (2010), applying that distribution into event-maximum method may provide more realistic results. Hence, the application of the Weibull distribution into event-maximum method should be studied in the future.

For the approximation of ice loads and pressures on hull of ships, various statistical methods have been proposed such as event-maximum method by Jordaan et al. (1993), and Gumbel asymptotic distribution by Kujala and Vurio (1985). The application of various methods into the same ice condition may provide different approximation of ice loads and pressures. Furthermore, the suitability of the method may also depend on the ice condition. Thus, comparison of these methods is required for providing a guideline for choosing the appropriate method according to the ice condition and the application of use.

9 Bibliography

[1] Bergström, M., Erikstad, S. & Ehlers, S., 2016. A simulation-based probabilistic design method for Arctic Sea transport systems. *Marine Science and Application,* 15(4), pp. 349-369.

[2] Castillo, E., 1988. *Extreme value theory in engineering.* s.l.:Harcourt Brace Jovanovich.

[3] Daley, C., 1992. *Aspects of ship-ice interaction in natural ice cover,* Helsinki: Helsinki University of Technology, Labratory of Naval Architecture and Marine Engineering.

[4] Daley, C., 2004. *A study of the process-spatial link in ice pressure-area relationships,* Newfoundland: National Reserach Concil of Canada.

[5] Daley, C., 2007. Reanalysis of ice pressure-area relationship. *Marine Technology,* 44(October 2007), pp. 234-244.

[6] Daley, C., ST John, J. & Blount, H., 1990. *Ice loads and ship response to ice,* s.l.: Ship Structures Committee.

[7] Ehlers, S. et al., 2015. *19th international ship and offshore structures congress.* Cascais: s.n.

[8] Frederking, R., 1999. *The local pressure-area relation in ship impact with ice.* Ottawa, s.n.

[9] Frederking, R., Jordaan, I. & JS, M., 1990. *Field test of ice indentation at medium scale.* Espoo, s.n.

[10] Hanninen, S., Lensu, M. & Riska, K., 2001. *Analysis of the ice load measurements during USCGC Healy ice trials, spring 2000,* Espoo: Helsiki University of Technology, Ship Labratory.

[11] IACS, I. A. o. C. S., 2016. *Requirements concerning POLAR CLASS.* s.l.:International Association of Classification Societies.

[12] ISO, 2010. *Petroleum and natural gas industries — Arctic offshore structure.* s.l.:International Standard Organization (ISO).

[13] Jordaan, I., 2005. *Decision under Uncertainty.* Cambridge: Cambridge University Press.

[14] Jordaan, I. et al., 2005b. *Principles for local and global ice design using pressures area relationship.* Newyork, POAC'05 Conference.

[15] Jordaan, I., Maes, M., Brown, P. & Herman, I., 1993. Probabilistic analysis of local ice pressure. *Offshore Mechanics and Arctic Engineering,* Volume 115.

[16] Kendrick, A. & Daley, C., 2011. *Structural challenges faced by arctic ships,* s.l.: Ship Structure Committee.

[17] Kheisin, D. & Popov, Y., 1973. *Ice navigation qualities of ships.* Hanover: Cold Regions Research and Engineering Laboratory.

[18] Kotilainen, M., 2014. *Statistical modeling of ice-induced loads on a research vessel.* Espoo: Aalto University, Department of Mechanical Engieering.

[19] Kotilainen, M., Suominen, M. & Kujala, P., 2018. *The influence of ice response to the peak ice load on ship's bow shoulder.* Vladivostok, IAHR International Symposium on Ice.

[20] Kotilainen, M., Vanhatalo, J., Suominen, M. & Kujala, P., 2017. Predicting ice-induced load amplitudes on ship bow conditional on ice thickness and ship speed in the Baltic Sea. *Cold Region Science and Technology,* Volume 135, pp. 116-126.

[21] Kotilainen, M., Vanhatalo, J., Suominen, M. & Kujala, P., 2018. Predicting local ice loads on ship bow as a function of ice and operational conditions in the Southern Sea. *Ship Technology Research,* 65(2), pp. 87-101.

[22] Kujala, P., 1994. *On the statistics of ice loads on ship hull in the Baltic.* Helsinki: Helsinki University of Technology.

[23] Kujala, P., Kulovesi, J., Lehtiranta, J. & Suominen, M., 2014. *Full-scale measurements on board S.A. Agulhas II in the Antarctic waters 2013-2014,* Espoo: Aalto University.

[24] Kujala, P. & Vuorio, J., 1985. *On the statstical nature of the ice-induced pressure measured on board I.B. Sisu.* Narssarssuaq, POAC 1985.

[25] Kujala, P. & Vuorio, J., 1986. *Results and statistical analysis of ice load measurements on board icebreaker Sisu in winters 1979 to 1985.,* Helsinki: Technical Research Centre of Finland,.

[26] Leira, N., Børsheim, L., Espeland, Ø. & Amdahl, J., 2009. Ice-load estimation for a ship hull based on continuous response monitoring. *Engineering for the Maritime Environment,* Volume 223, pp. 529-540.

[27] Lensu, M., 2002. *Short Term Prediction of Ice Loads Experienced by Ice Going Ships,* Espoo: Helsinki University of Technology.

[28] Maes, M. A. & Jordaan, I., 1986. *Arctic environmental design using short data extremal techniques.* Tokyo, OMAE 1986.

[29] Ochi, M., 1981. *Principle of extreme value statistics and their application.* Arlington, The Society of Naval Architects and Marine Engineers.

[30] Ralph, F., 2016. *Design of Ships and Offshore Structures:A Probabilistic Approach for Multi-Year Ice and Iceberg Impact Loads for Decision-making with Uncertainty.* Newfoundland: Memorial University.

[31] Ralph, F. & Jordaan, I., 2013. *Probabilistic methodology for design of arctic ships.* Nantes, ASME.

[32] Riska, K., 2010. Design of ice breaking ships. *Cold Region Science and Marine Technology.*

[33] Riska, K. & Kämäräinen, J., 2012. *A review of ice loading and the evolution of the Finnish-Swedish Ice Class rules.* s.l.:SNAME Transactions.

[34] Sanderson, T. J. O., 1988. Full-scale measurements. In: *Ice mechanics- Risk of offshore structures.* London: Graham and Tortman, p. 140.

[35] Suominen, M., 2018. *Uncertainty and variation in measured ice-induced loads on a ship hull.* Espoo: Aalto University.

[36] Suominen, M. et al., 2017. *Visual Antarctic Sea ice condition observations during Austral summers 2012-2016.* Busan, Proceedings of the 24th International Conference on Port and Ocean Engineering under Arctic Conditions.

[37] Suominen, M. & Kujala, P., 2010. *Analysis of short-term ice load measurements on board MSKemira during the winters 1987 and 1988,* Espoo: Aalto University, School of Science and Technology, Department of Applied Mechanics,.

[38] Suominen, M., Kujala, P. & Kotilainen, M., 2015. *The encountered extreme events and predicted maximum ice-induced loads on the ship hull in the Southern Ocean.* Newfoundland, s.n.

[39] Suyuthi, A., Leira, B. & Riska, K., 2010. *Variation of the short term extreme ice loads along a ship hull.* Shanghai, OMAE.

[40] Suyuthi, A., Leira, B. & Riska, K., 2012a. Short term extreme statistics of local ice loads on ship hulls. *Cold Regions Science and Technology,* 82(May 2012), pp. 130-143.

[41] Suyuthi, A., Leira, B. & Riska, K., 2012b. Statistics of local ice load peaks on ship hulls. *Structural Safety,* 40(September 2012), pp. 1-10.

[42] Taylor, R., Jordaan, I., Li, L. & Sudom, D., 2010. Local design pressure for structures in ice. *Offshore Mechanics and Arctic Engineering,* Volume 132.

[43] Vuorio, J., Riska, K. & Varsta, P., 1978. *Long term measurement of ice pressure and ice-induced stresses on the icebreaker Sisu in winter 1978,* s.l.: Winter Navigation Research Board.

[44] WMO, 2014. *WMO Sea-Ice Nomenclature.* s.l. :World Meteorological Organization.

Appendix A: Stiffness matrix for different locations of hull

Stiffness matrix for the bow (a_b), bow shoulder (a_{bs}), and the stern shoulder (a_{ss})

$$a_b = \begin{pmatrix} 1.195 \times 10^6 & -1.255 \times 10^5 \\ -1.859 \times 10^5 & 1.198 \times 10^6 \end{pmatrix} kN$$

$$a_{bs} = \begin{pmatrix} 6.292 \times 10^5 & -3.659 \times 10^4 & 1.991 \times 10^4 \\ 1.364 \times 10^4 & 7.452 \times 10^5 & -6.002 \times 10^5 \\ -4.707 \times 10^4 & -3.155 \times 10^5 & 1.558 \times 10^6 \end{pmatrix} kN$$

$$a_{ss} = \begin{pmatrix} 2.876 \times 10^5 & 1.021 \times 10^3 & -8.243 \times 10^1 & 2.793 \times 10^2 \\ 5.586 \times 10^3 & 3.341 \times 10^5 & -7.997 \times 10^4 & 1.5959 \times 10^4 \\ -3.962 \times 10^3 & -6.984 \times 10^4 & 3.632 \times 10^5 & -6.983 \times 10^4 \\ -1.519 \times 10^3 & 1.276 \times 10^4 & -6.3356 \times 10^4 & 3.309 \times 10^5 \end{pmatrix} kN$$

Appendix B: Ten-minute maximum ice forces histograms

Ten-minute maximum ice forces histograms for different frames at the bow

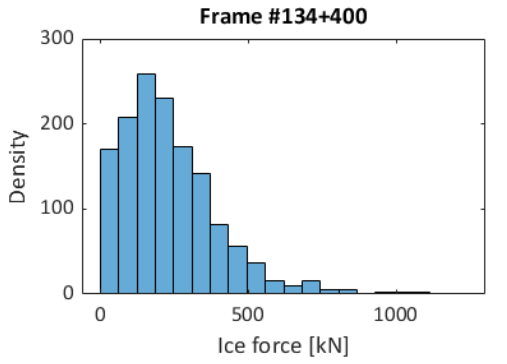

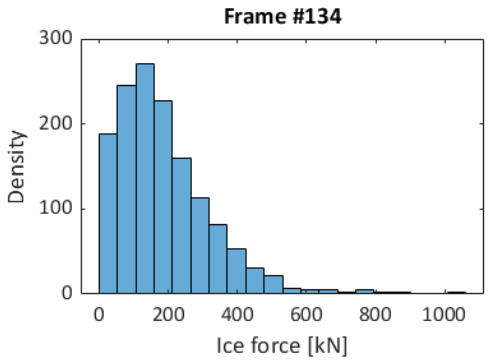

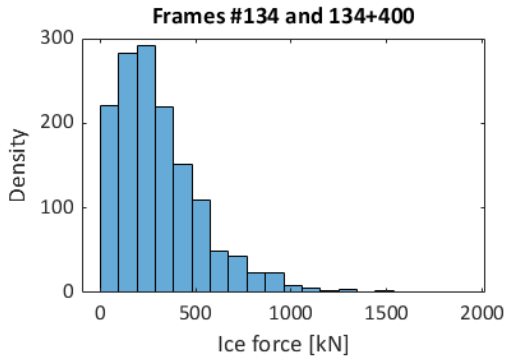

Ten-minute maximum ice forces histograms for different frames at the bow shoulder

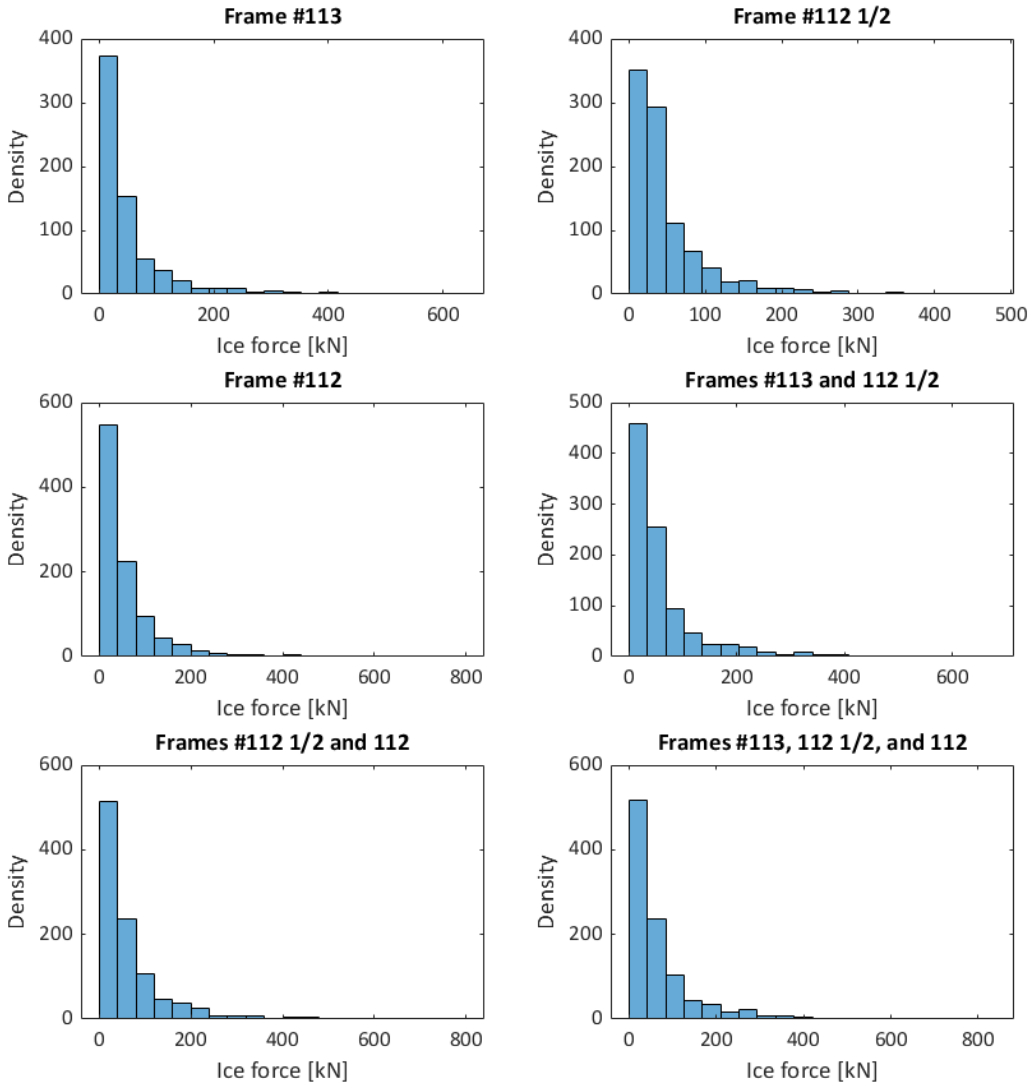

Ten-minute maximum ice forces histograms for different frames at the stern shoulder

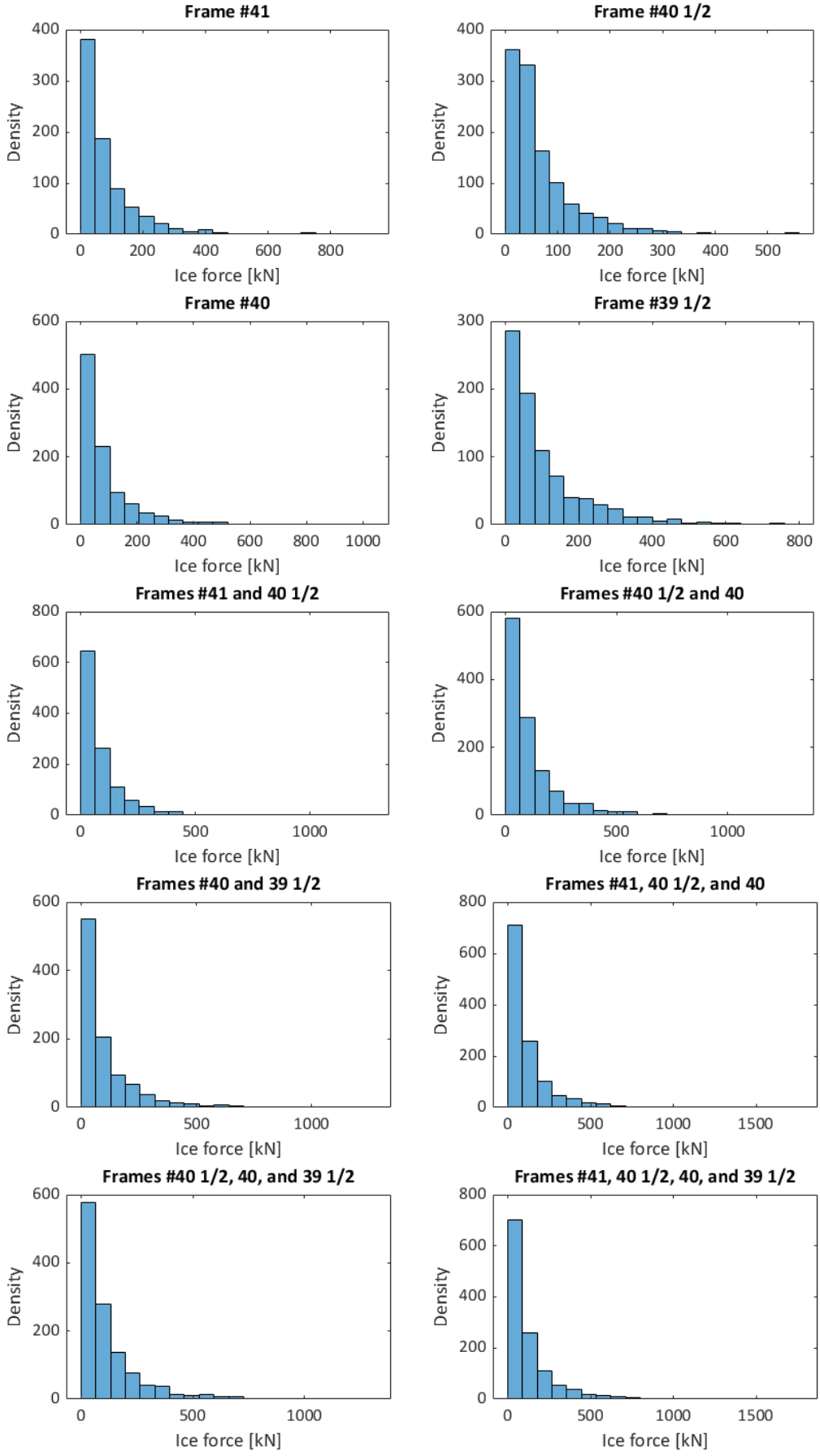

Appendix C: Ten-minute maximum ice pressures histograms

Ten-minute maximum ice pressures histograms for different frames at the bow

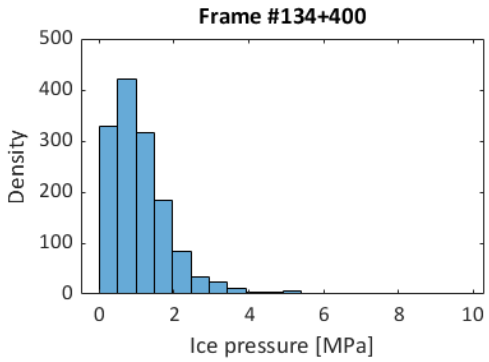

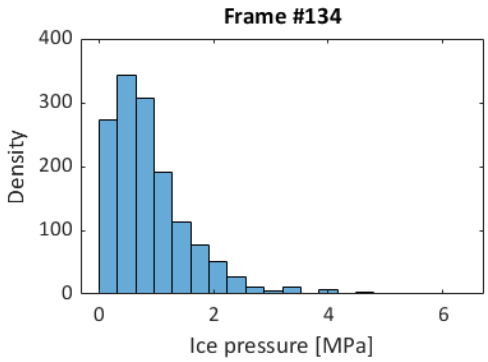

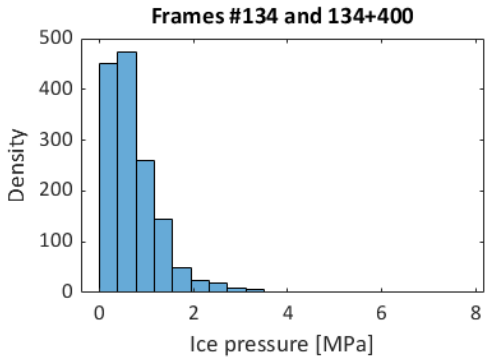

Ten-minute maximum ice pressures histograms for different frames at the bow shoulder

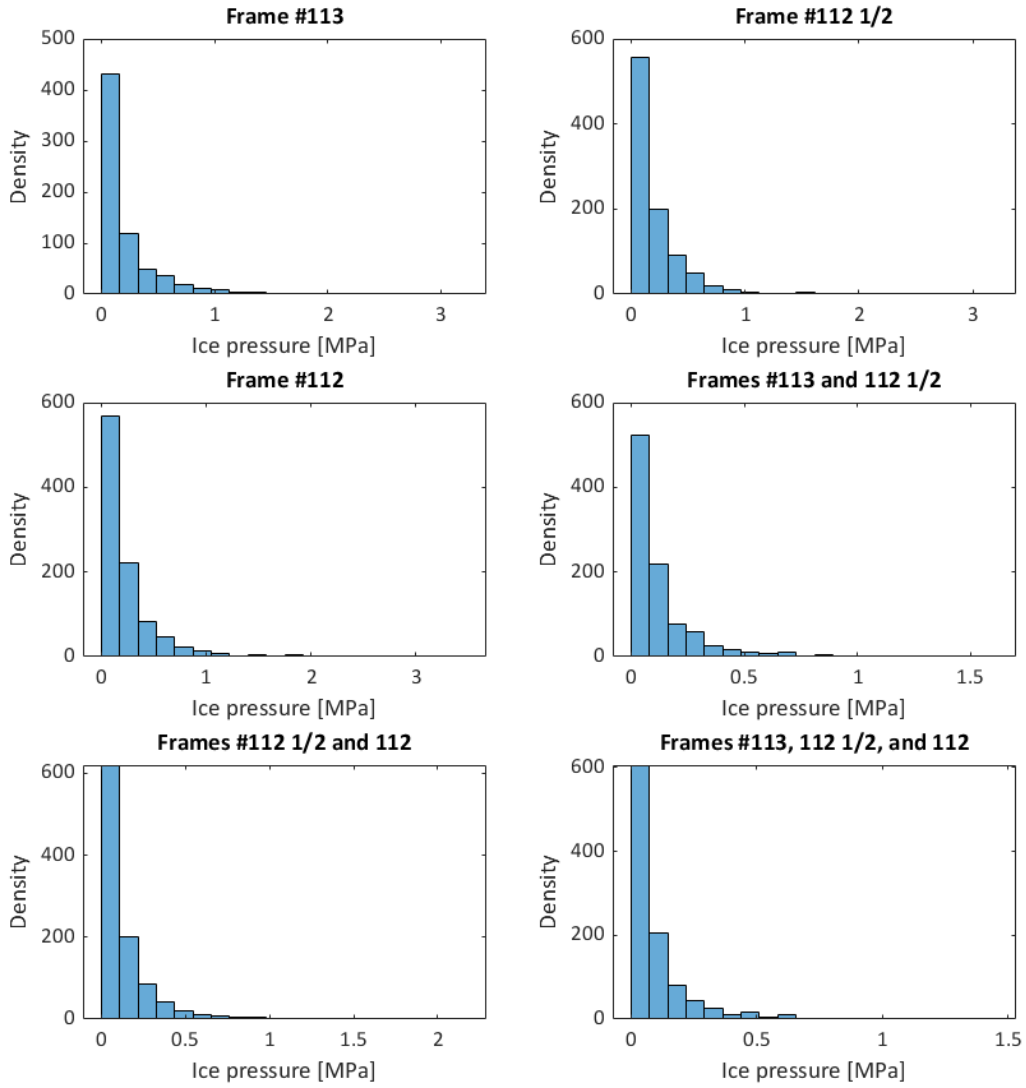

Ten-minute maximum ice pressures histograms for different frames at the stern shoulder

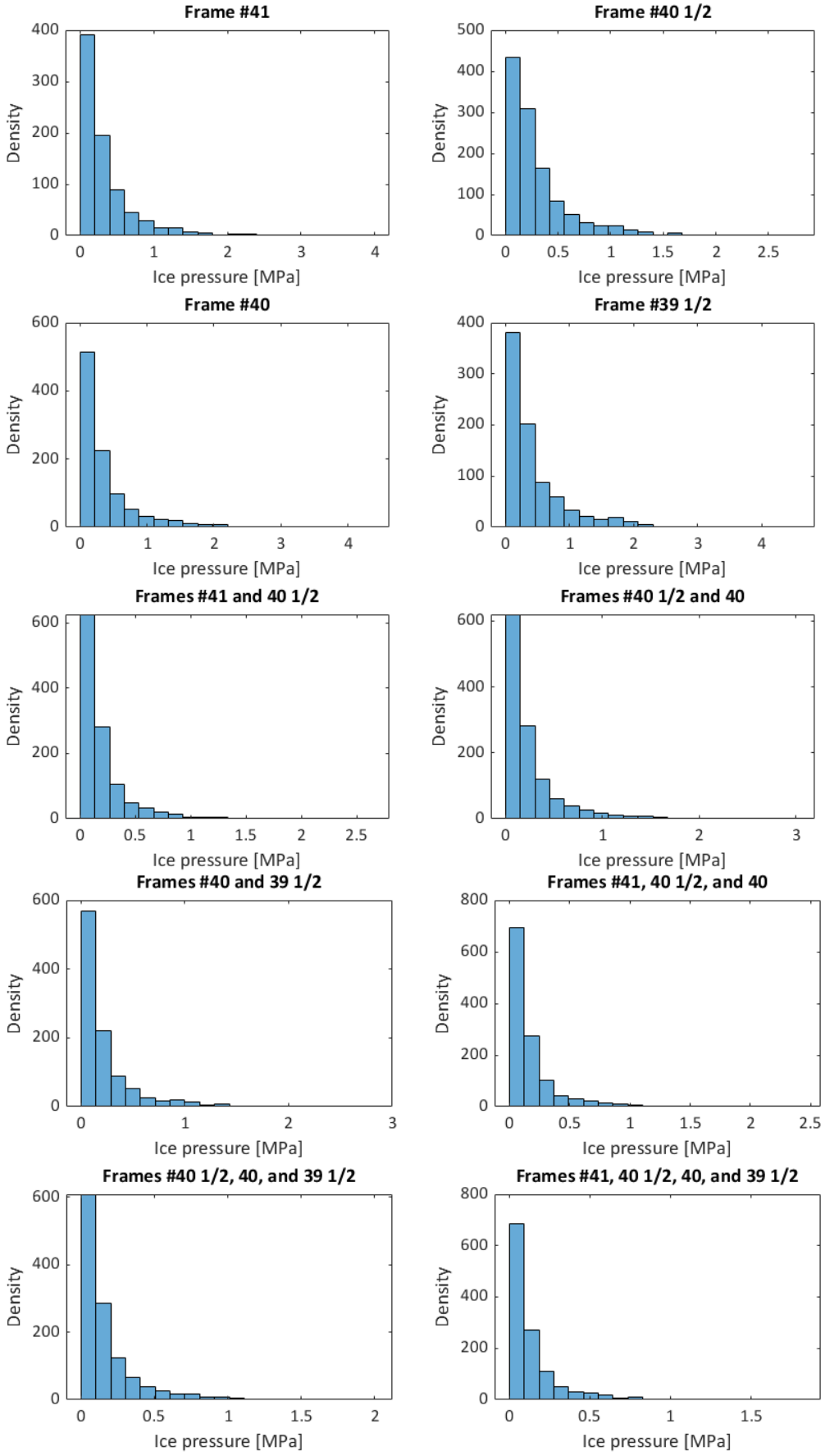

Appendix D: Results of analysis of various frames at different locations of hull

Local pressures vs contact areas at the bow for frame #134+400

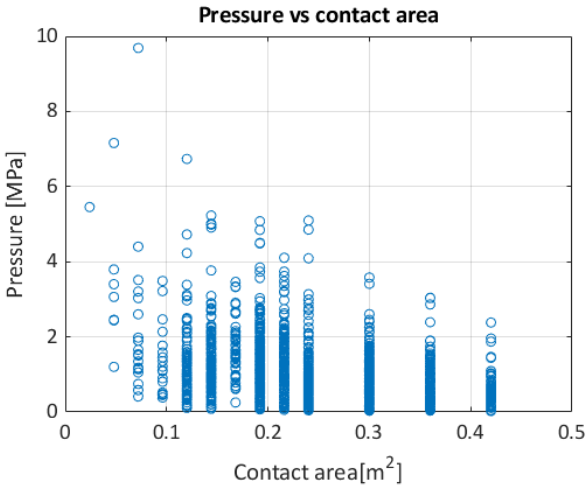

Best fitting lines for the pressures at the tail, for frame #134+400

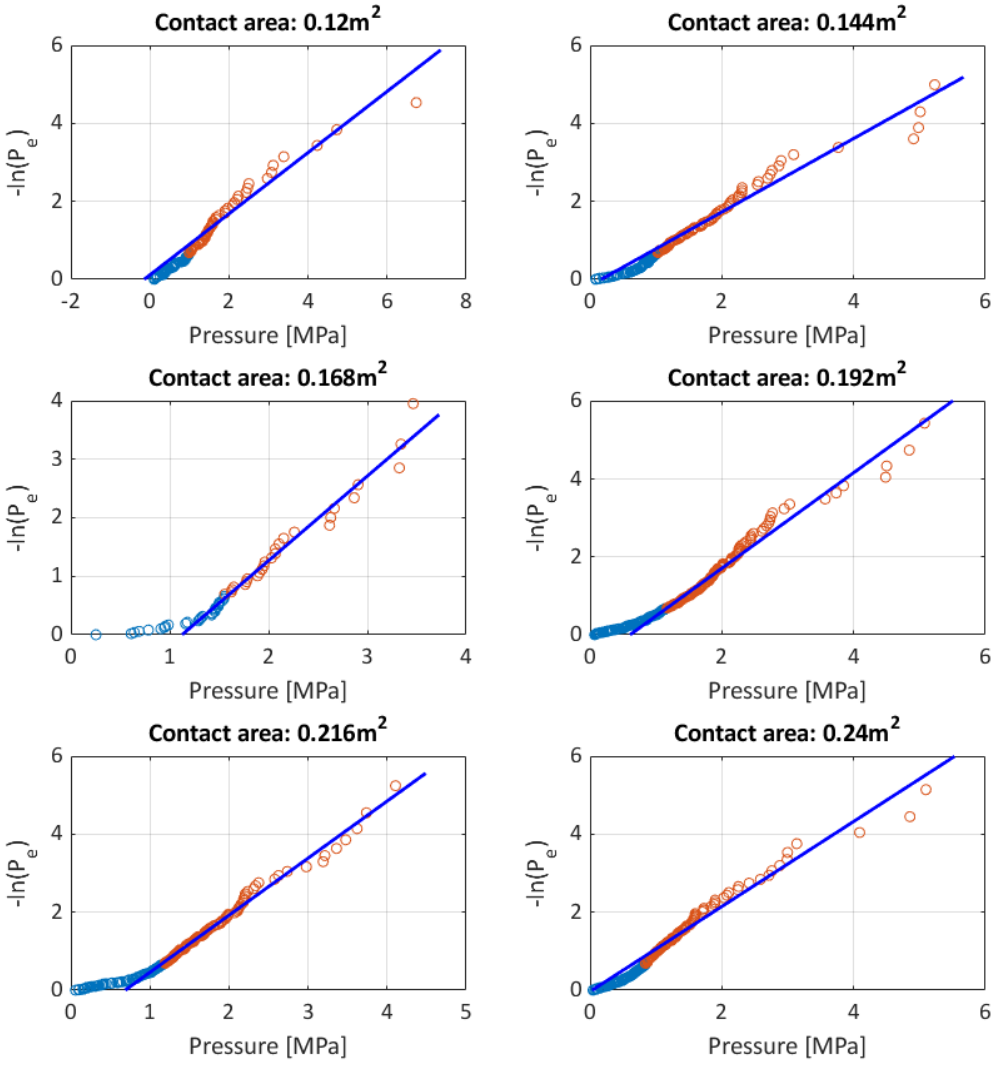

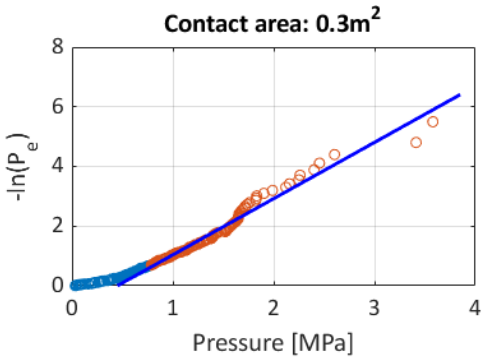

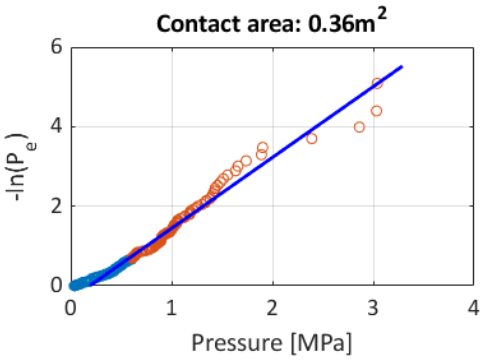

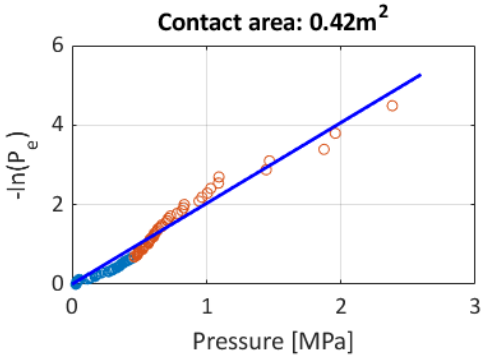

Parameters of best fitting lines to the pressures at the tail, for frame #134+400

Contact area [m^2]	a	b	α [MPa]	X_0 [MPa]
0.120	0.784	0.115	-0.146	1.275
0.144	0.942	-0.158	0.168	1.061
0.168	1.447	-1.629	1.125	0.691
0.192	1.227	-0.745	0.607	0.815
0.216	1.463	-1.005	0.687	0.683
0.240	1.090	-0.035	0.032	0.918
0.300	1.885	-0.848	0.450	0.531
0.360	1.782	-0.338	0.190	0.561
0.420	2.028	0.009	-0.004	0.493

The α-area curve and X_0 versus contact for frame #134+400

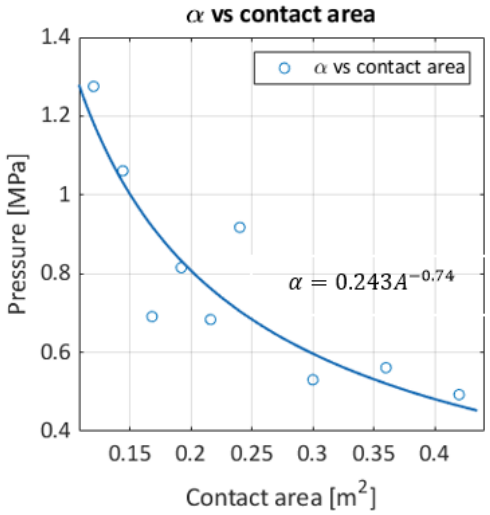

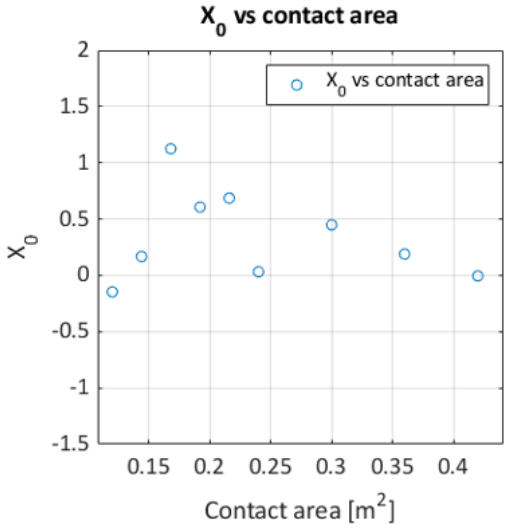

Local pressures vs contact areas at the bow for frame #134

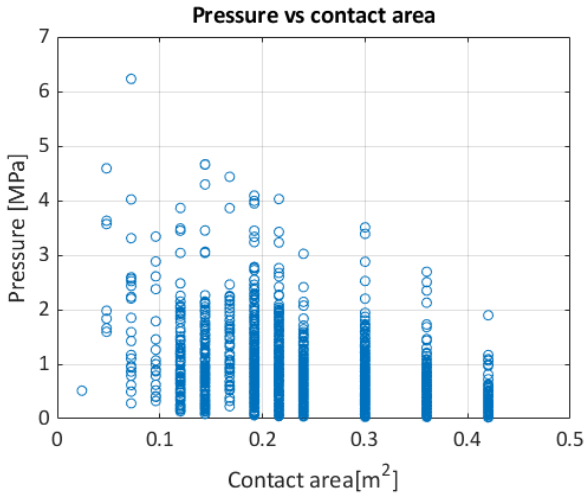

Best fitting lines for the pressures at the tail, for frame #134

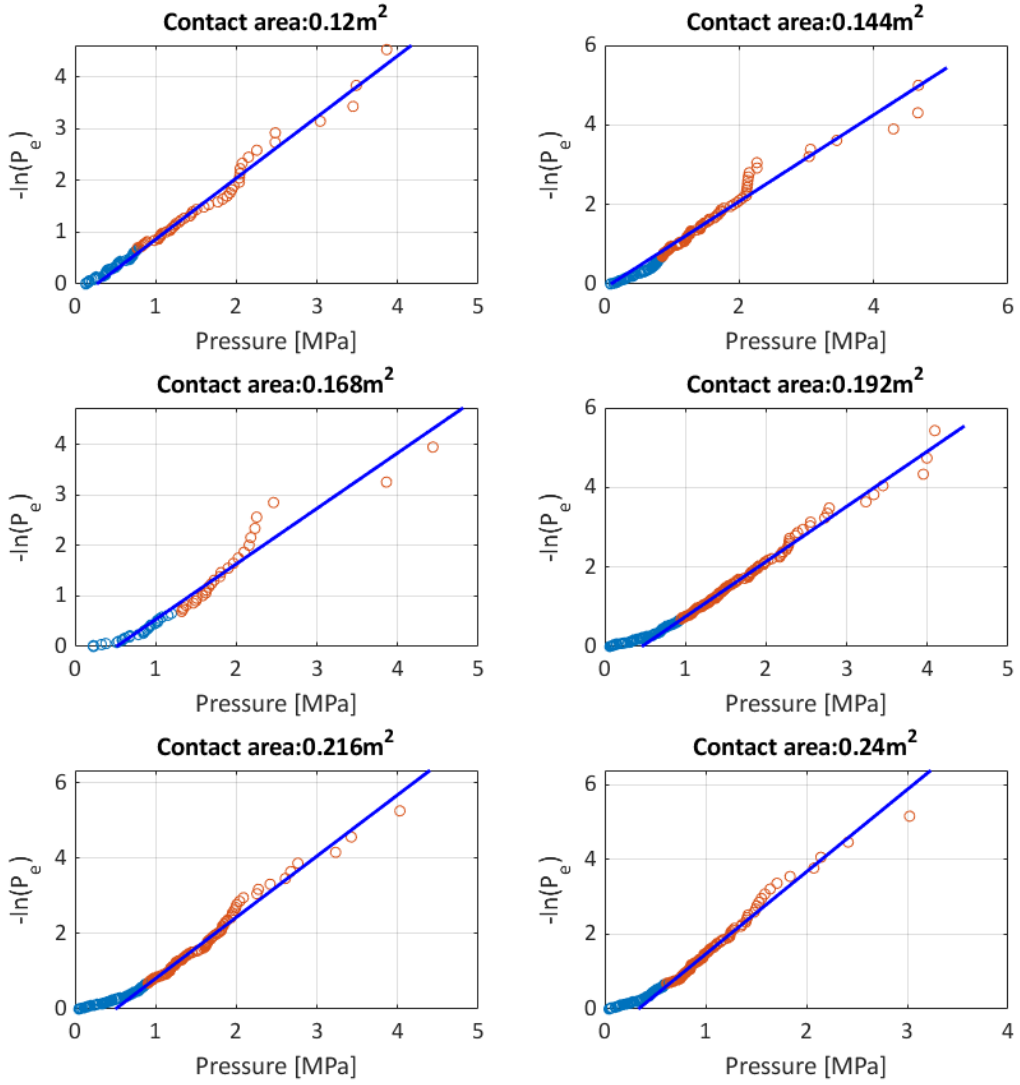

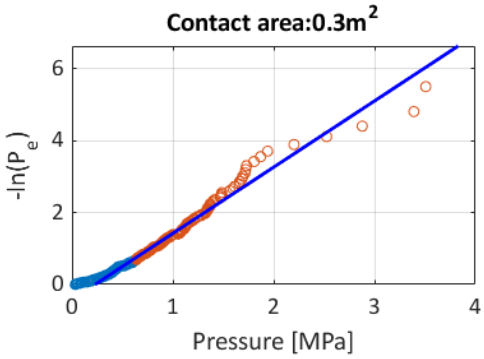

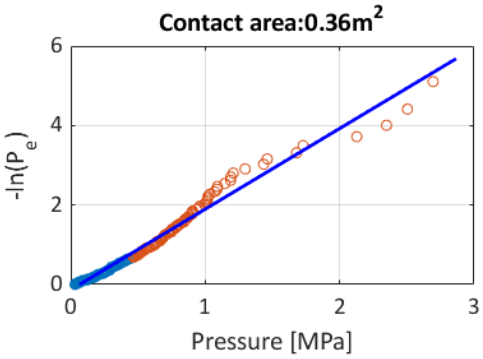

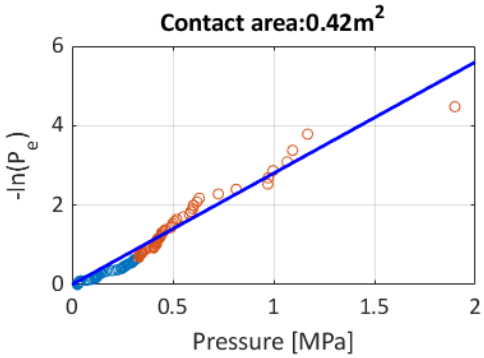

Parameters of best fitting lines to the pressures at the tail, for frame #134

Contact area [m^2]	a	b	α [MPa]	X_0 [MPa]
0.120	1.183	-0.319	0.269	0.845
0.144	1.088	-0.098	0.091	0.919
0.168	1.100	-0.562	0.512	0.909
0.192	1.386	-0.636	0.459	0.721
0.216	1.622	-0.811	0.500	0.617
0.240	2.199	-0.733	0.333	0.455
0.300	1.840	-0.421	0.229	0.543
0.360	2.029	-0.133	0.065	0.493
0.420	2.799	0.004	-0.001	0.357

The α-area curve and X_0 versus contact for frame #134

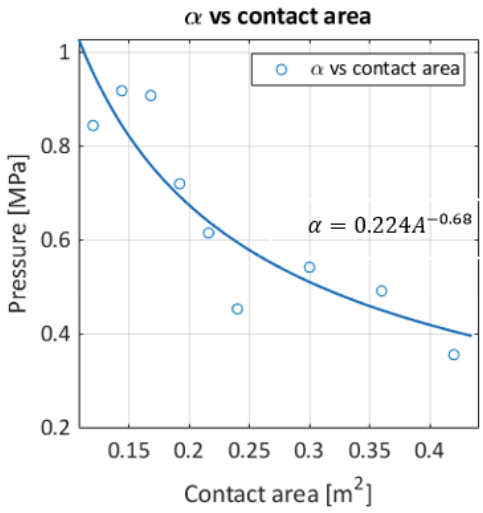

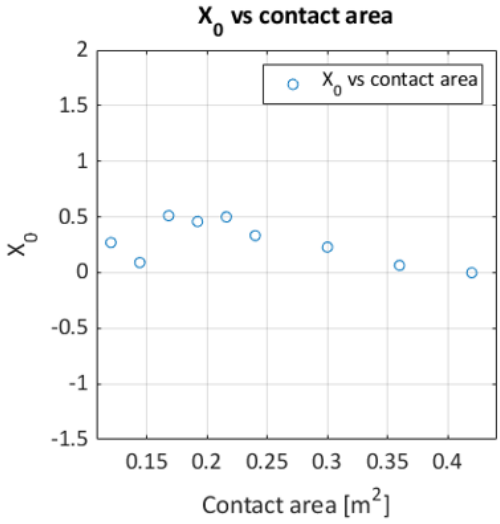

Local pressures vs contact areas at the bow shoulder for frame #113

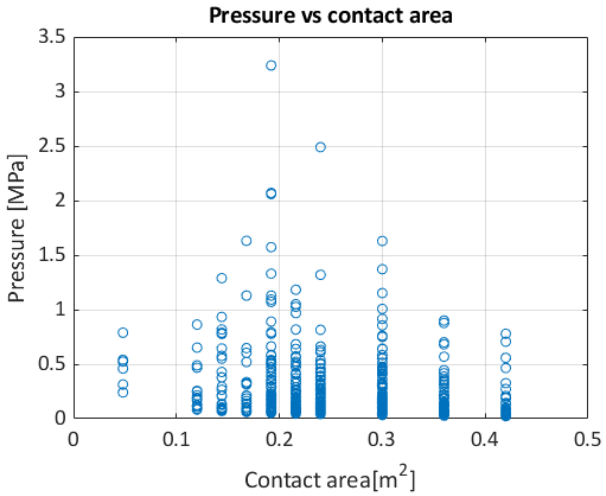

Best fitting lines for the pressures at the tail, for frame #113

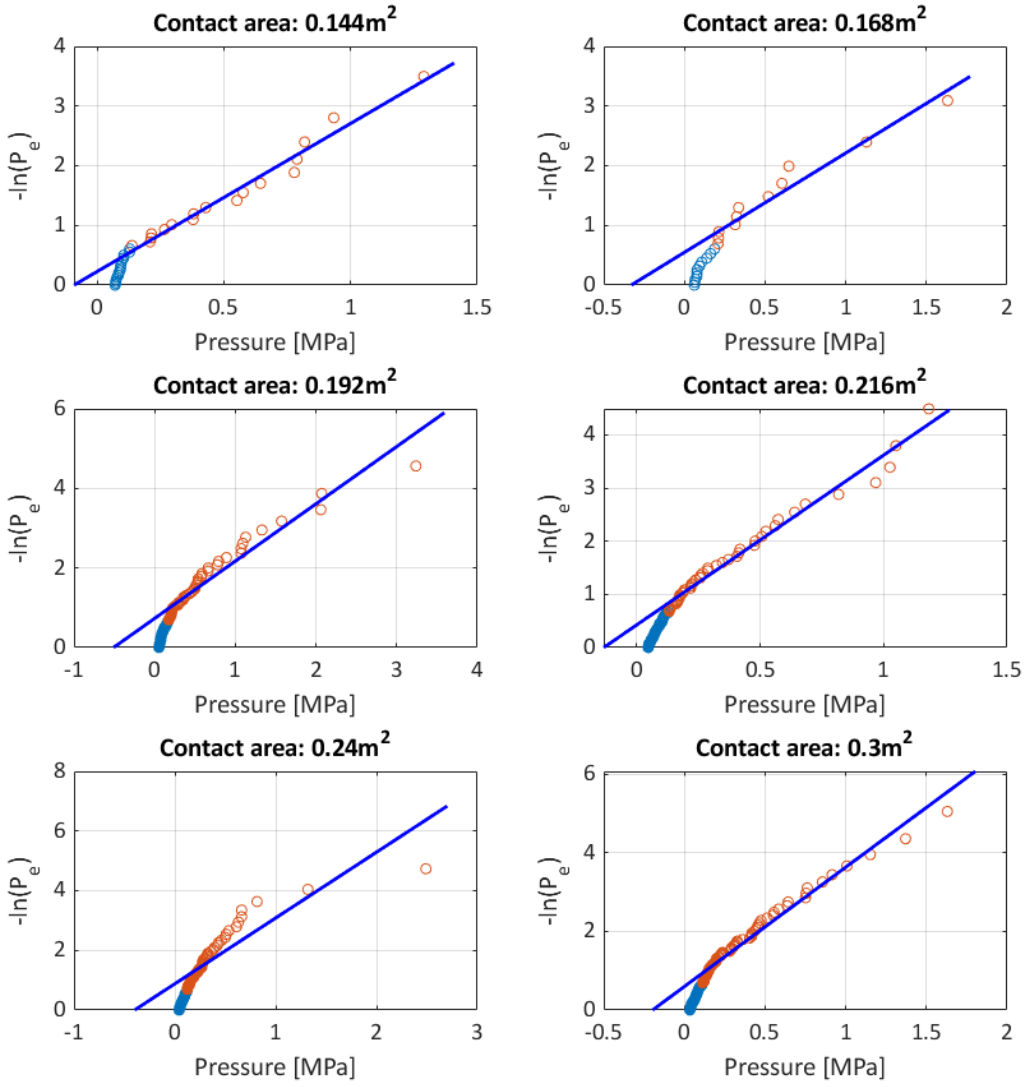

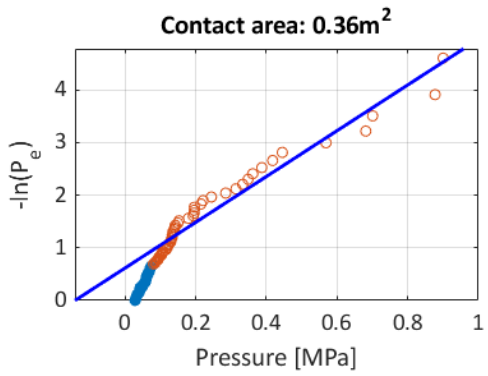

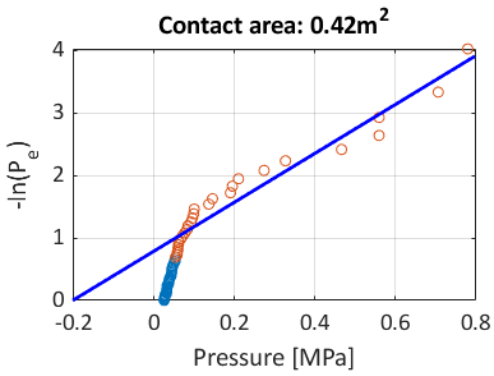

Parameters of best fitting lines to the pressures at the tail, for frame #113

Contact area [m^2]	a	b	α [MPa]	X_0 [MPa]
0.144	2.481	0.228	-0.092	0.403
0.168	1.664	0.548	-0.329	0.601
0.192	1.440	0.733	-0.509	0.695
0.216	3.192	0.426	-0.133	0.313
0.240	2.206	0.880	-0.399	0.453
0.300	3.035	0.598	-0.197	0.330
0.360	4.348	0.617	-0.142	0.230
0.420	3.907	0.793	-0.203	0.256

The α-area curve and X_0 versus contact for frame #113

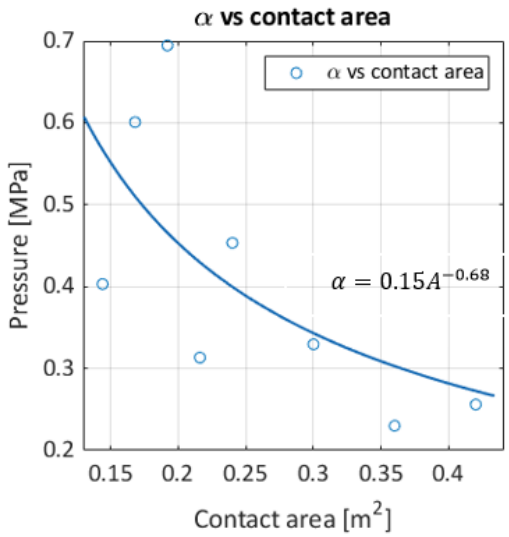

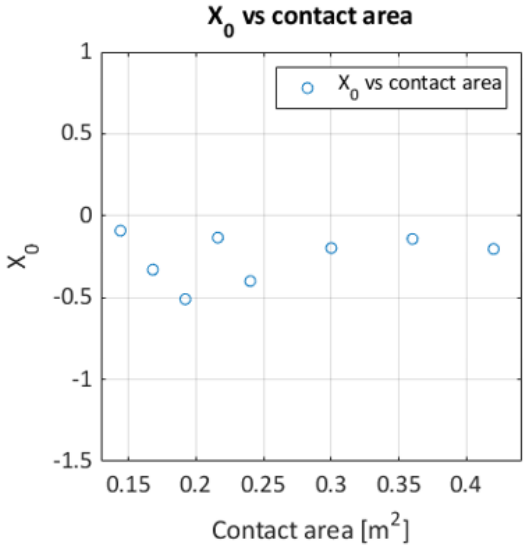

Local pressures vs contact areas at the bow shoulder for frame #112 ½

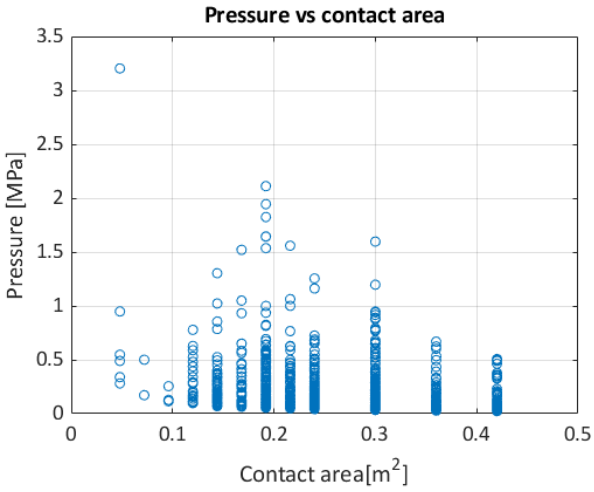

Best fitting lines for the pressures at the tail, for frame #112 ½

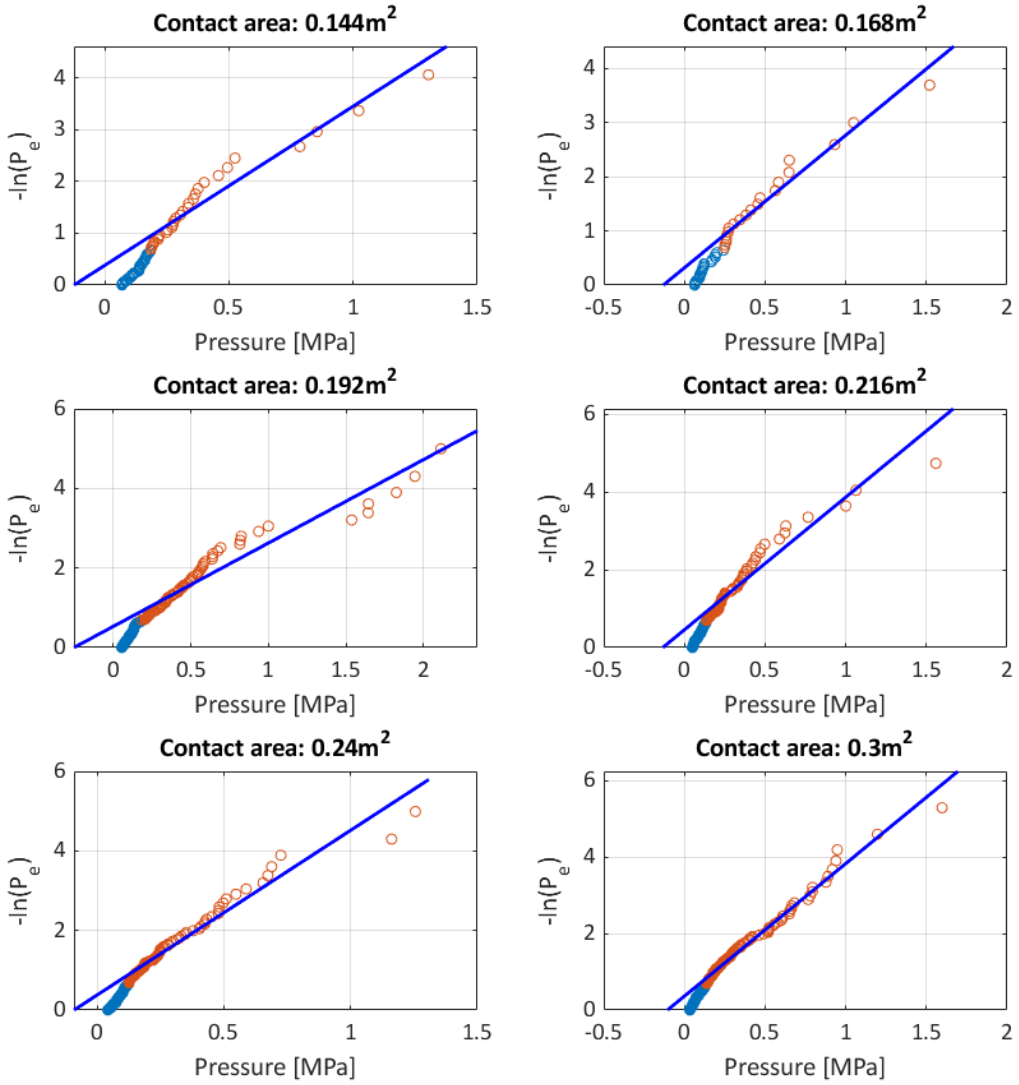

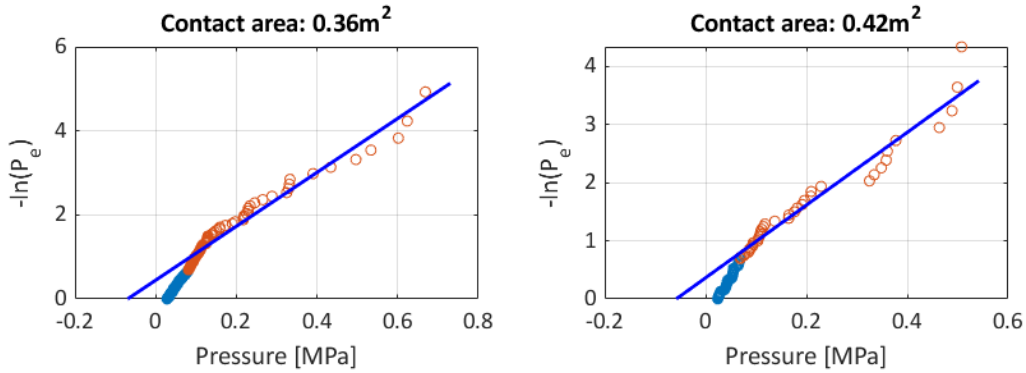

Parameters of best fitting lines to the pressures at the tail, for frame #112 ½

Contact area [m^2]	a	b	α [MPa]	X_0 [MPa]
0.144	3.072	0.379	-0.123	0.325
0.168	2.446	0.319	-0.130	0.409
0.192	2.097	0.532	-0.254	0.477
0.216	3.409	0.457	-0.134	0.293
0.240	4.139	0.380	-0.092	0.242
0.300	3.467	0.363	-0.105	0.288
0.360	6.415	0.447	-0.070	0.156
0.420	6.247	0.363	-0.058	0.160

The α-area curve and X_0 versus contact for frame #112 ½

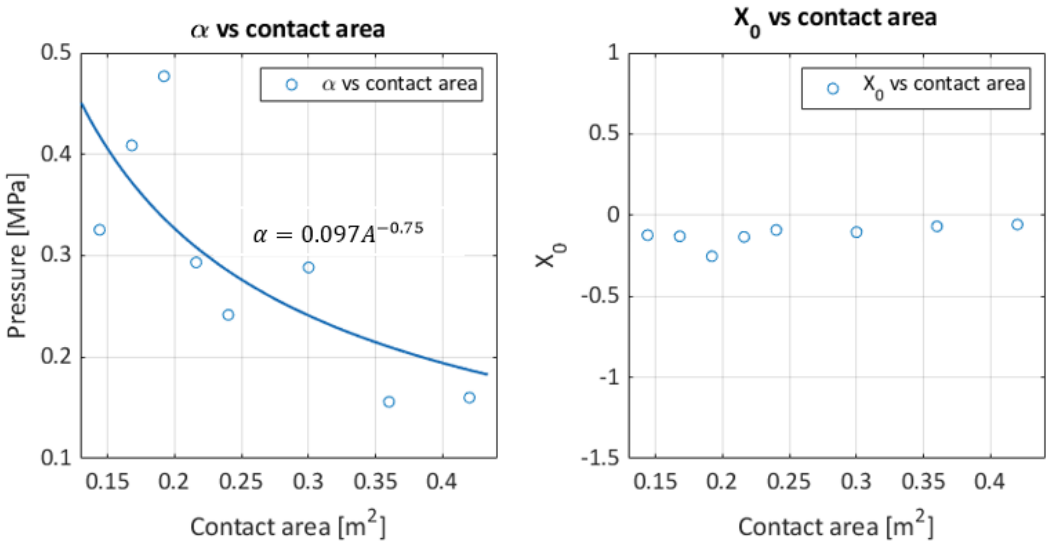

Local pressures vs contact areas at the bow shoulder for frame #112

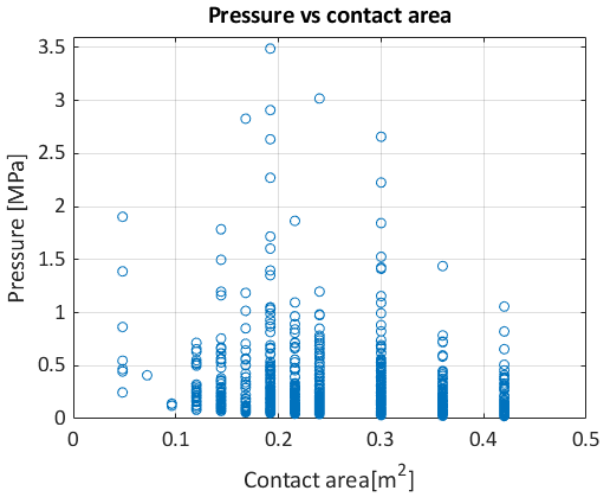

Best fitting lines for the pressures at the tail, for frame #112

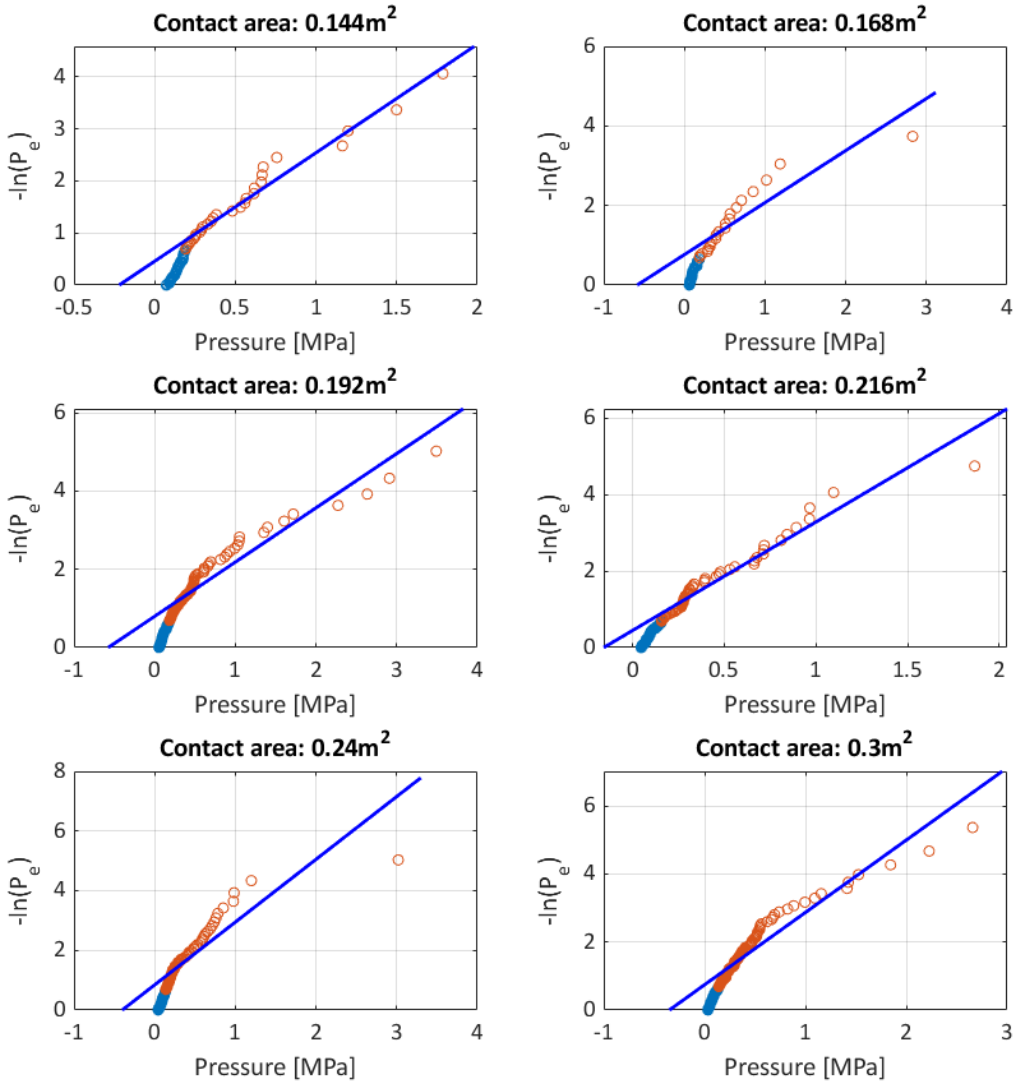

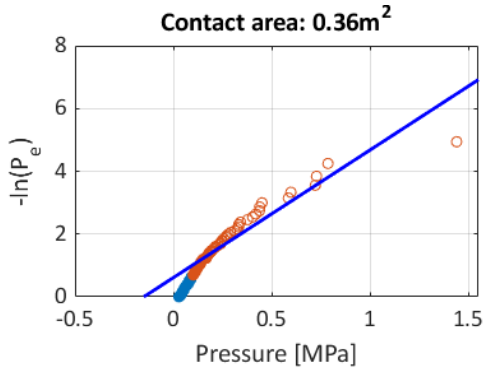

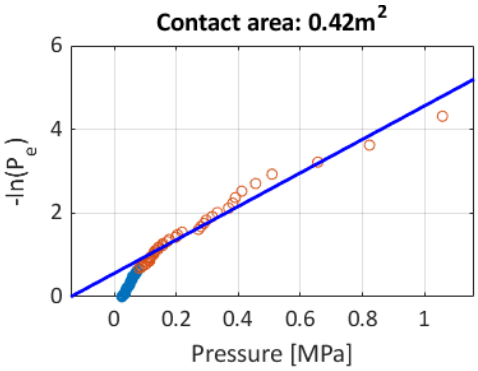

Parameters of best fitting lines to the pressures at the tail, for frame #112

Contact area [m^2]	a	b	α [MPa]	X_0 [MPa]
0.144	2.084	0.458	-0.220	0.480
0.168	1.308	0.765	-0.585	0.764
0.192	1.388	0.799	-0.576	0.721
0.216	2.841	0.447	-0.157	0.352
0.240	2.104	0.844	-0.401	0.475
0.300	2.128	0.744	-0.349	0.470
0.360	4.070	0.611	-0.150	0.246
0.420	4.002	0.561	-0.140	0.250

The α-area curve and X_0 versus contact for frame #112

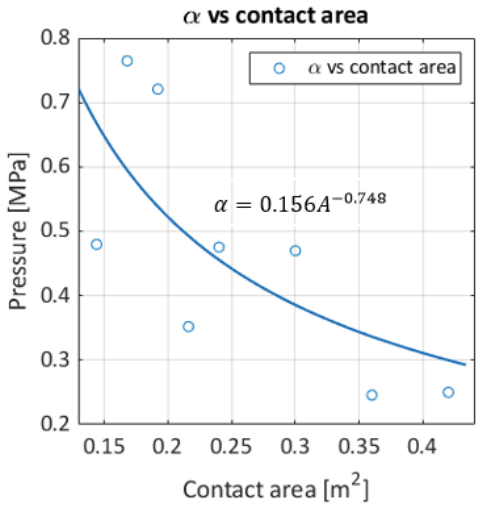

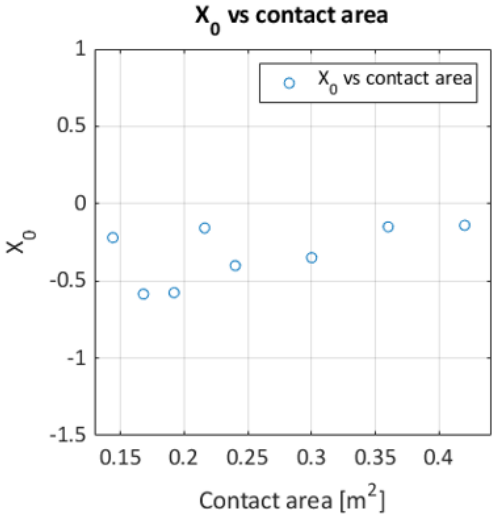

Local pressures vs contact areas at the bow shoulder for frames #113 and 112 ½

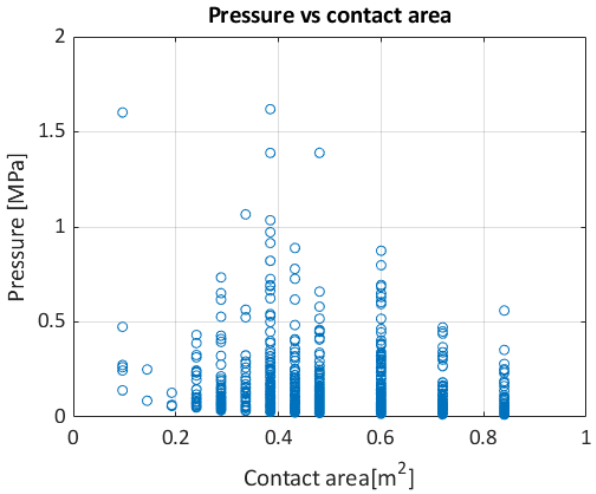

Best fitting lines for the pressures at the tail, for frames #113 and 112 ½

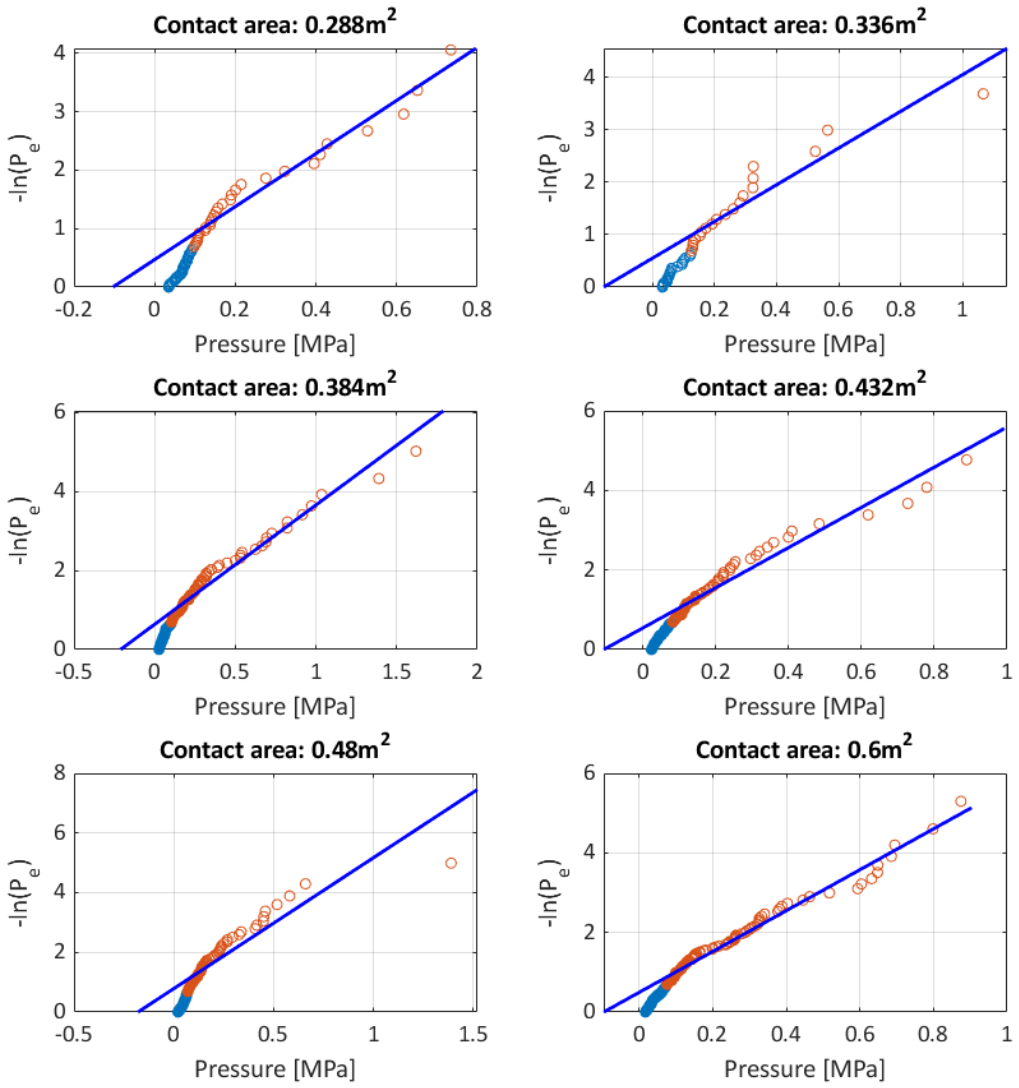

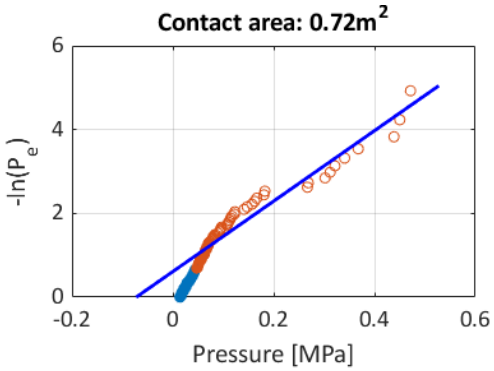

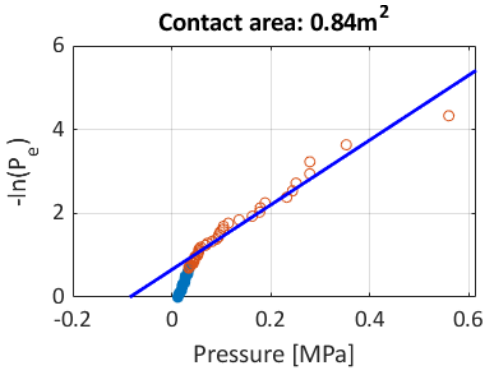

Parameters of best fitting lines to the pressures at the tail, for frames #113 and 112 ½

Contact area $[m^2]$	a	b	α [MPa]	X_0 [MPa]
0.288	4.540	0.470	-0.104	0.220
0.336	3.505	0.551	-0.157	0.285
0.384	3.022	0.639	-0.211	0.331
0.432	5.050	0.544	-0.108	0.198
0.480	4.385	0.786	-0.179	0.228
0.600	5.136	0.496	-0.097	0.195
0.720	8.410	0.611	-0.073	0.119
0.840	7.733	0.654	-0.085	0.129

The α-area curve and X_0 versus contact for frames #113 and 112 ½

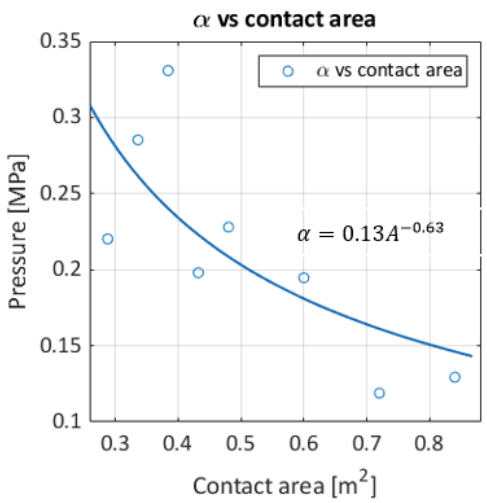

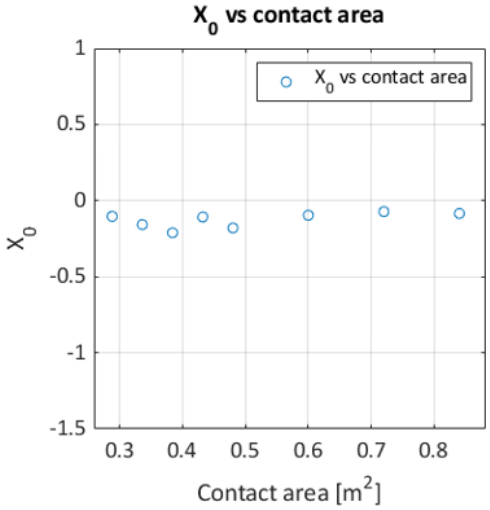

Local pressures vs contact areas at the bow shoulder for frames # 112 ½ and 112

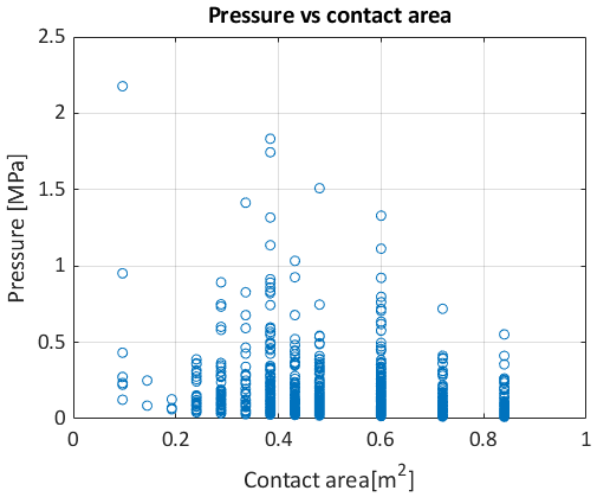

Best fitting lines for the pressures at the tail, for frames # 112 ½ and 112

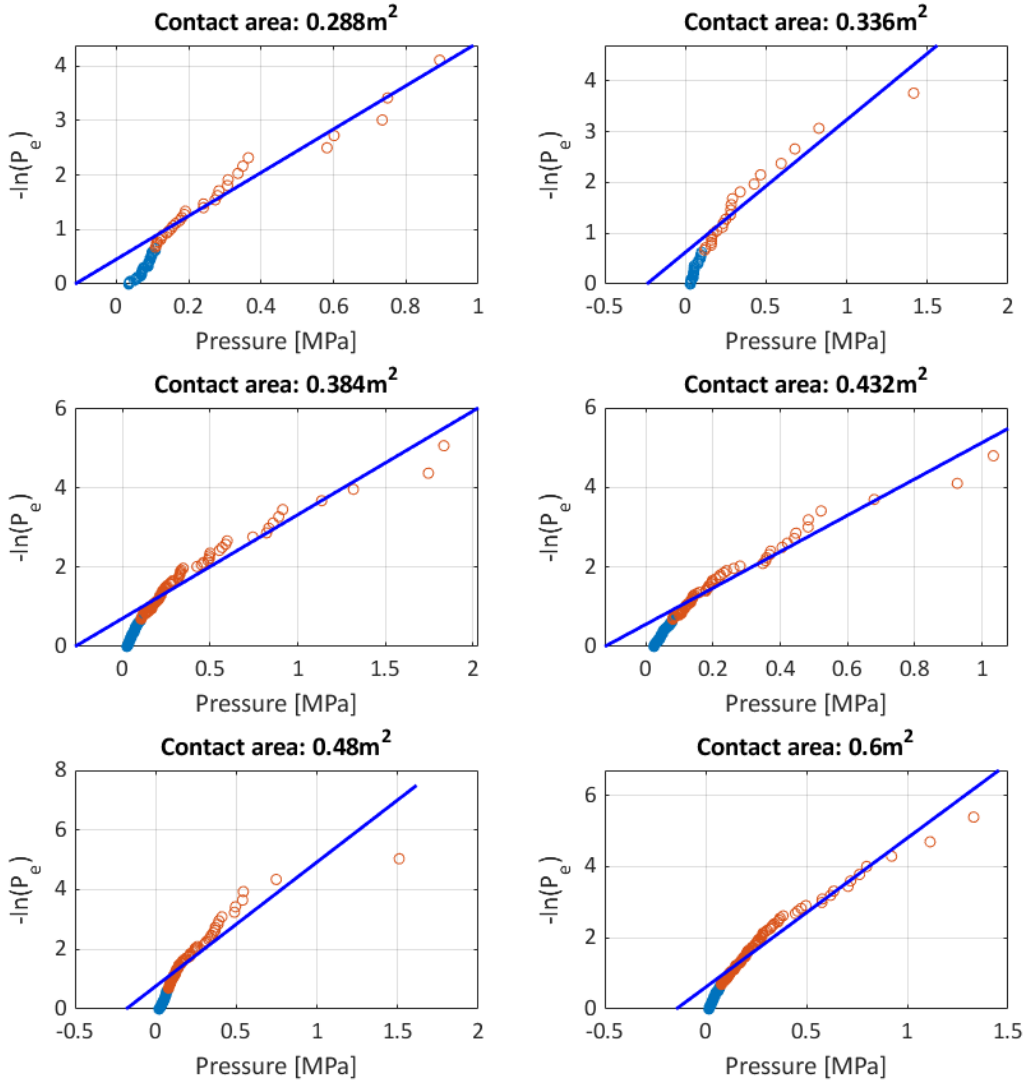

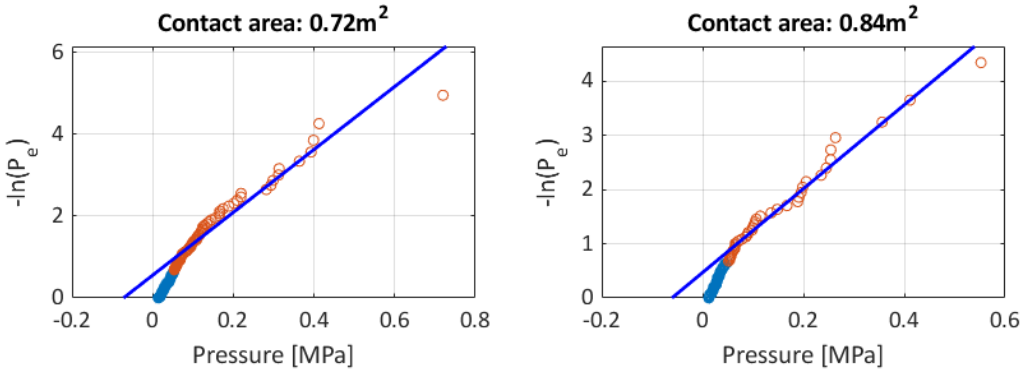

Parameters of best fitting lines to the pressures at the tail, for frames # 112 ½ and 112

Contact area $[m^2]$	a	b	α [MPa]	X_0 [MPa]
0.288	3.984	0.454	-0.114	0.251
0.336	2.612	0.625	-0.239	0.383
0.384	2.616	0.707	-0.270	0.382
0.432	4.566	0.559	-0.122	0.219
0.480	4.163	0.763	-0.183	0.240
0.600	4.189	0.611	-0.146	0.239
0.720	7.676	0.554	-0.072	0.130
0.840	7.738	0.469	-0.061	0.129

The α-area curve and X_0 versus contact for frames # 112 ½ and 112

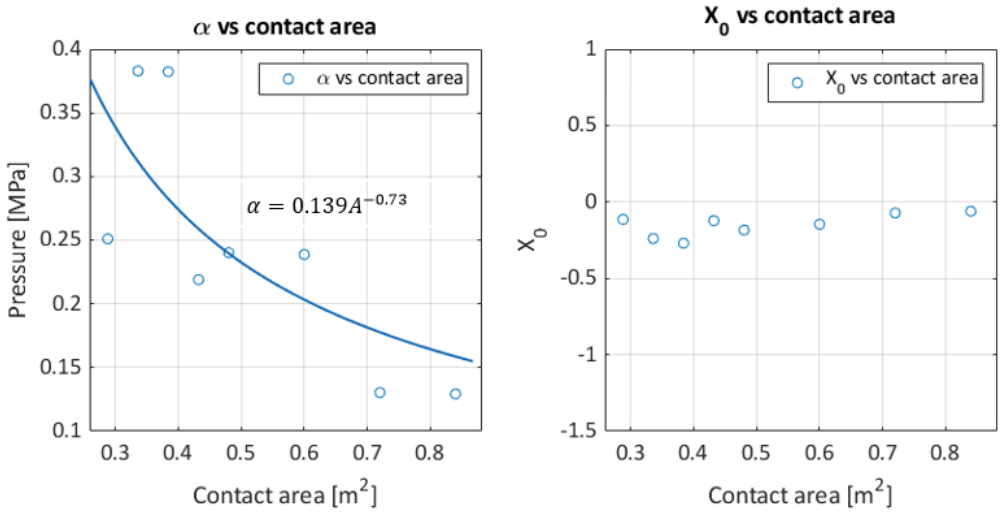

Local pressures vs contact areas at the bow shoulder for frames #113, 112 ½, and 112

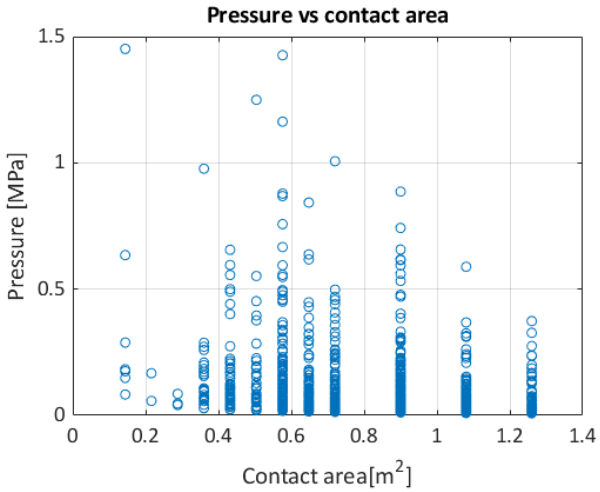

Best fitting lines for the pressures at the tail, for frames #113, 112 ½, and 112

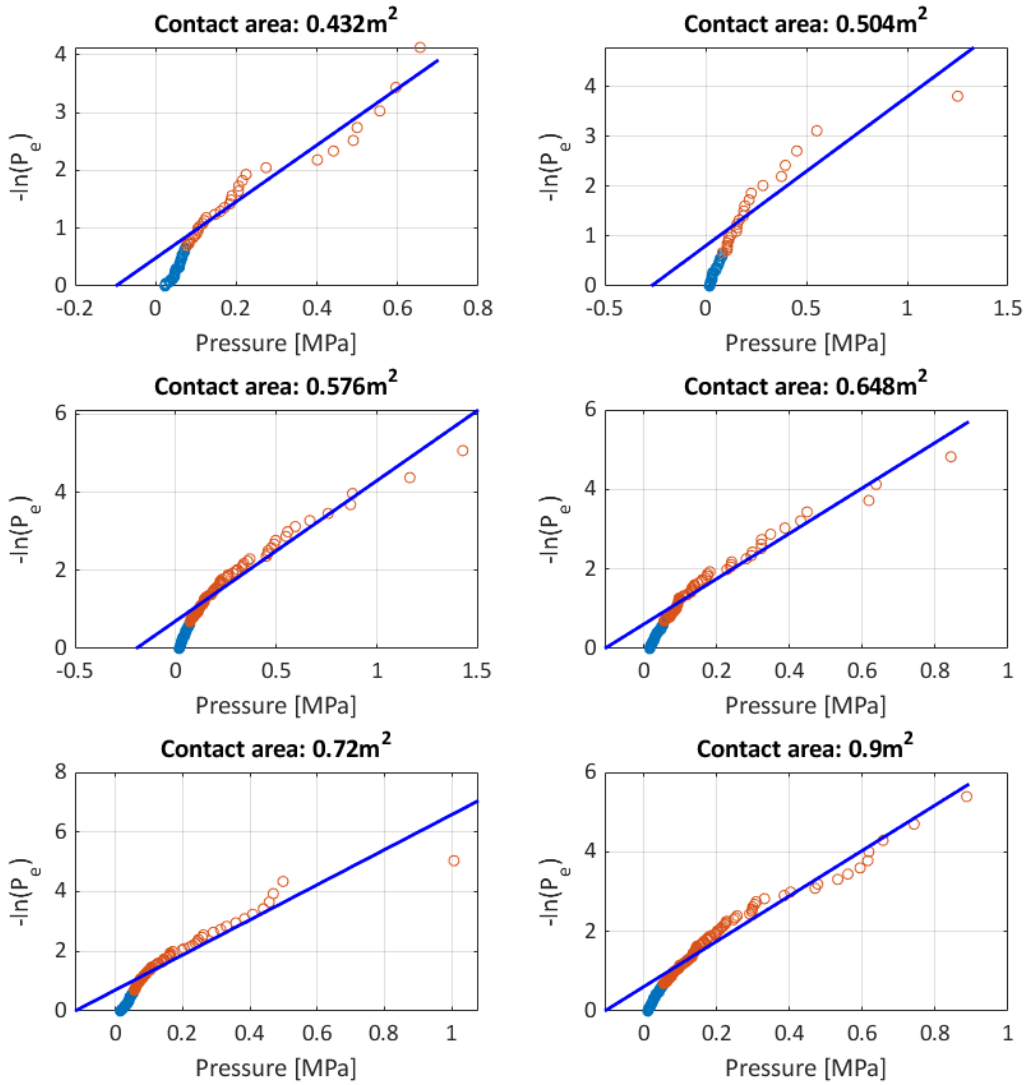

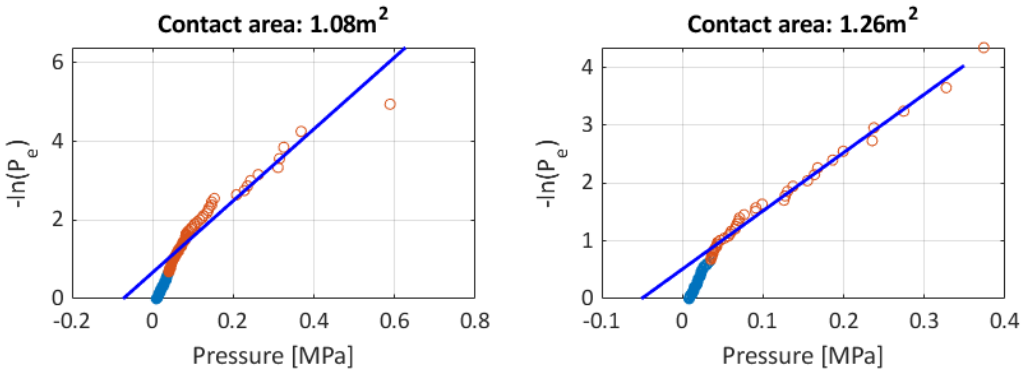

Parameters of best fitting lines to the pressures at the tail, for frames #113, 112 ½, and 112

Contact area $[m^2]$	a	b	α [MPa]	X_0 [MPa]
0.432	4.887	0.483	-0.099	0.205
0.504	2.990	0.805	-0.269	0.334
0.576	3.594	0.706	-0.196	0.278
0.648	5.702	0.616	-0.108	0.175
0.720	5.872	0.710	-0.121	0.170
0.900	5.706	0.611	-0.107	0.175
1.080	9.123	0.669	-0.073	0.110
1.260	10.083	0.513	-0.051	0.099

The α-area curve and X_0 versus contact for frames #113, 112 ½, and 112

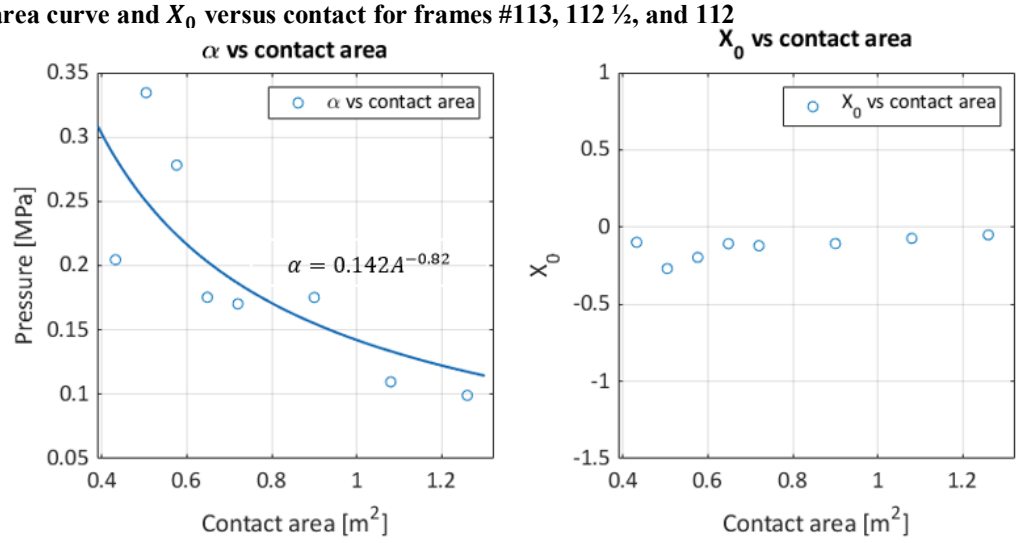

Local pressures vs contact areas at the stern shoulder for frame #41

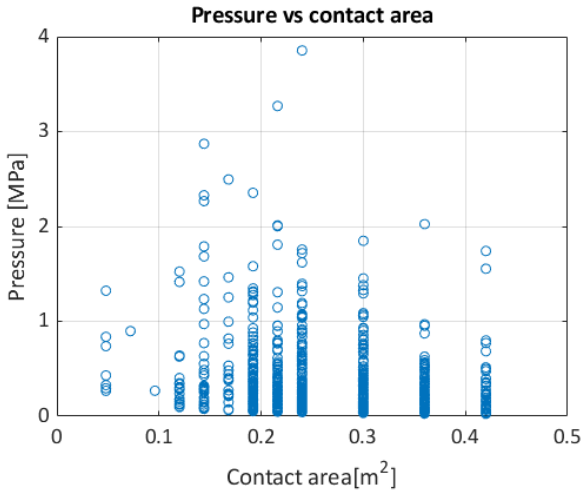

Best fitting lines for the pressures at the tail, for frame #41

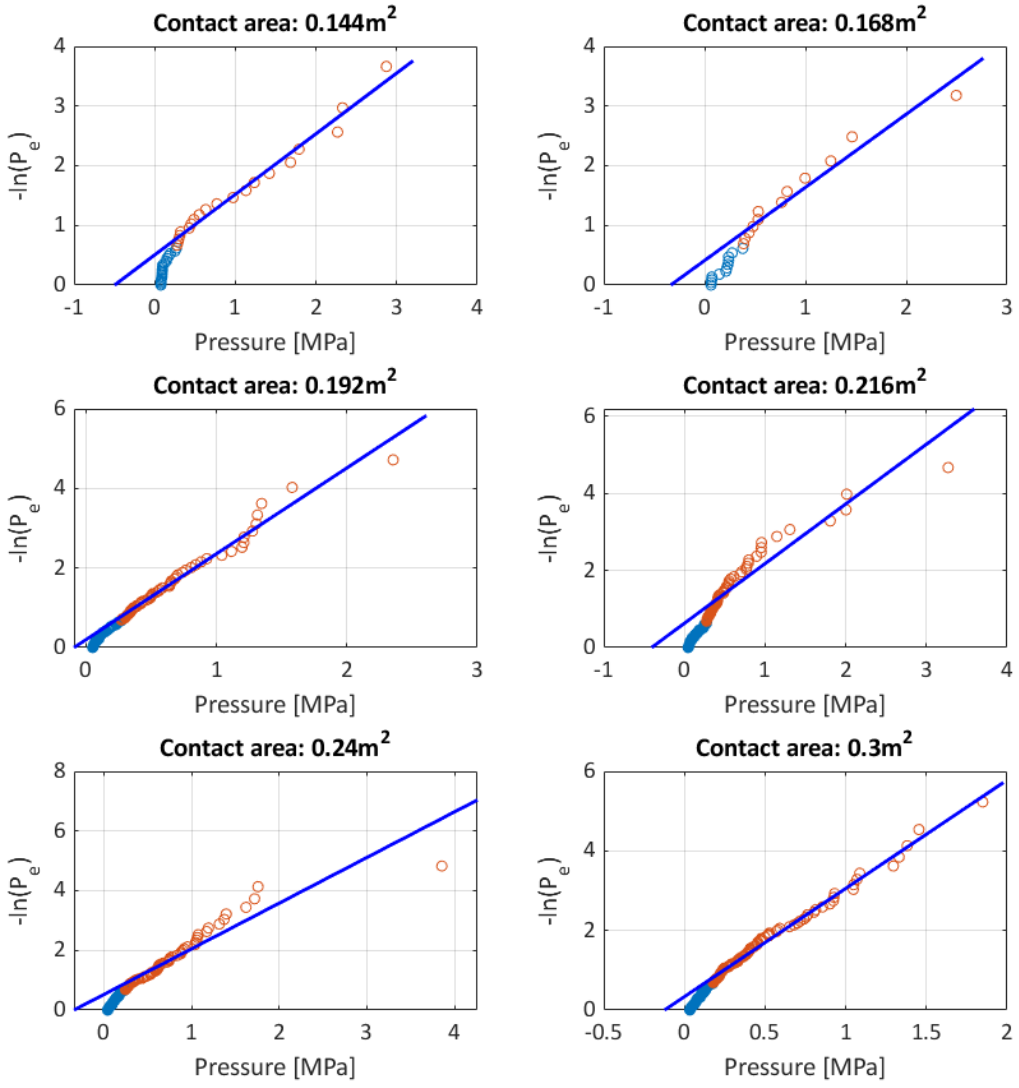

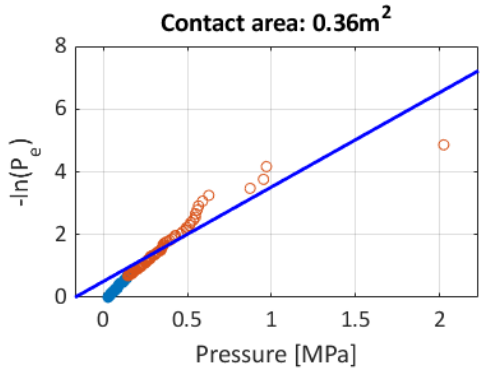

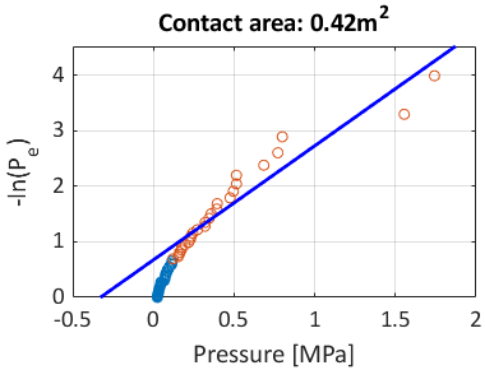

Parameters of best fitting lines to the pressures at the tail, for frame #41

Contact area [m^2]	a	b	α [MPa]	X_0 [MPa]
0.144	1.016	0.505	-0.497	0.984
0.168	1.226	0.411	-0.336	0.816
0.192	2.160	0.196	-0.091	0.463
0.216	1.549	0.630	-0.407	0.646
0.240	1.531	0.521	-0.340	0.653
0.300	2.723	0.335	-0.123	0.367
0.360	3.008	0.509	-0.169	0.332
0.420	2.054	0.674	-0.328	0.487

The α-area curve and X_0 versus contact area for frame #41

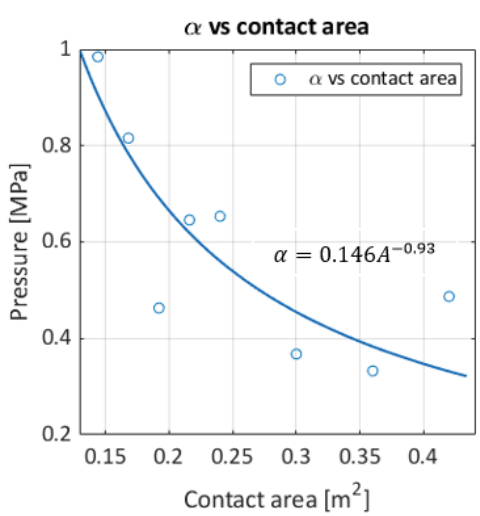

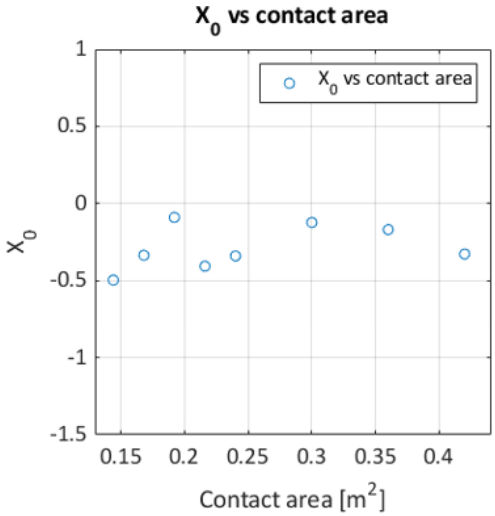

Local pressures vs contact areas at the stern shoulder for frame #40 ½

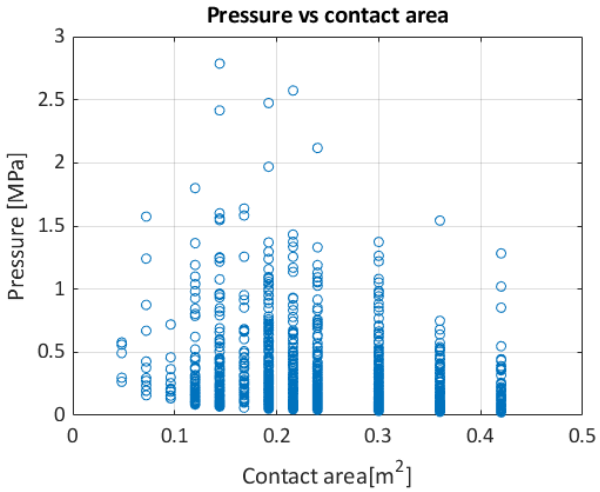

Best fitting lines for the pressures at the tail, for frame #40 ½

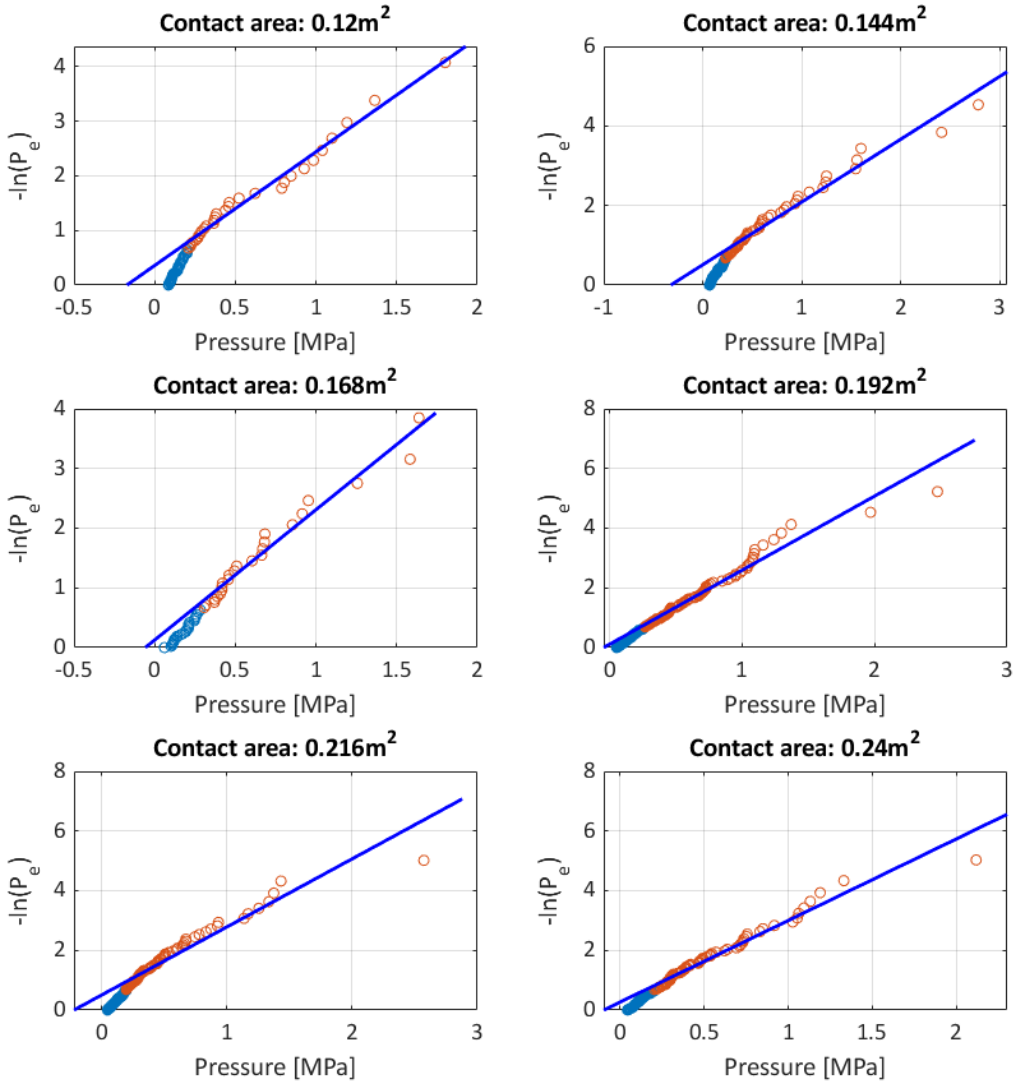

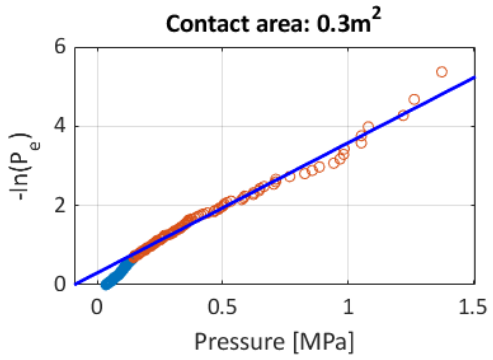

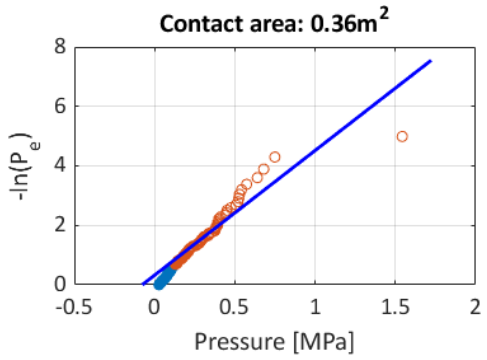

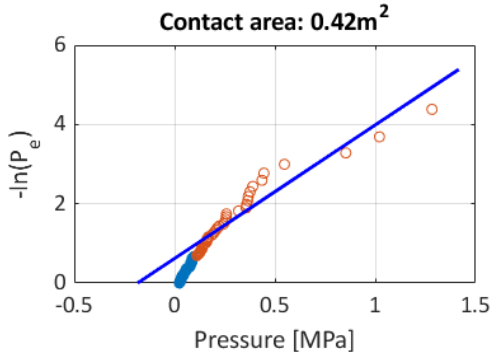

Parameters of best fitting lines to the pressures at the tail, for frame #40 ½

Contact area $[m^2]$	a	b	α [MPa]	X_0 [MPa]
0.120	2.083	0.359	-0.172	0.480
0.144	1.577	0.509	-0.323	0.634
0.168	2.184	0.126	-0.058	0.458
0.192	2.483	0.111	-0.045	0.403
0.216	2.282	0.503	-0.221	0.438
0.240	2.734	0.268	-0.098	0.366
0.300	3.281	0.301	-0.092	0.305
0.360	4.195	0.323	-0.077	0.238
0.420	3.368	0.620	-0.184	0.297

The α-area curve and X_0 versus contact area for frame #40 ½

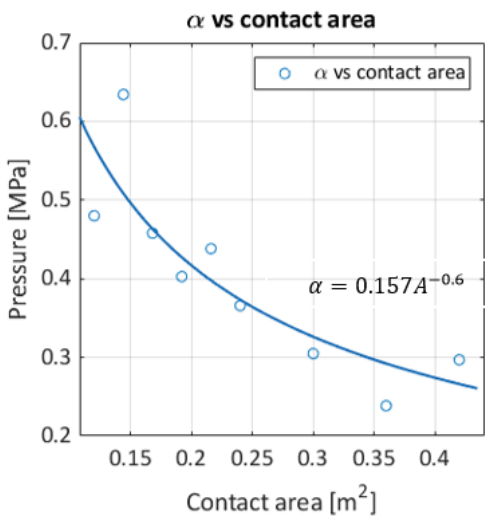

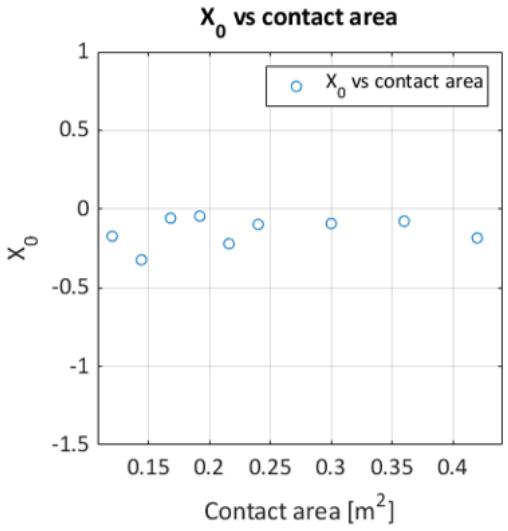

Local pressures vs contact areas at the stern shoulder for frame #40

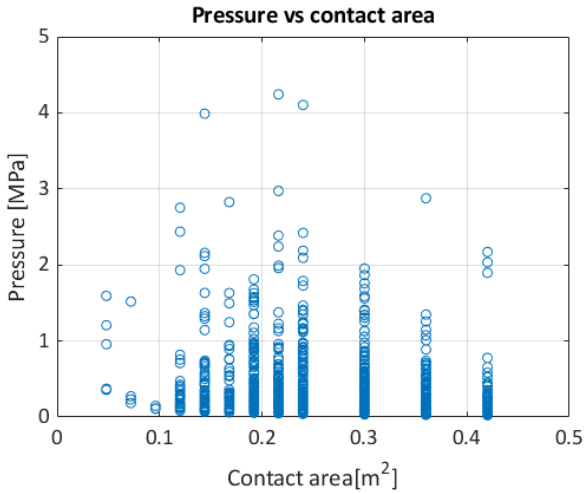

Best fitting lines for the pressures at the tail, for frame #40

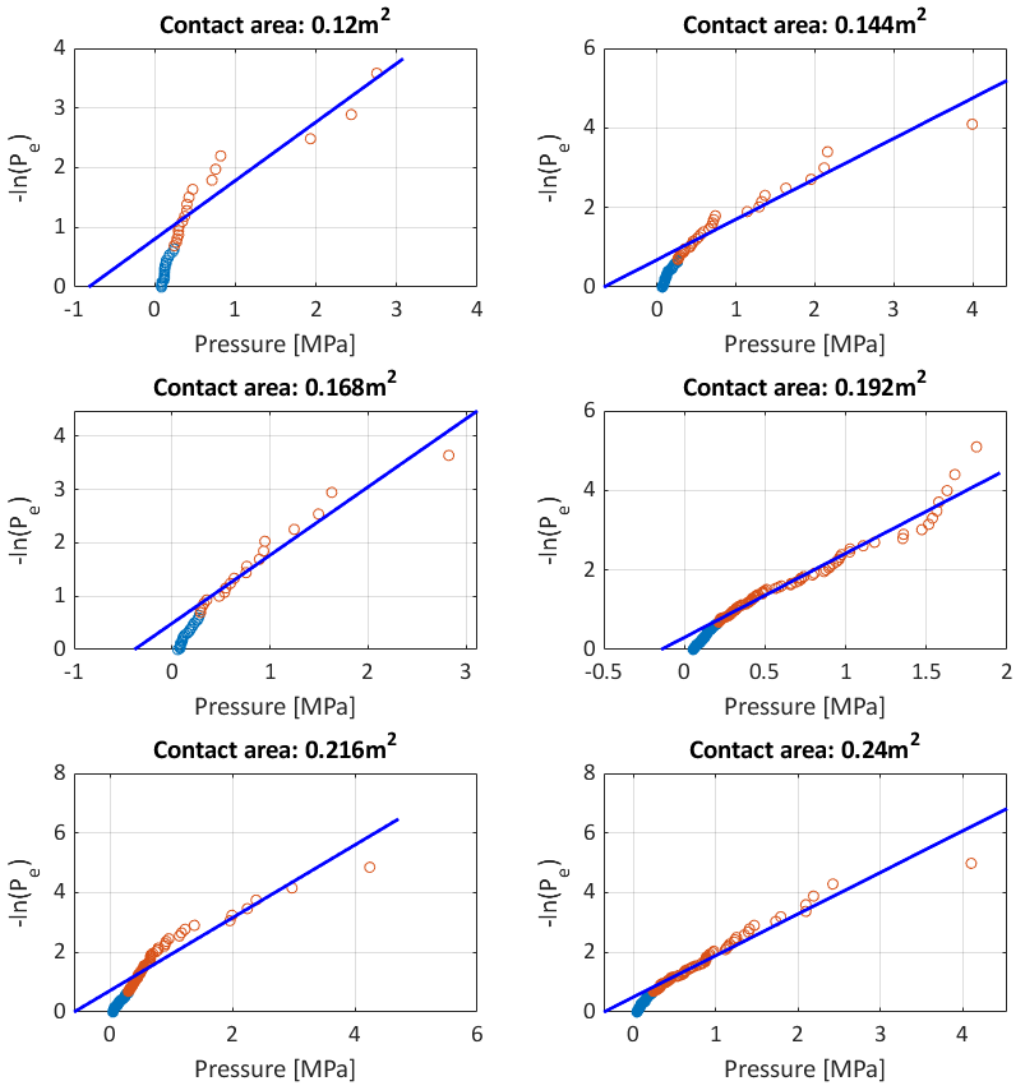

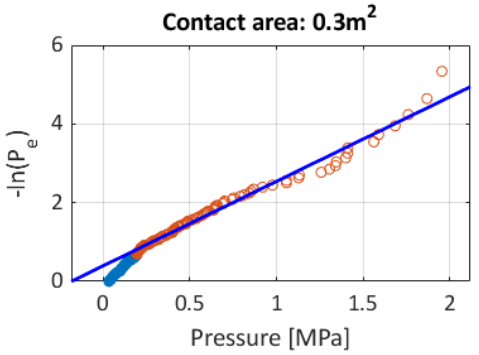

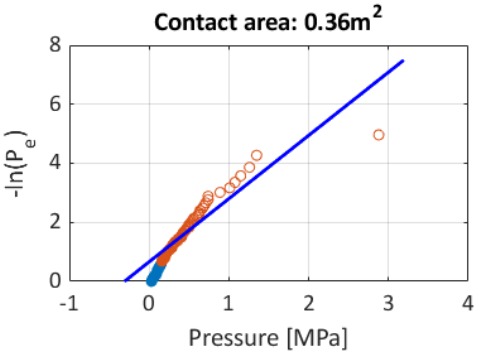

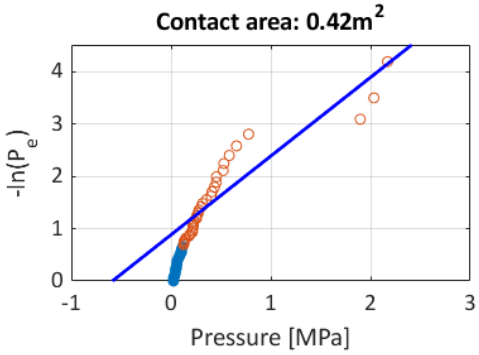

Parameters of best fitting lines to the pressures at the tail, for frame #40

Contact area [m^2]	a	b	α [MPa]	X_0 [MPa]
0.120	0.981	0.803	-0.819	1.019
0.144	1.019	0.683	-0.671	0.982
0.168	1.278	0.489	-0.383	0.783
0.192	2.114	0.305	-0.144	0.473
0.216	1.221	0.719	-0.589	0.819
0.240	1.392	0.504	-0.362	0.718
0.300	2.149	0.394	-0.183	0.465
0.360	2.142	0.662	-0.309	0.467
0.420	1.503	0.883	-0.588	0.665

The α-area curve and X_0 versus contact area for frame #40

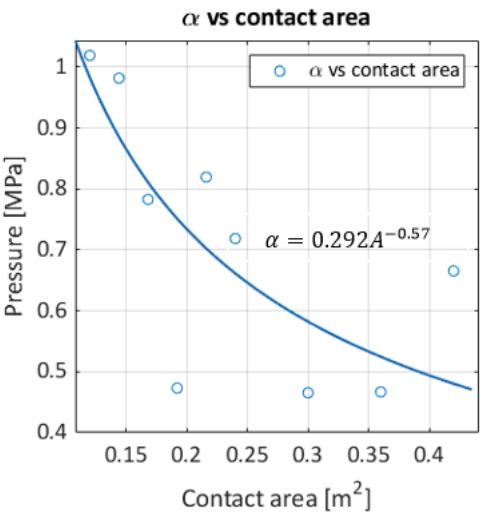

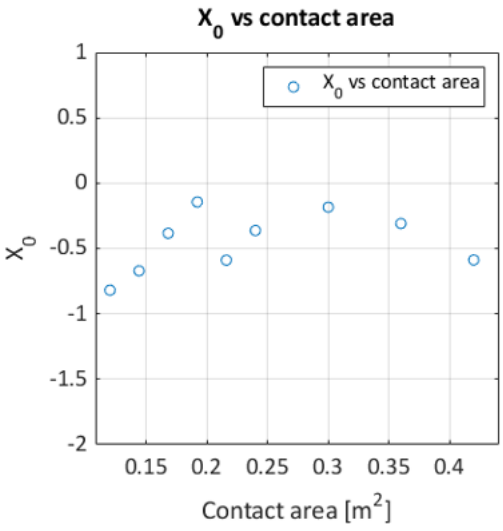

Local pressures vs contact areas at the stern shoulder for frame #39 ½

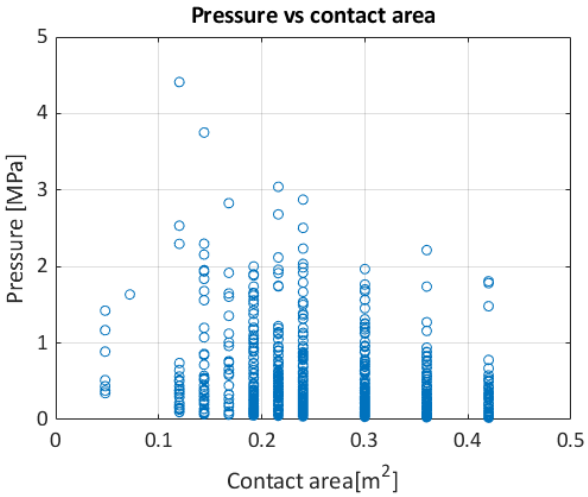

Best fitting lines for the pressures at the tail, for frame #39 ½

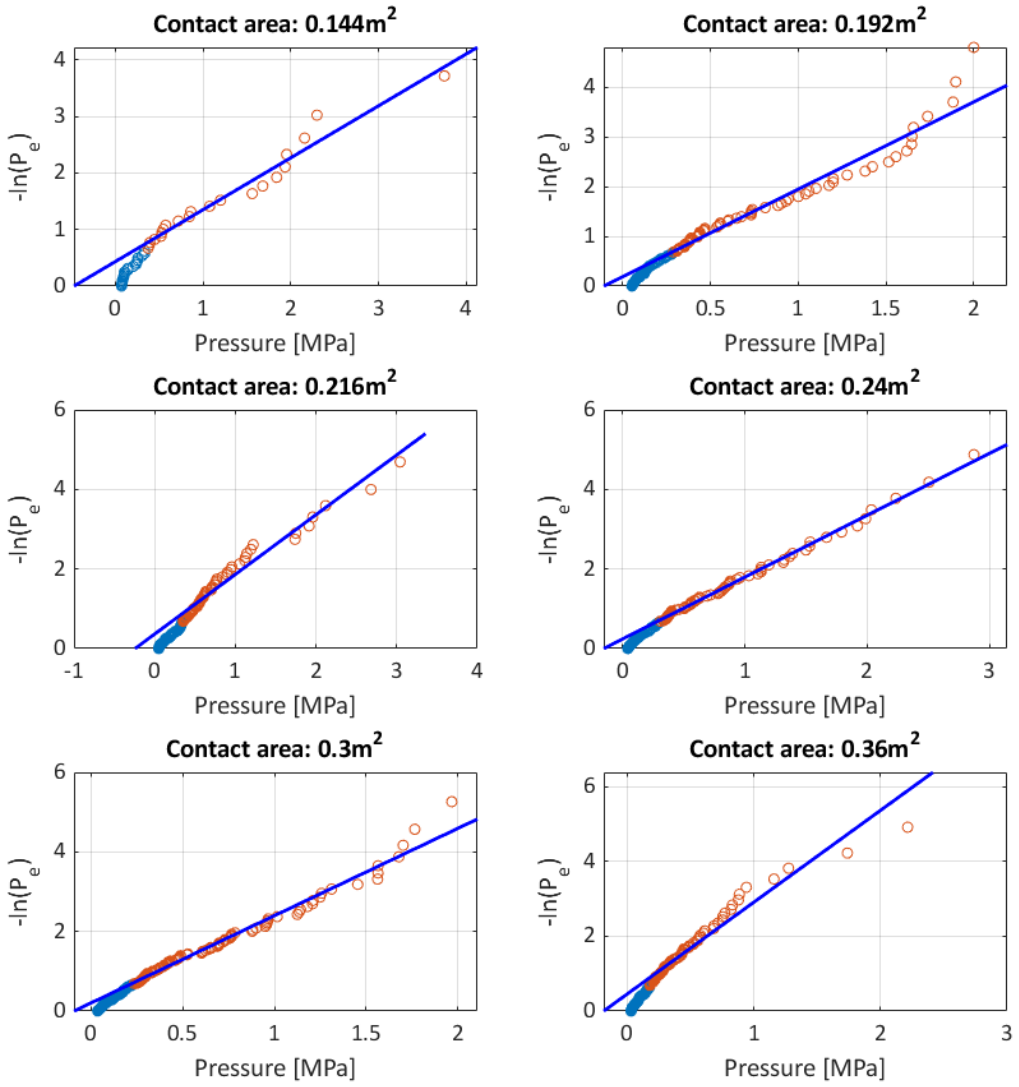

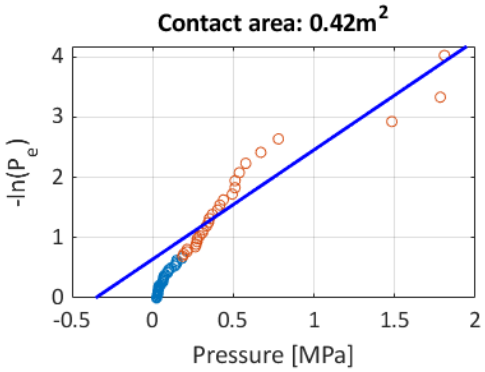

Parameters of best fitting lines to the pressures at the tail, for frame #39 ½

Contact area [m^2]	a	b	α [MPa]	X_0 [MPa]
0.144	0.917	0.434	-0.473	1.090
0.192	1.753	0.191	-0.109	0.570
0.216	1.500	0.364	-0.243	0.666
0.240	1.554	0.240	-0.155	0.643
0.300	2.193	0.205	-0.093	0.456
0.360	2.457	0.457	-0.186	0.407
0.420	1.815	0.642	-0.354	0.551

The α-area curve and X_0 versus contact area for frame #39 ½

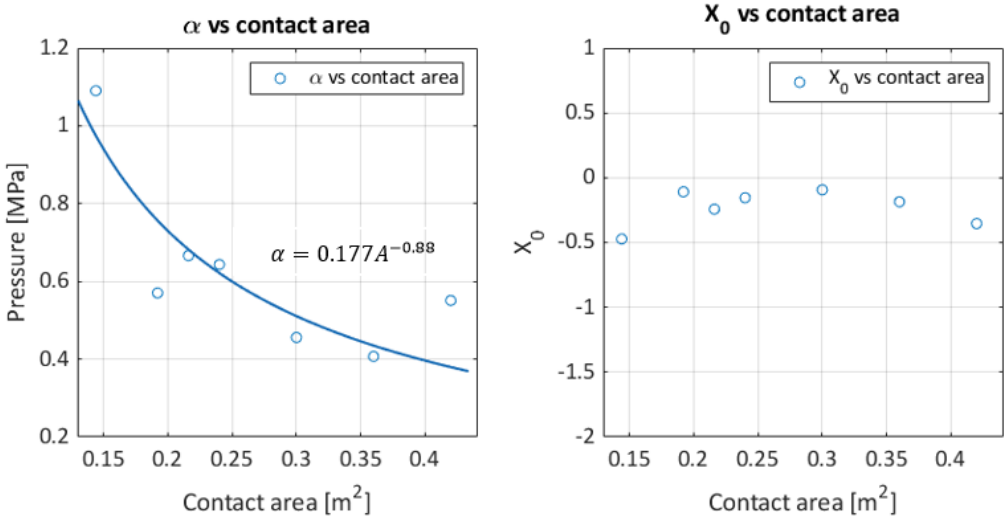

Local pressures vs contact areas at the stern shoulder for frames #41, and #40 ½

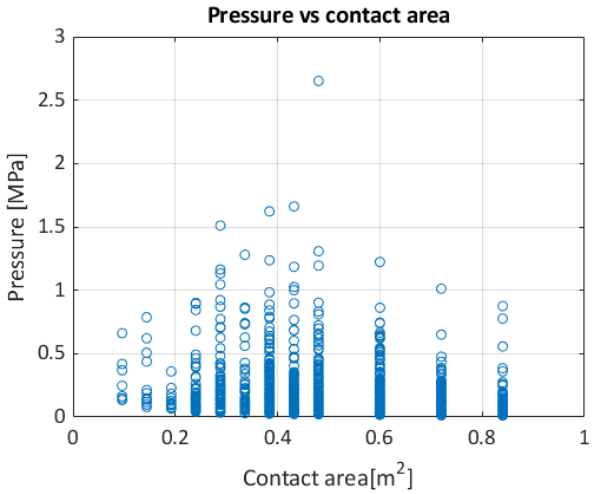

Best fitting lines for the pressures at the tail, for frames #41, and #40 ½

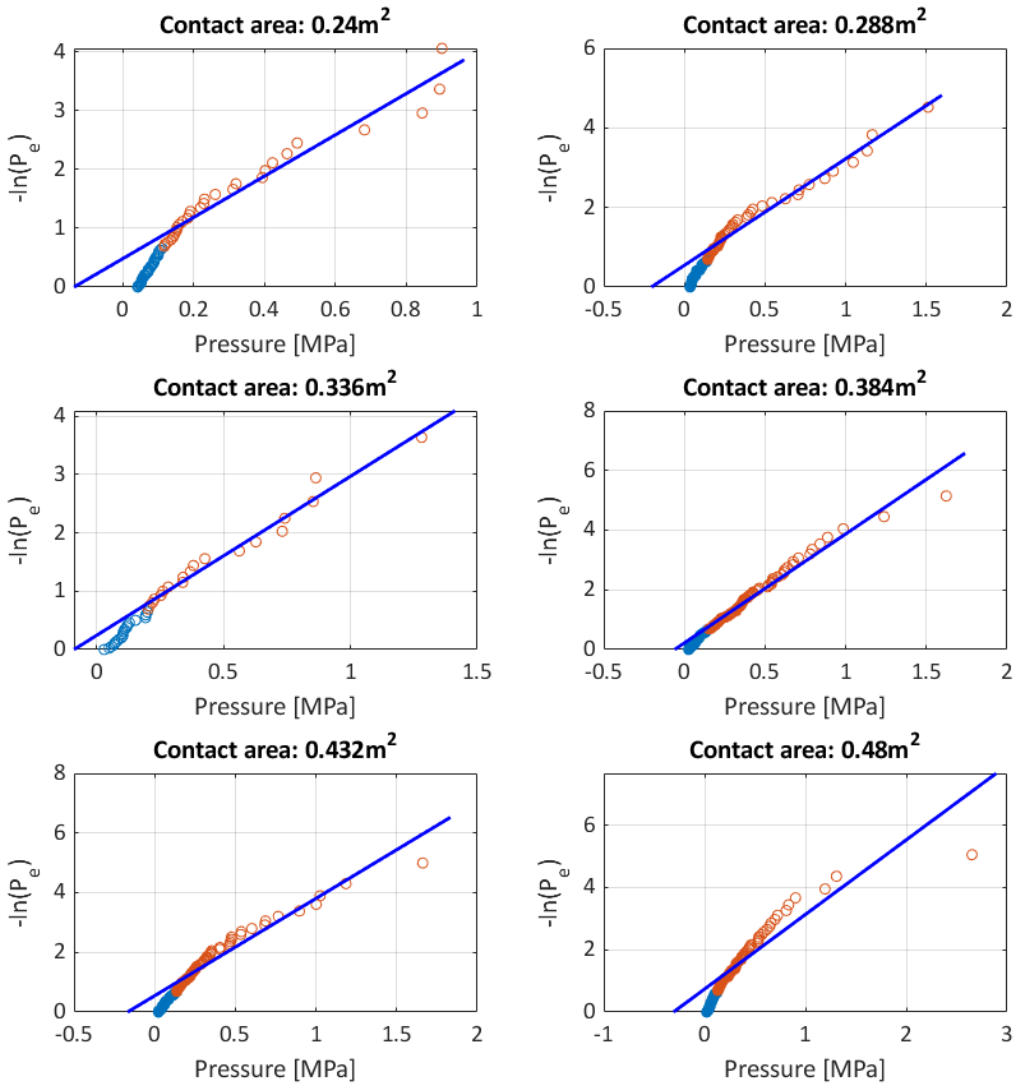

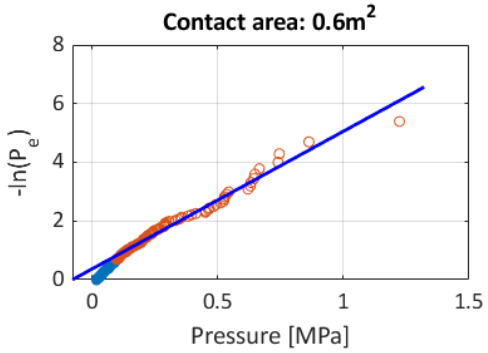

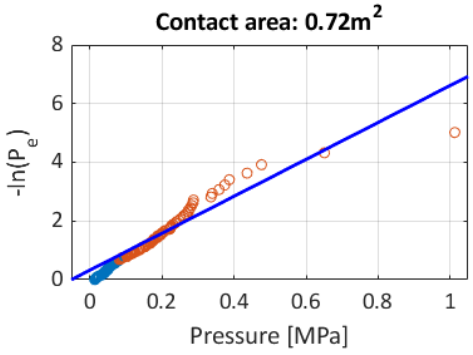

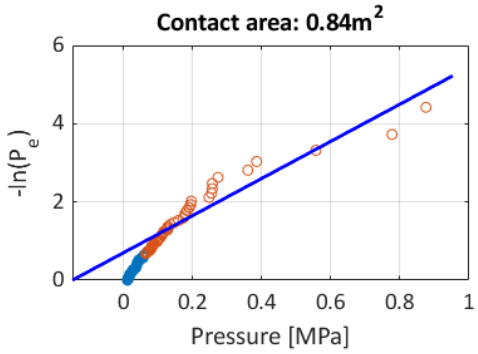

Parameters of best fitting lines to the pressures at the tail, for frames #41, and #40 ½

Contact area $[m^2]$	a	b	α [MPa]	X_0 [MPa]
0.240	3.515	0.481	-0.137	0.285
0.288	2.678	0.547	-0.204	0.373
0.336	2.729	0.241	-0.088	0.366
0.384	3.656	0.221	-0.060	0.274
0.432	3.262	0.547	-0.168	0.307
0.480	2.394	0.737	-0.308	0.418
0.600	4.688	0.370	-0.079	0.213
0.720	6.298	0.321	-0.051	0.159
0.840	4.748	0.700	-0.147	0.211

The α-area curve and X_0 versus contact area for frames #41, and #40 ½

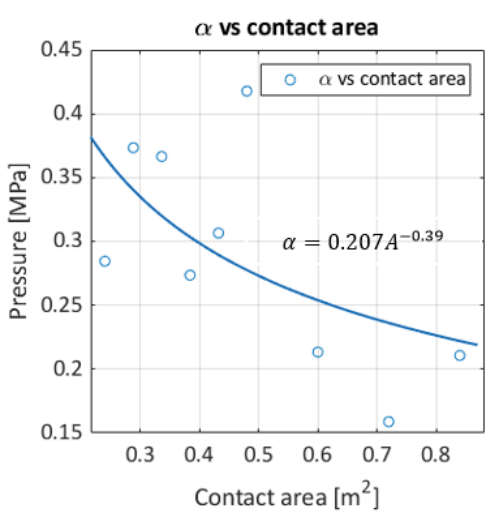

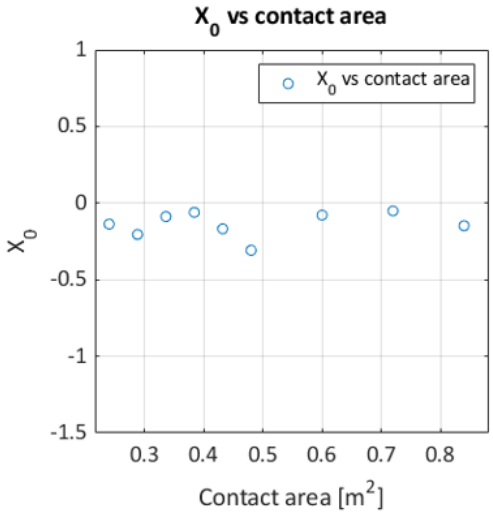

Local pressures vs contact areas at the stern shoulder for frames #40 ½ , and #40

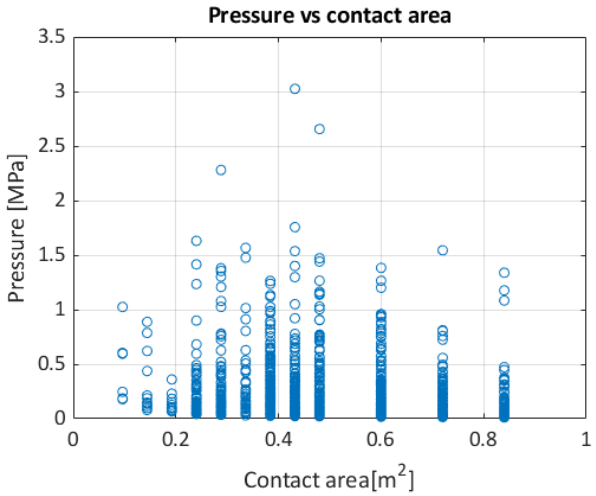

Best fitting lines for the pressures at the tail, for frames #40 ½ , and #40

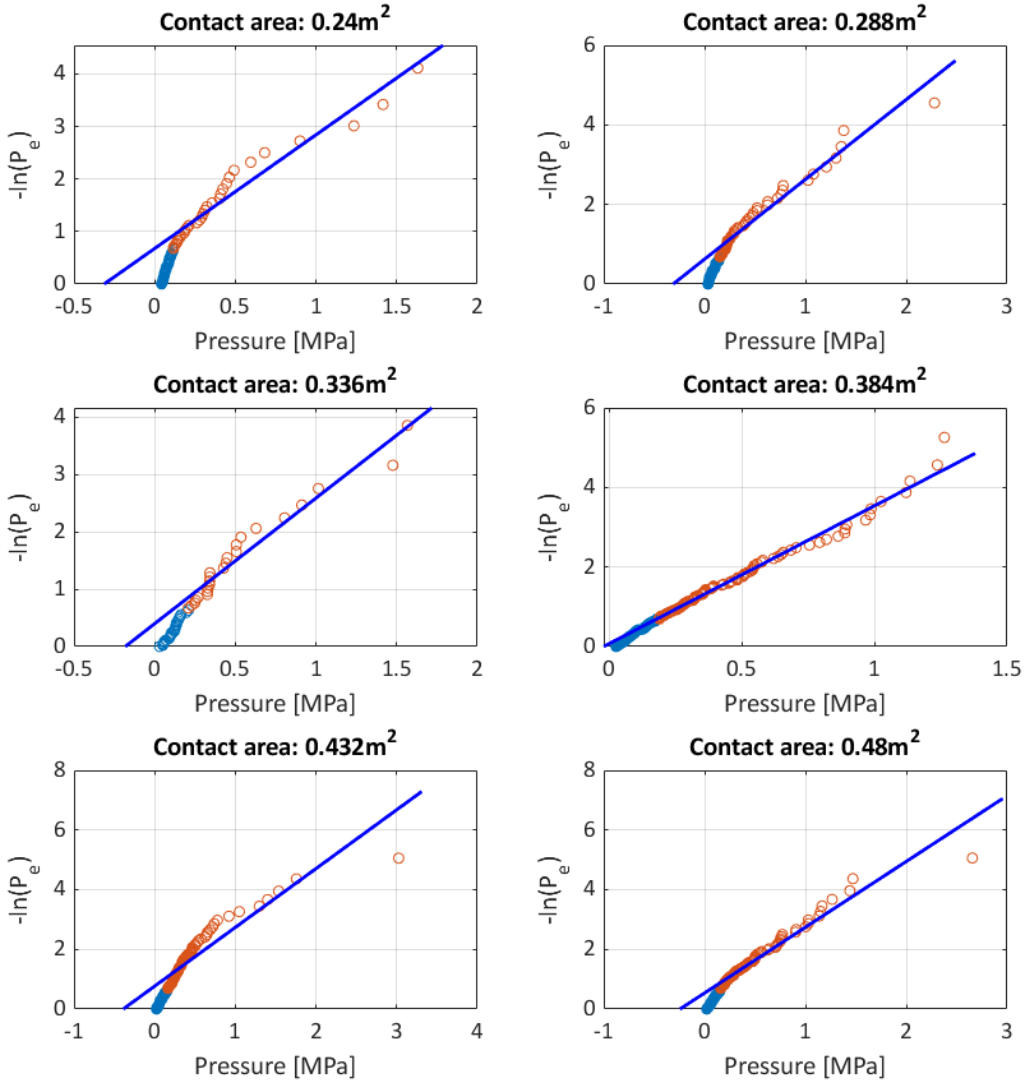

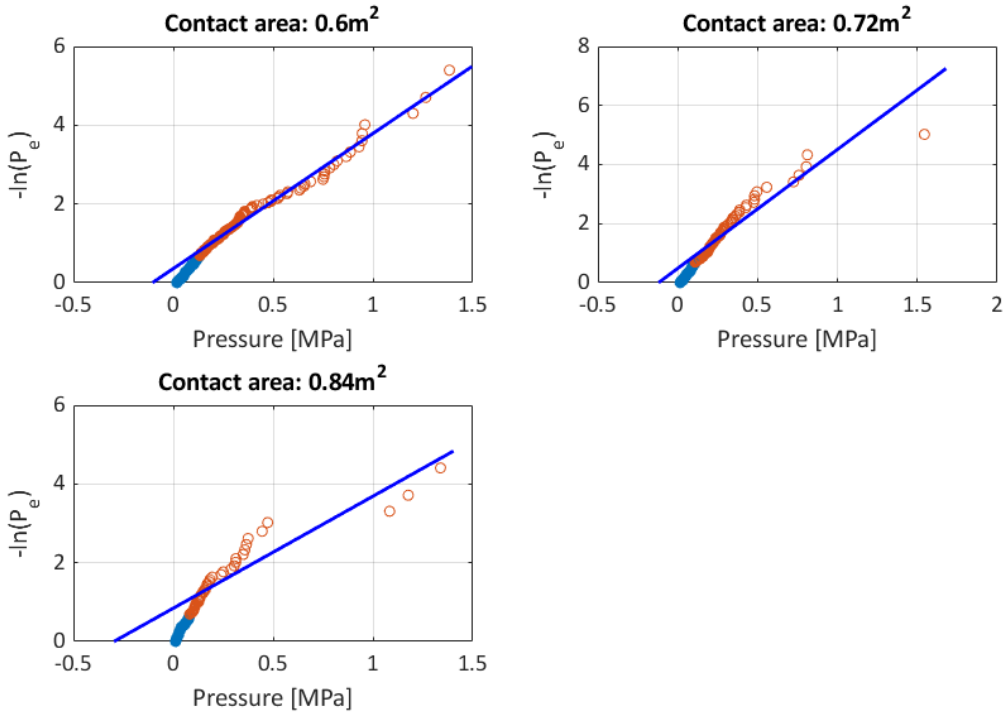

Parameters of best fitting lines to the pressures at the tail, for frames #40 ½ , and #40

Contact area [m^2]	a	b	α [MPa]	X_0 [MPa]
0.240	2.163	0.677	-0.313	0.462
0.288	2.006	0.626	-0.312	0.498
0.336	2.187	0.399	-0.182	0.457
0.384	3.468	0.071	-0.020	0.288
0.432	1.970	0.767	-0.390	0.508
0.480	2.205	0.537	-0.244	0.454
0.600	3.432	0.358	-0.104	0.291
0.720	4.029	0.485	-0.120	0.248
0.840	2.845	0.844	-0.297	0.352

The α-area curve and X_0 versus contact area for frames #40 ½ , and #40

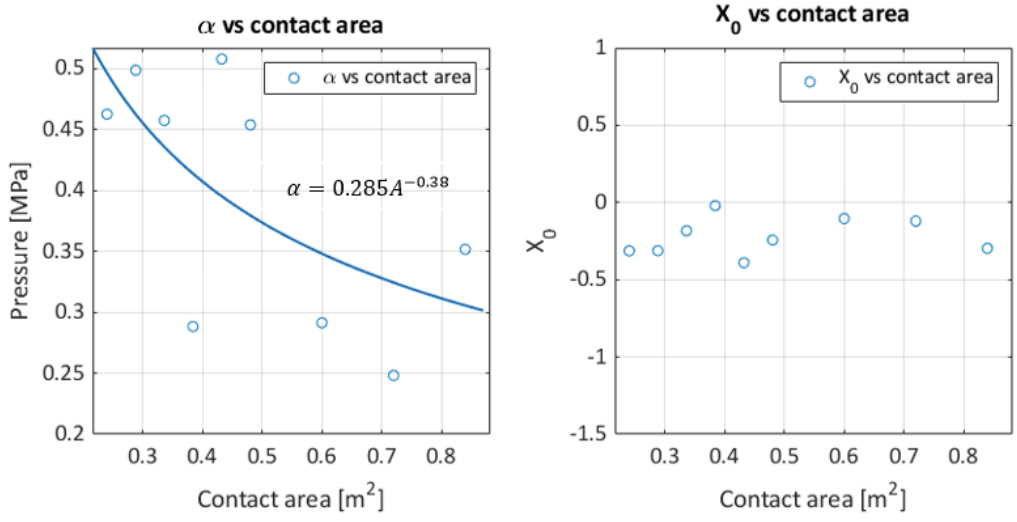

Local pressures vs contact areas at the stern shoulder for frames #40, and #39 ½

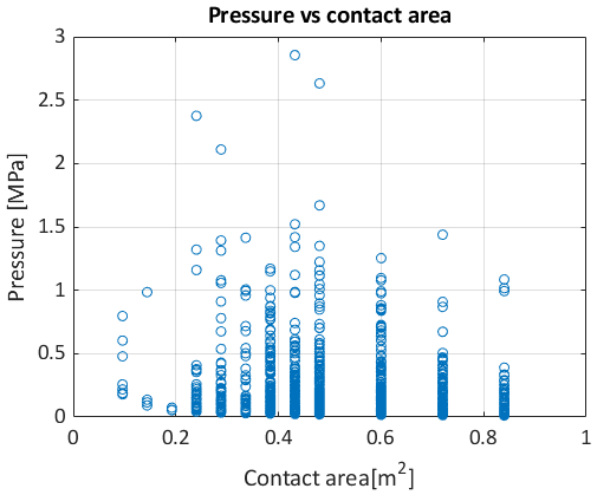

Best fitting lines for the pressures at the tail, for frames #40, # and 39 ½

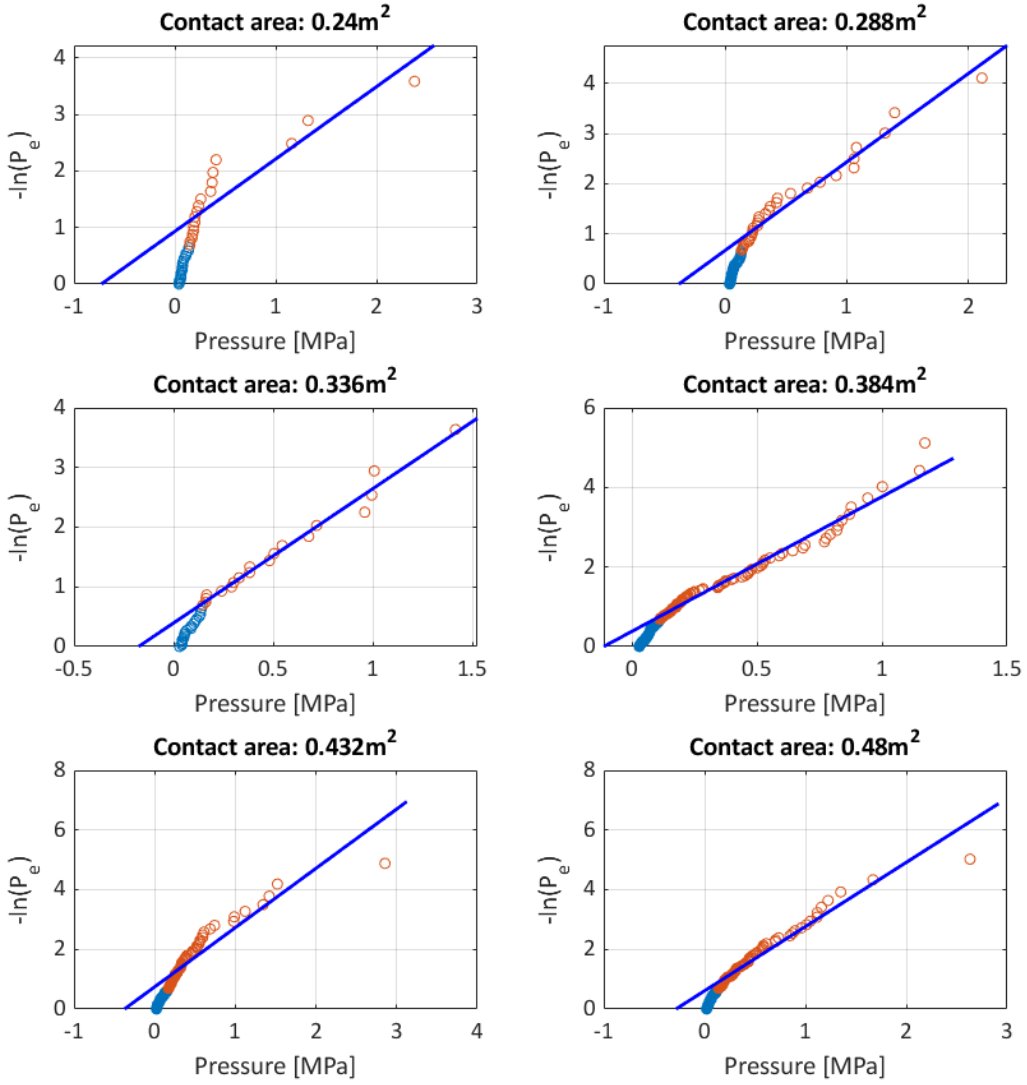

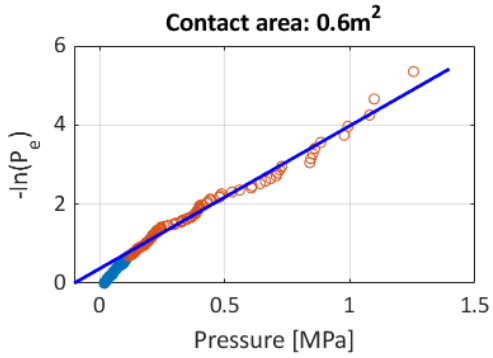

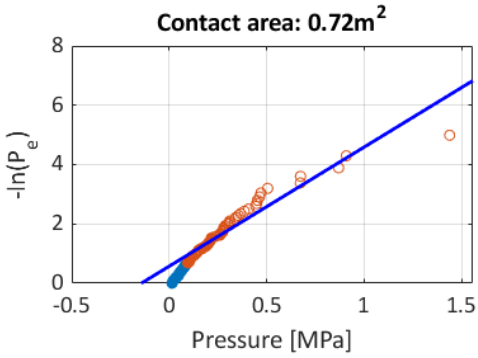

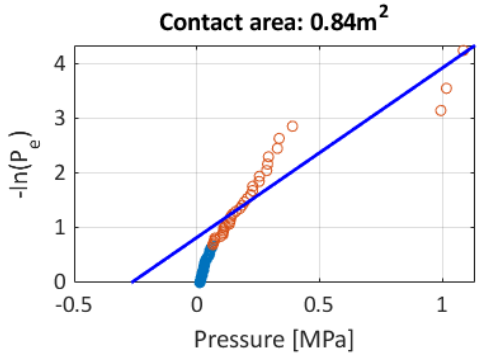

Parameters of best fitting lines to the pressures at the tail, for frames #40, # and 39 ½

Contact area $[m^2]$	a	b	α [MPa]	X_0 [MPa]
0.240	1.279	0.932	-0.729	0.782
0.288	1.763	0.674	-0.382	0.567
0.336	2.251	0.396	-0.176	0.444
0.384	3.381	0.389	-0.115	0.296
0.432	1.987	0.744	-0.374	0.503
0.480	2.152	0.611	-0.284	0.465
0.600	3.611	0.374	-0.104	0.277
0.720	4.017	0.573	-0.143	0.249
0.840	3.101	0.827	-0.267	0.322

The α-area curve and X_0 versus contact area for frames #40, # and 39 ½

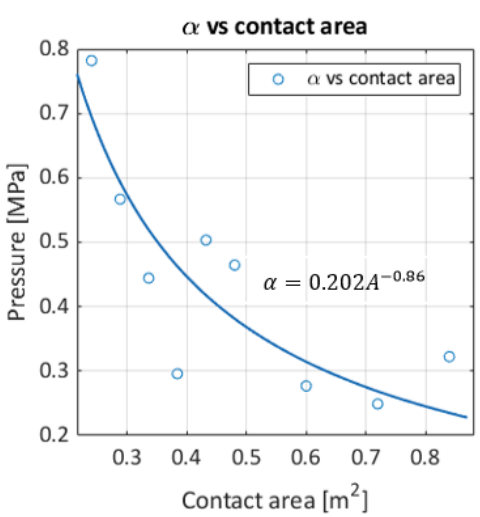

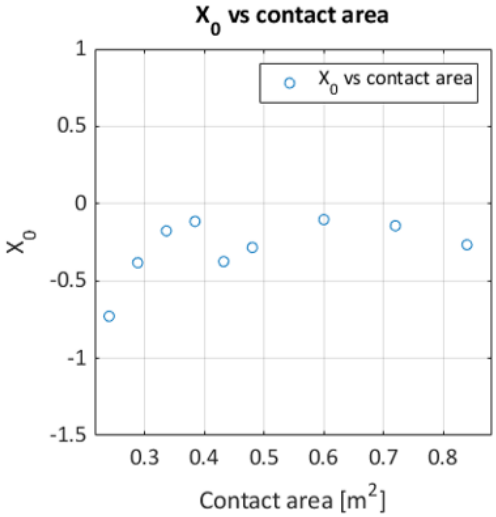

Local pressures vs contact areas at the stern shoulder for frames #41, #40 ½ , and #40

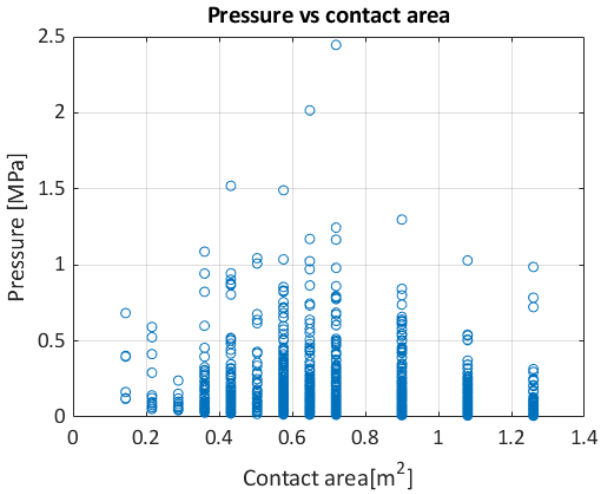

Best fitting lines for the pressures at the tail, for frames #41, #40 ½ , and #40

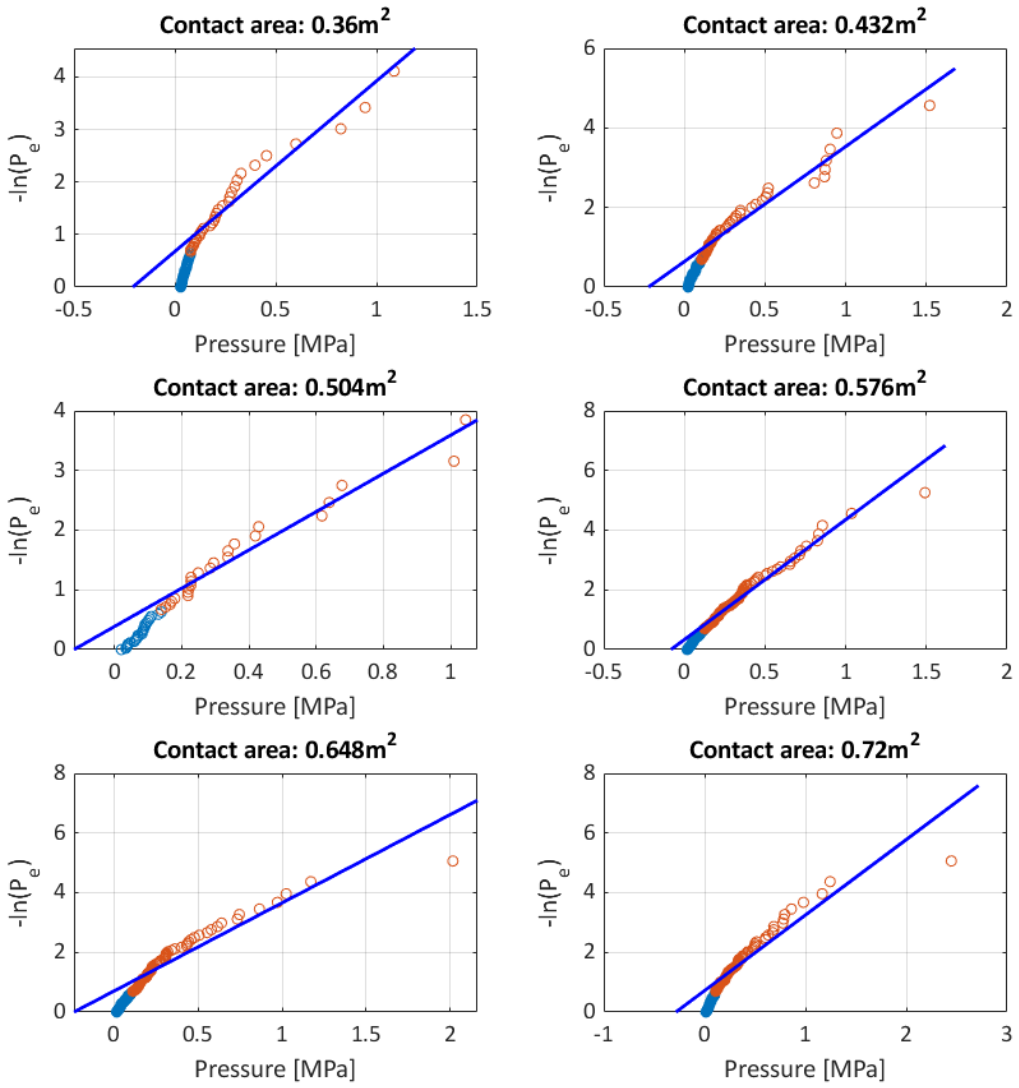

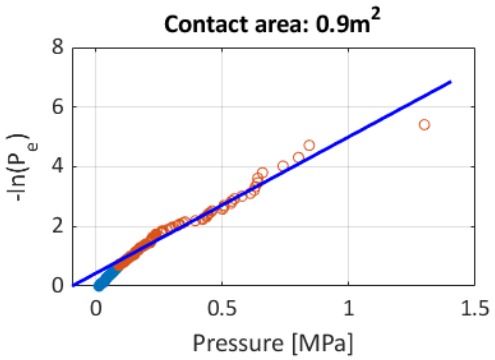

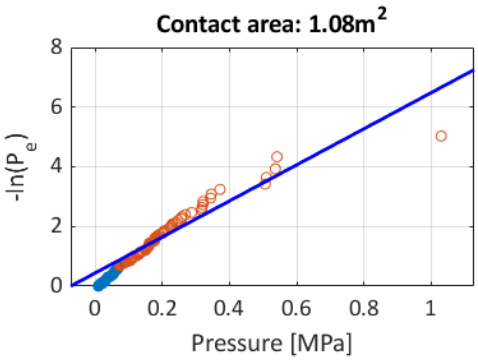

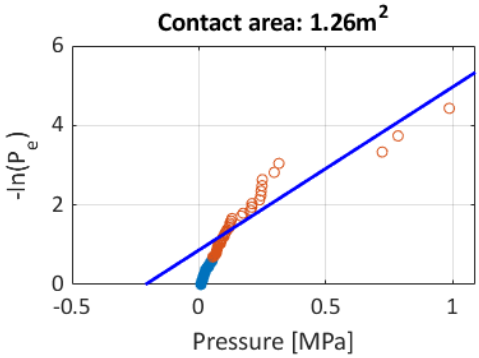

Parameters of best fitting lines to the pressures at the tail, for frames #41, #40 ½ , and #40

Contact area $[m^2]$	a	b	α [MPa]	X_0 [MPa]
0.360	3.245	0.677	-0.209	0.308
0.432	2.891	0.643	-0.222	0.346
0.504	3.206	0.387	-0.121	0.312
0.576	4.022	0.334	-0.083	0.249
0.648	2.956	0.704	-0.238	0.338
0.720	2.531	0.719	-0.284	0.395
0.900	4.572	0.436	-0.095	0.219
1.080	6.046	0.440	-0.073	0.165
1.260	4.103	0.865	-0.211	0.244

The α-area curve and X_0 versus contact area for frames #41, #40 ½ , and #40

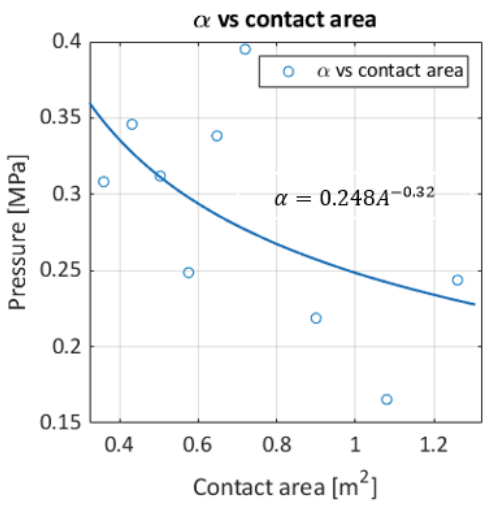

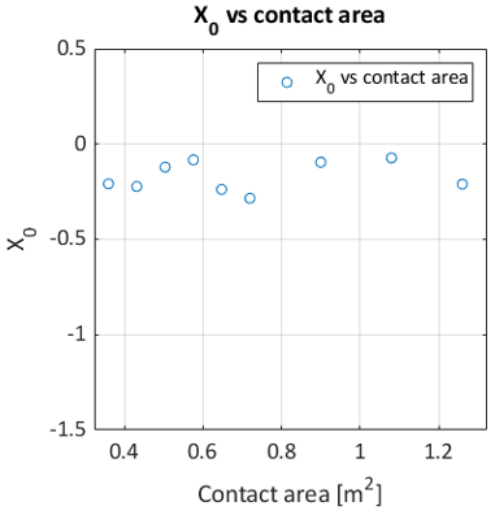

Local pressures vs contact areas at the stern shoulder for frames #40 ½ , 40, and #39 ½

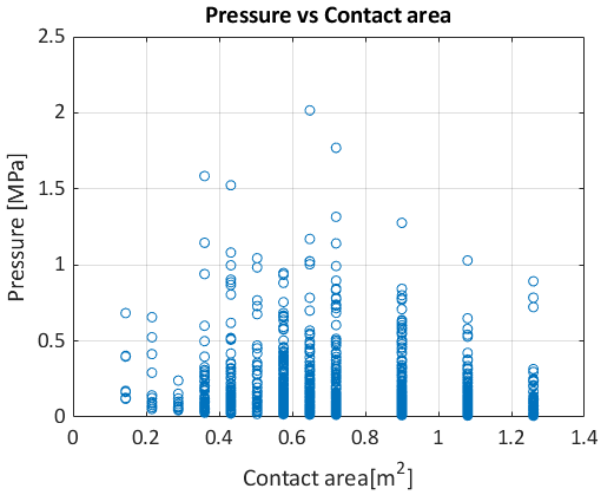

Best fitting lines for the pressures at the tail, for frames #40 ½ , 40, and #39 ½

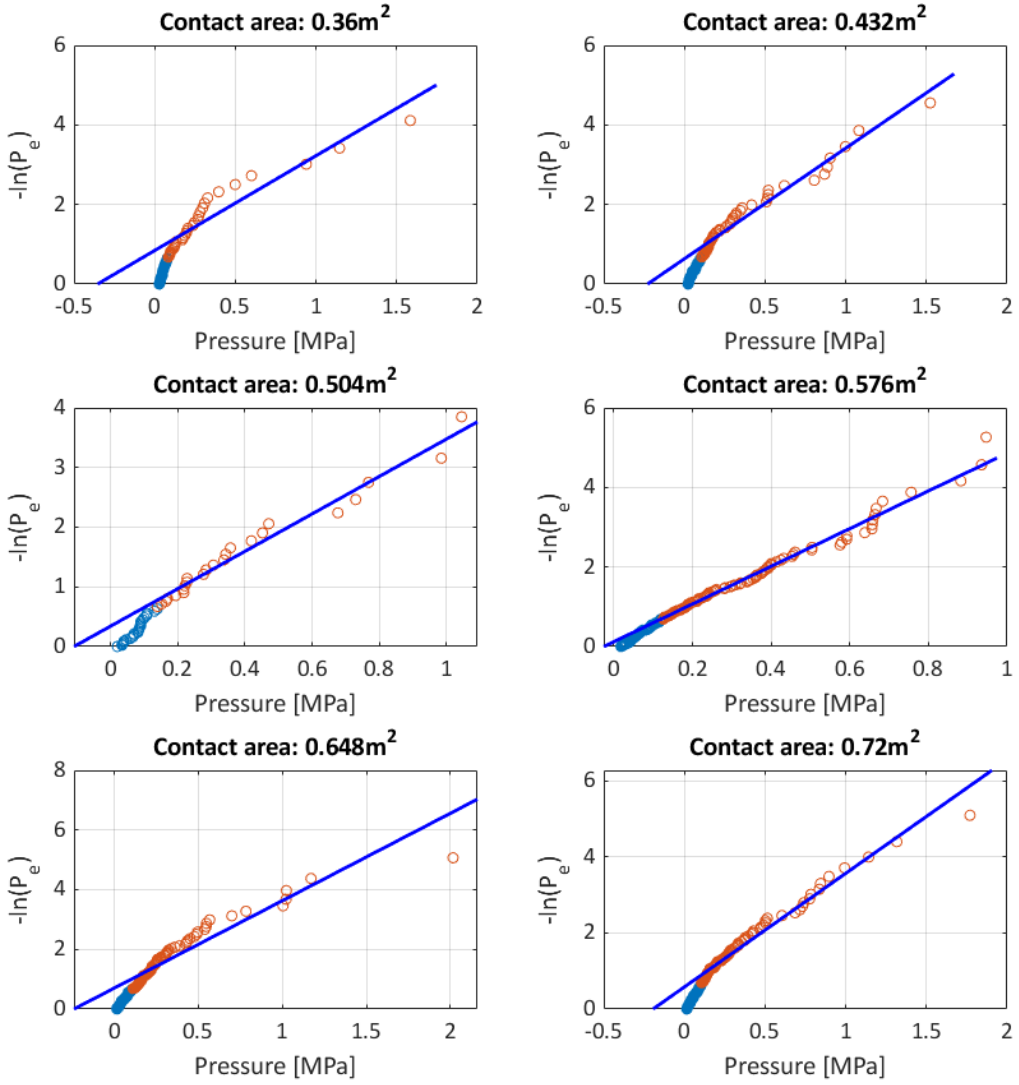

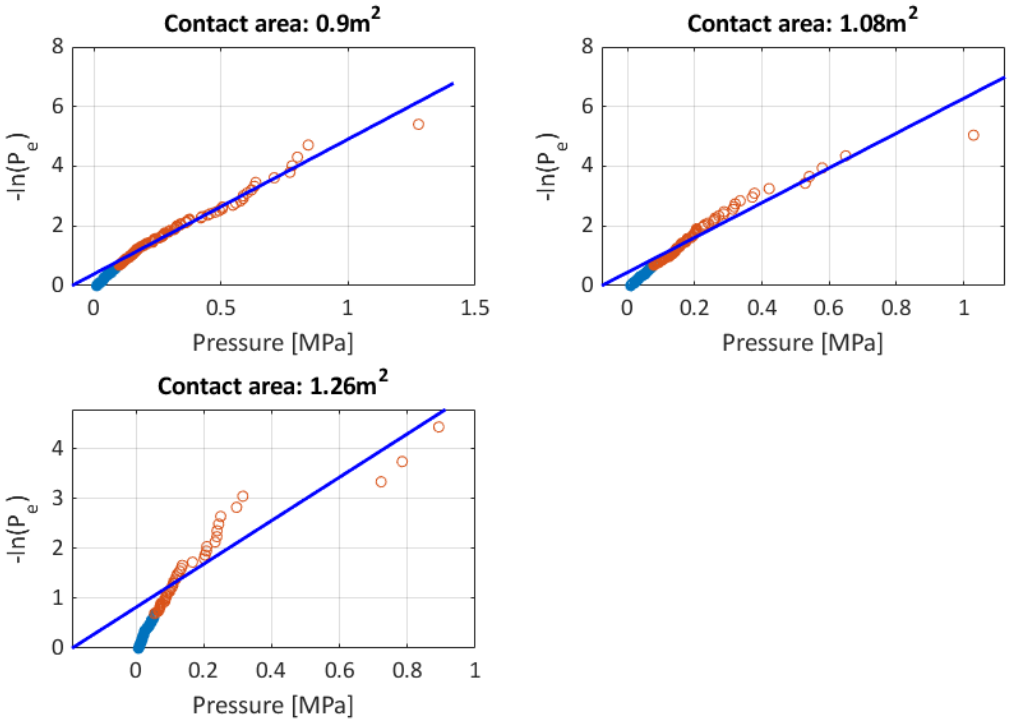

Parameters of best fitting lines to the pressures at the tail, for frames #40 ½ , 40, and #39 ½

Contact area $[m^2]$	a	b	α [MPa]	X_0 [MPa]
0.360	2.383	0.843	-0.354	0.420
0.432	2.781	0.635	-0.228	0.360
0.504	3.138	0.341	-0.109	0.319
0.576	4.737	0.122	-0.026	0.211
0.648	2.929	0.701	-0.239	0.341
0.720	2.992	0.581	-0.194	0.334
0.900	4.524	0.387	-0.086	0.221
1.080	5.828	0.447	-0.077	0.172
1.260	4.346	0.817	-0.188	0.230

The α-area curve and X_0 versus contact area for frames #40 ½ , 40, and #39 ½

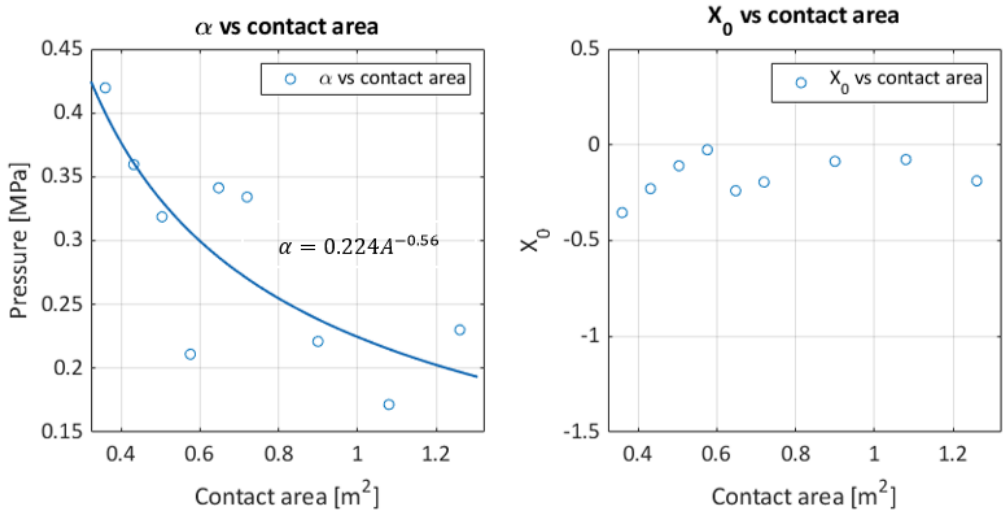

Local pressures vs contact areas at the stern shoulder for frames #41, #40 ½, #40, # and 39 ½

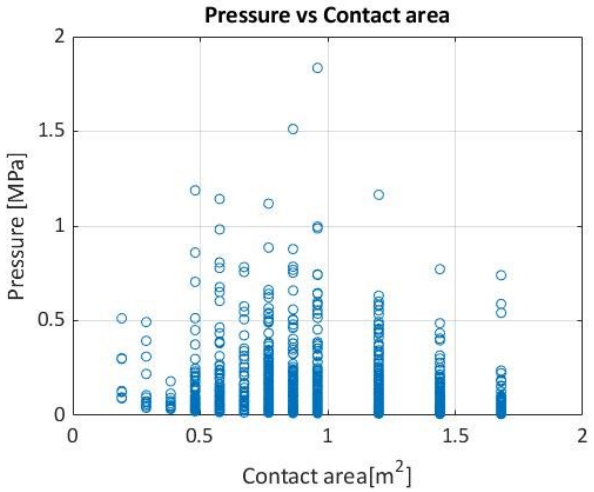

Best fitting lines for the pressures at the tail, for frames #41, #40 ½, #40, # and 39 ½

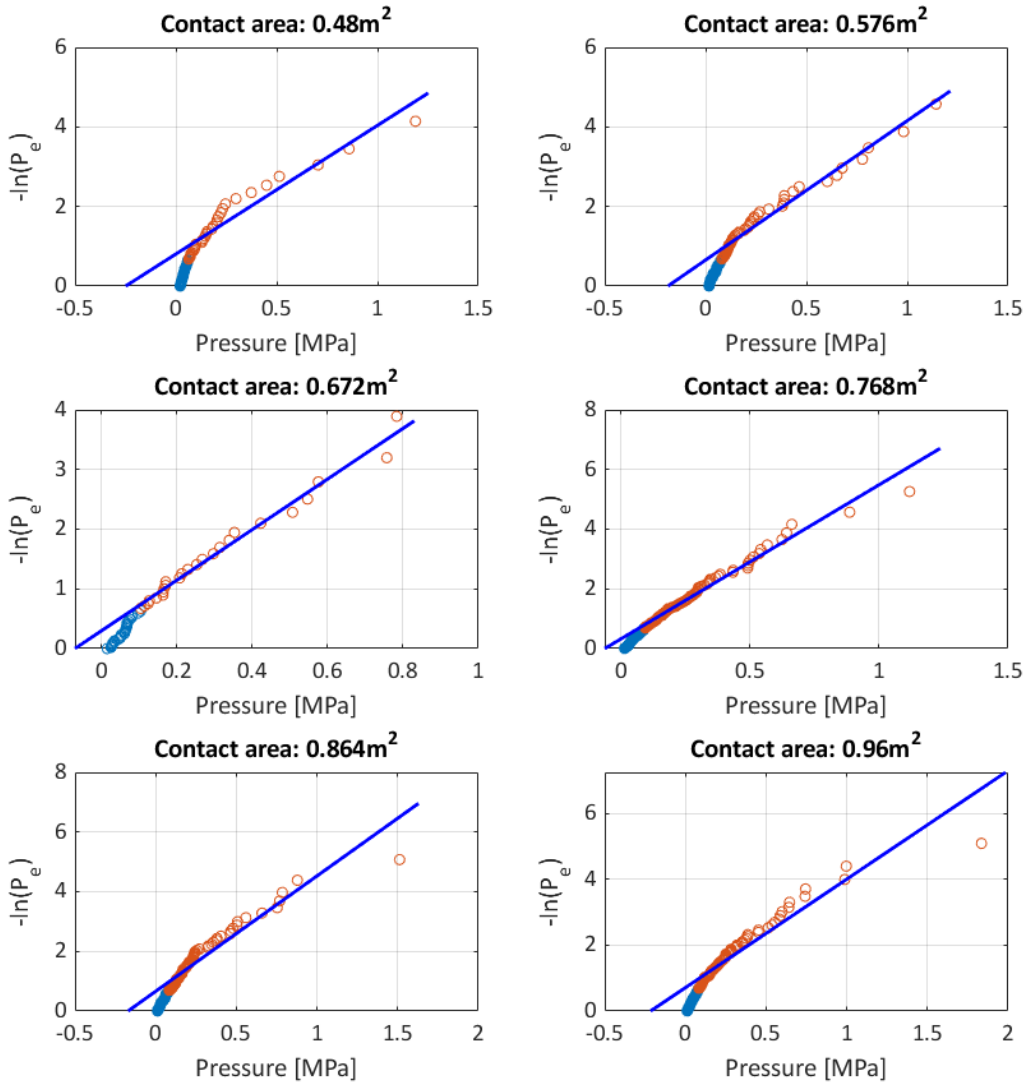

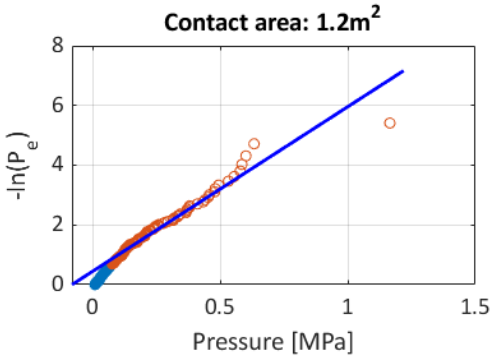

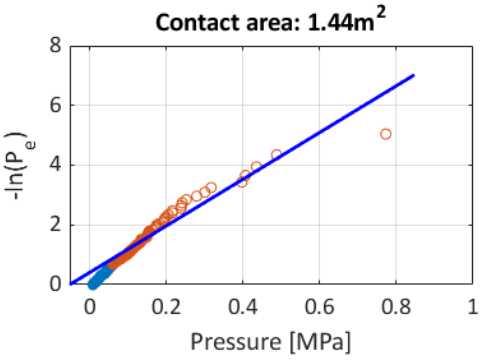

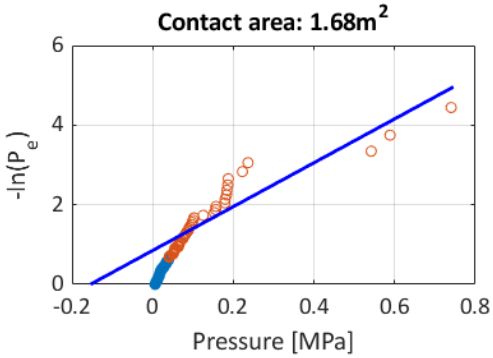

Parameters of best fitting lines to the pressures at the tail, for frames #41, #40 ½, #40, # and 39 ½

Contact area [m^2]	a	b	α [MPa]	X_0 [MPa]
0.480	3.234	0.805	-0.249	0.309
0.576	3.502	0.654	-0.187	0.286
0.672	4.239	0.297	-0.070	0.236
0.768	5.162	0.326	-0.063	0.194
0.864	3.866	0.662	-0.171	0.259
0.960	3.300	0.712	-0.216	0.303
1.200	5.511	0.449	-0.082	0.181
1.440	7.808	0.416	-0.053	0.128
1.680	5.511	0.851	-0.154	0.181

The α-area curve and X_0 versus contact area for frames #41, #40 ½, #40, # and 39 ½

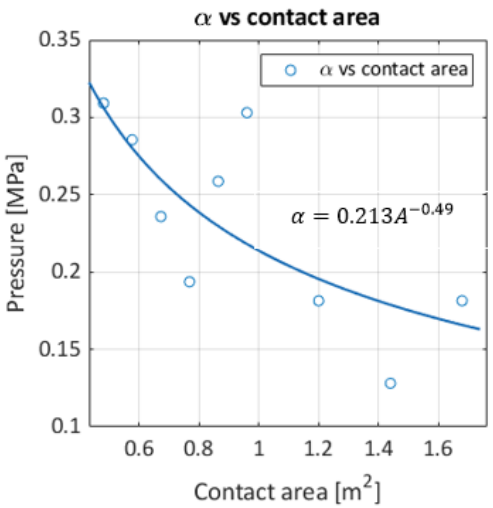

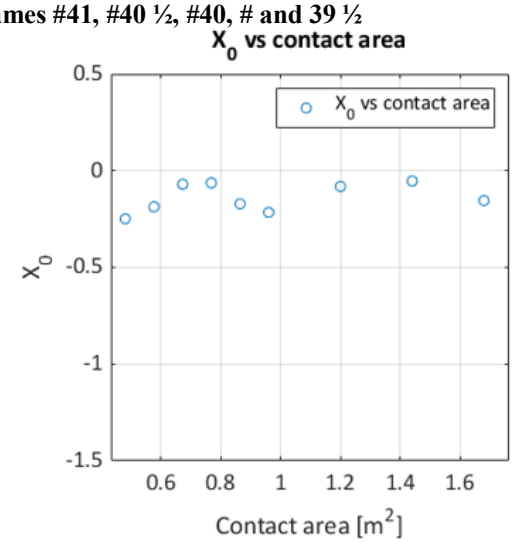

Appendix E: Comparison of the obtained α-area curves with the previous studies

Obtained α-area curves of the bow frames

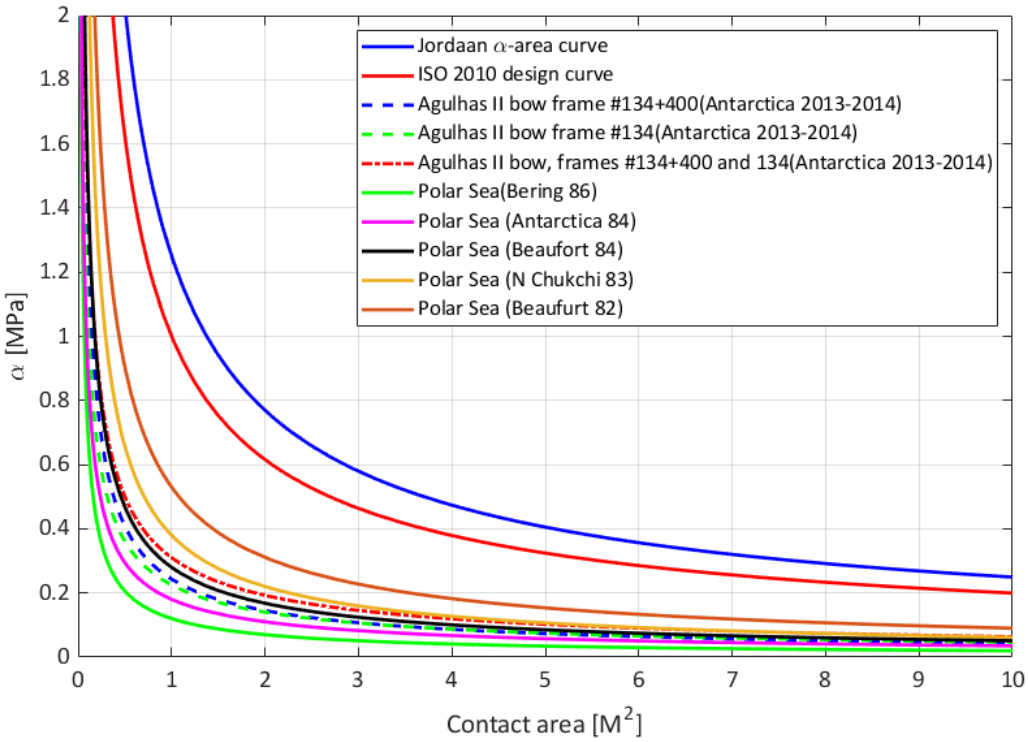

Obtained α-area curves for individual frames at the bow shoulder

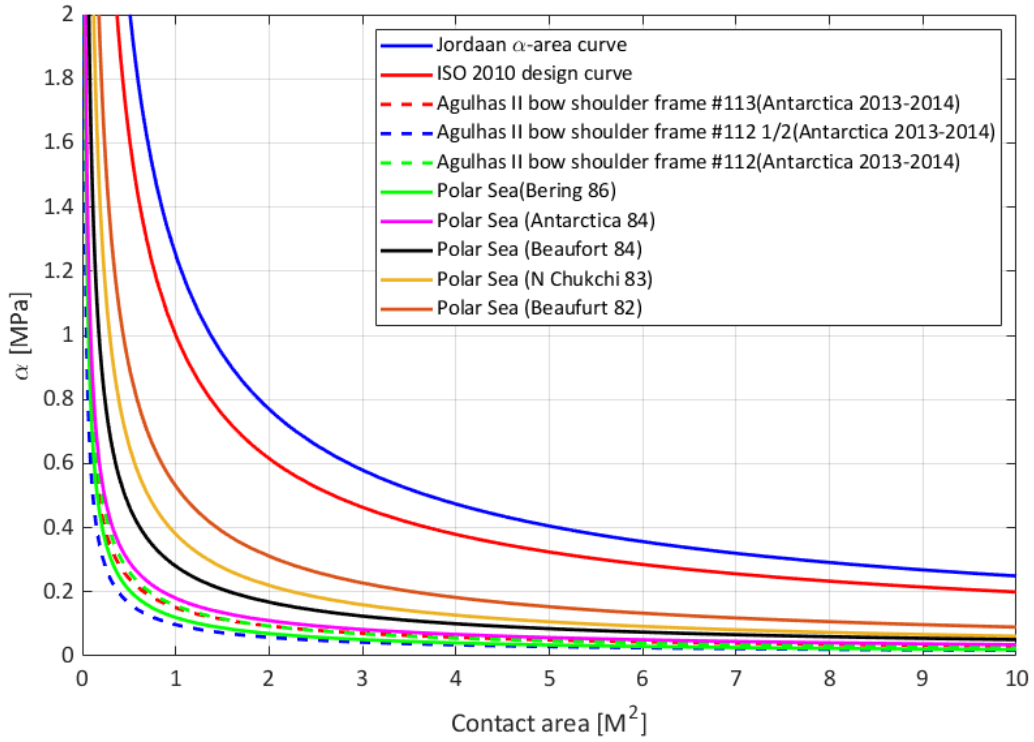

Obtained α-area curves for two frames at the bow shoulder

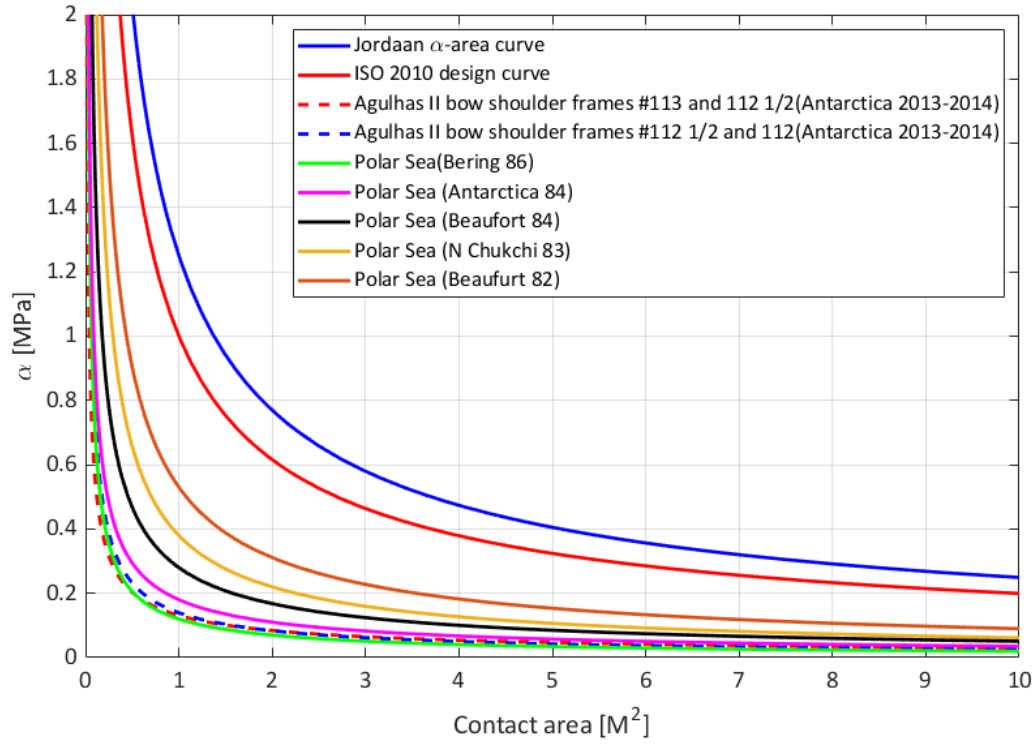

Obtained α-area curves for three frames at the bow shoulder

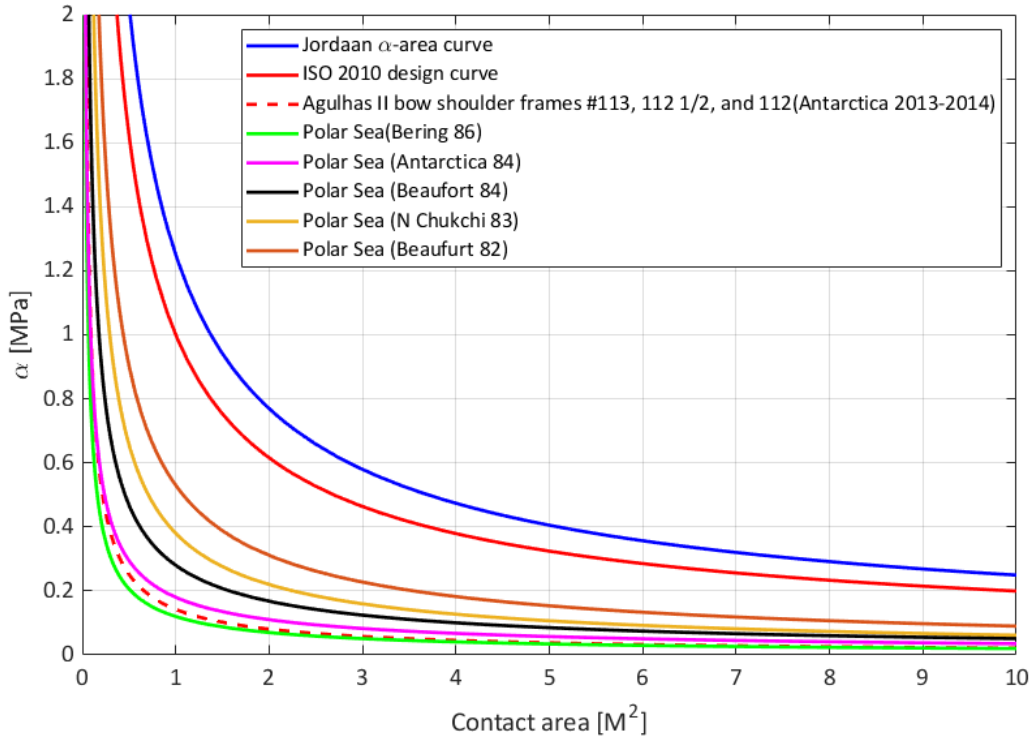

Obtained α-area curves for individual frames at the stern shoulder

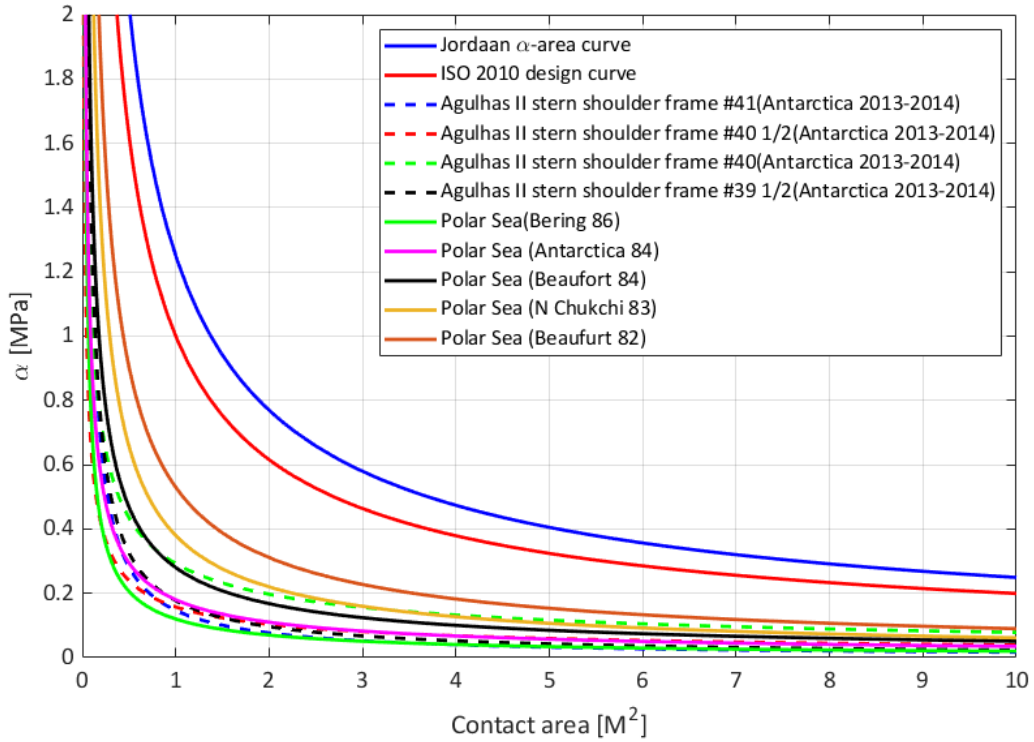

Obtained α-area curves for two frames at the stern shoulder

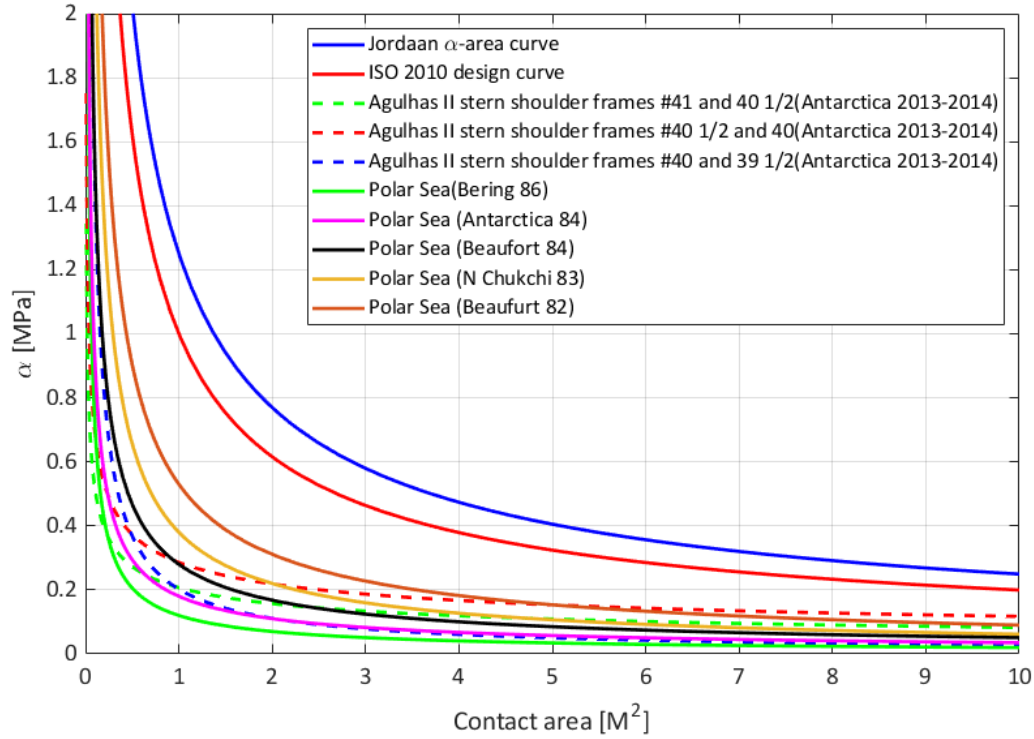

Obtained α-area curves for three frames at the stern shoulder

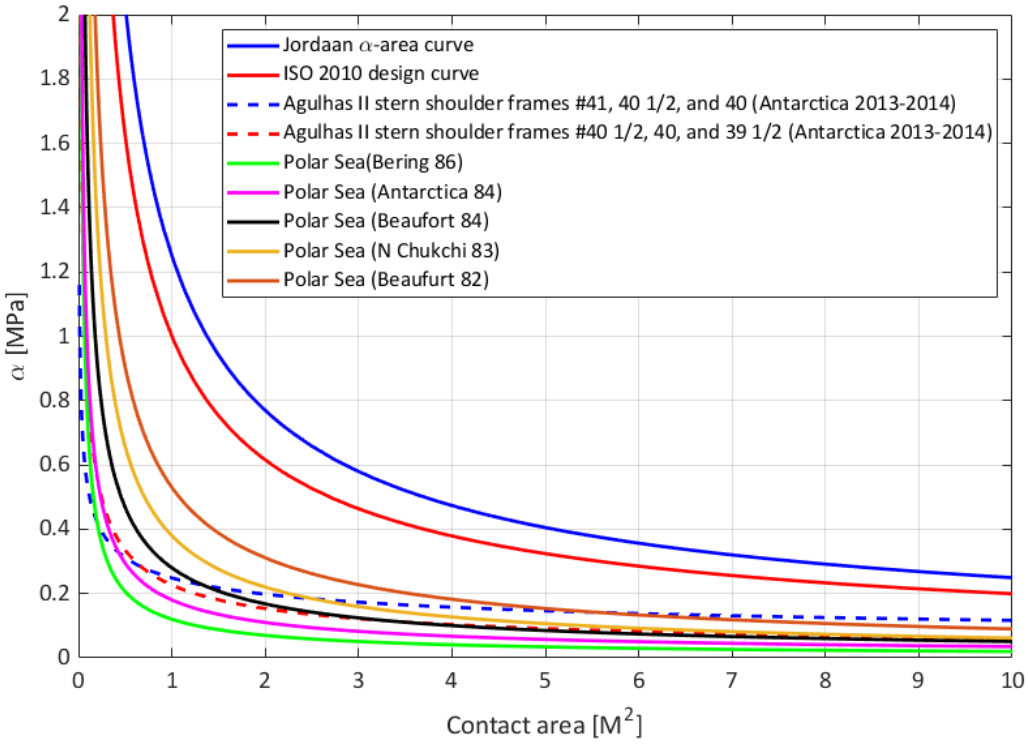

Obtained α-area curves for four frames at the stern shoulder

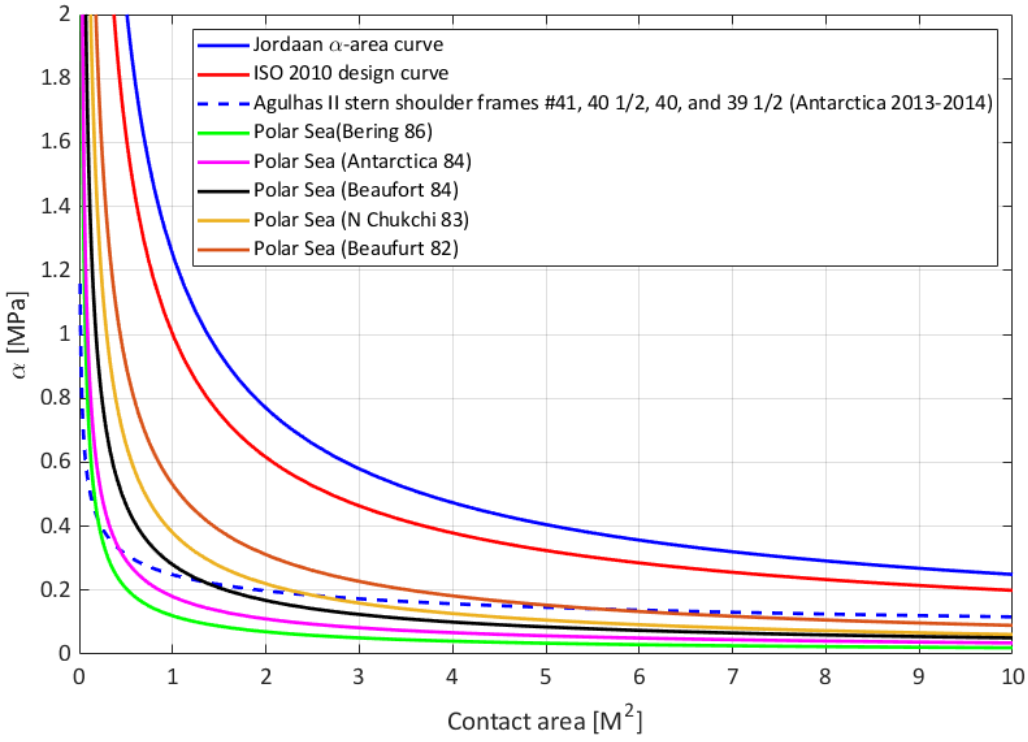

Appendix F: The expected number of MYI exposure for different ice class

The expected number of MYI exposure for different ice classes (Ralph, 2016)**.**

IACS Polar Class	MY Ice Exposure	Can. ASPPR	FIN	DnV	ABS	RUS
PC1				Polar 30		LL1/L9
	10000	CAC1				
PC2	**1000**	CAC2		Polar 20	A5	
PC3	**100**	CAC3		Polar 10	A4	LL2/L8
PC4	**10**	CAC4		ICE 15	A3	LL3/L7/ ULA
	5			ICE 10		
PC5	**1**	**Type A**		**ICE 5**	**A2**	**LL4/L6**
PC6	**1/10**	Type A	**1A Super**	ICE 1A*/ 1A Super	A1	L5/UL
PC7	**1/20**	Type B	1A	DnV 1A	A0	L4/L1

Appendix G: The effect of variation of load height on ice pressures vs different contact areas and x_0 at two frames at the bow

The effect of variation of load height on ice pressures vs different contact areas for two frames at the bow

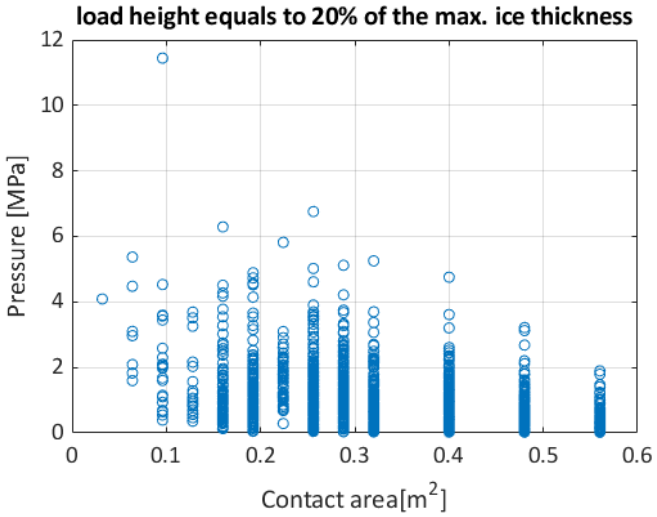

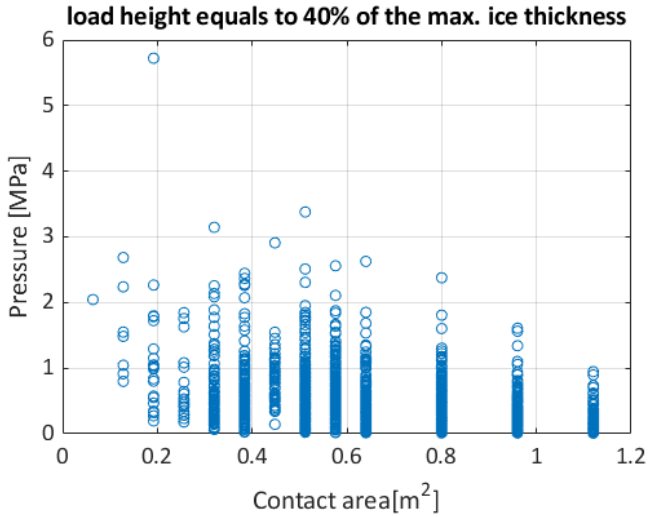

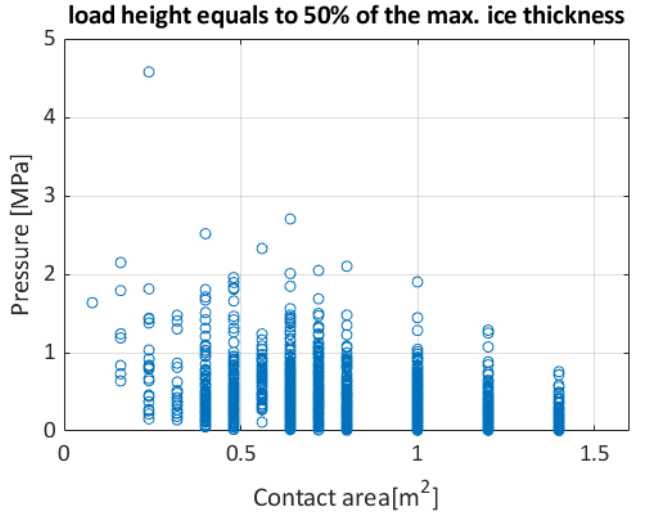

The effect of variation of load height on x_0 for two frames at the bow